EXPERIMENTAL AND FEM INVESTIGATION OF THE PERFORMANCE OF CONCRETE MASONRY WALLS RETROFITTED USING STEEL FIBER REINFORCED MORTAR ADMIXED WITH MICROSILICA

BY

MADYAN ABDULWAHAB SALEH ALSHUGAA

A Thesis Presented to the
DEANSHIP OF GRADUATE STUDIES

KING FAHD UNIVERSITY OF PETROLEUM & MINERALS

DHAHRAN, SAUDI ARABIA

In Partial Fulfillment of the
Requirements for the Degree of

MASTER OF SCIENCE

In

CIVIL ENGINEERING

May 2016

KING FAHD UNIVERSITY OF PETROLEUM & MINERALS

DHAHRAN- 31261, SAUDI ARABIA

DEANSHIP OF GRADUATE STUDIES

This thesis, written by **MADYAN ABDULWAHAB SALEH ALSHUGAA** under the direction of his thesis advisor and approved by his thesis committee, has been presented and accepted by the Dean of Graduate Studies, in partial fulfillment of the requirements for the degree of **MASTER OF SCIENCE IN CIVIL ENGINEERING**.

Dr. Ali H. Al-Gadhib
(Advisor)

Dr. Salah U. Al-Dulaijan
Department Chairman

Prof. Mohammed H. Baluch
(Co-Advisor)

Prof. Salam A. Zummo
Dean of Graduate Studies

Dr. Muhammad K. Rahman
(Member)

15/5/16
Date

Prof. Omar S. Baghabra Al-Amoudi
(Member)

Dr. Mohammed A. Al-Osta
(Member)

Dedicated

to

My parents, brothers & sisters

and

my wife & daughter

for their help and support

ACKNOWLEDGMENTS

First and foremost, all praise and glory be to ALLAH for giving me the good health, courage and patience to complete this work. Acknowledgment is due to KFUPM for granting me the opportunity to pursue my graduate MS with financial support. I am also indebted to the Department Chairman, Dr. Salah Al-Dulaijan, and to other faculty members for their support. I also acknowledge the Deanship of Scientific Research at KFUPM for funding this work under project number of RG 1403-1/2. Acknowledgments are due to Advanced Concrete Products Company (Ltd.) for providing the hollow concrete blocks needed for finishing this work.

I acknowledge, with deep gratitude and appreciation, the valuable time and guidance given to me by Dr. Ali H. Al-Gadhib, who served as my major advisor. Further, I am deeply indebted and grateful to Prof. Mohammed H. Baluch, my co-advisor, and Dr. Muhammad K. Rahman, as a committee member and a Principal Investigator of this research, for their extensive guidance, continuous support, and personal involvement in all phases of this research. I am also grateful to my committee members, Dr. Mohammed A. Al-Osta and Prof. Omar S. Baghabra Al-Amoudi, for their constructive guidance, valuable advice and cooperation. I also acknowledge the sincere and untiring efforts of the laboratory technicians Eng. Imran, Eng. Omer and Eng. Najamuddin for their tremendous help. I would like to express my heartfelt love and gratitude to my parents and family in Yemen and US for their support and help in overcoming the challenges I have faced during my study. Also, I would like to thank my brother Mohammed Alshugaa in the US for his sacrifice and support. Finally, I would like to thank, my colleagues at KFUPM for their friendship during my studies.

TABLE OF CONTENTS

LIST OF TABLES

LIST OF FIGURES

LIST OF ABBREVIATIONS

CDP: Concrete Damage Plasticity

FEM: Finite Element Modeling

NCM: Normal Concrete Masonry Wall

NCMWJ: Normal Concrete Masonry Wall Joined by SFRM

NCMWR: Normal Concrete Masonry Wall Retrofitted

SFRM: Steel Fiber Reinforced Mortar

URM: Unreinforced Masonry

ABSTRACT

Full Name: Madyan Abdulwahab Saleh Alshugaa

Thesis Title: Experimental and FEM Investigations of the Performance of Concrete Masonry Walls Retrofitted Using Steel Fiber Reinforced Mortar Admixed with Microsilica

Major Field: Civil Engineering

Date of Degree: May 2016

Although the constructions of buildings are nowadays built using mainly reinforcement concrete and steel, still the use of concrete unreinforced masonry buildings is very common. Because of easy installing, low cost and availability in different types, people keep using the unreinforced masonry (URM) wall and it represents the majority of the residential building in the developing countries. The URM walls can act as a compressive element with a high capacity. However, it shows weak performance when exposed to in-plane lateral loads such as wind and earthquake. Unfortunately, most of the existing URM buildings were constructed without taking the earthquake hazards into account. Therefore, a need has emerged in the direction of strengthening these walls to improve their ability to withstand potential seismic damage.

This work was aiming to retrofit the URM walls using steel fiber reinforced mortar (SFRM) as coating layers. The advancement of micro-mineral additions to cement as cementitious materials has been exploited where the microsilica was used as a cement replacement in the SFRM. Microsilica enhances the mortar strength, increases the density and reduces the permeability and porosity. Consequently, steel fiber was employed in the mix of the SFRM in order to increase the tensile strength and mortar ductility. URM hollow concrete prisms

and walls were prepared and retrofitted in one side and both sides and using SFRM in the joint in order to study the performance against lateral load as well as axial stress. In addition, FEM modeling was conducted using Concrete Damage Plasticity (CDP) available in ABAQUS. Laboratory tests for mechanical properties of the masonry components were conducted in order to be used in the FEM input for actual calibration with the experimental tests.

Results of this work have indicated that there is a significant increase in the shear capacity of the URM walls retrofitted using SFRM. Furthermore, the FEM simulations showed a good agreement with the experimental results for both prisms and walls in terms of failure mode, stiffness and strength capacity.

ملخص الرسالة

الاسم الكامل: مدين عبدالوهاب صالح الشجاع

عنوان الرسالة: دراسة معملية وحسابية (FEM) لأداء جدران الطوب الخرسانية المطلية بملاط مُقَوَّى بألياف حديدية ومخلوط بمادة الميكروسيليكا.

التخصص: هندسة مدنية

تاريخ الدرجة العلمية: مايو 2016

على الرغم من أنَّ معظم المنشآت في الوقت الحاضر مبنية باستخدام الخرسانة المسلحة والحديد، فإنه لا يزال استخدام مباني الطوب الخرسانية هو شائع جداً. ونظراً لسهولة تركيب جدران الطوب الخرسانية وانخفاض التكلفة وتوفرها في أنواع مختلفة، ما زال الناس يستخدمونها في البناء، بحيث أنها تمثل غالبية المباني السكنية في الدول النامية. تعتبر جدران البناء غير المدعمَّة عنصر فعَّال في مقاومة إجهاد الضغط لكن أداءها يكون ضعيفاً عند تعرضها لأي أحمال جانبية مثل الرياح والزلازل. ومن الملاحظ أن أغلب المباني القائمة قد شُيدت بدون أخذ مخاطر الزلازل في الإعتبار عند التصميم، ولذلك ظهرت الحاجة لتقوية جدران هذه المباني لتحسين قدرتها في مقاومة الدمار المحتمل للزلازل.

يهدف هذا العمل إلى تقوية جدران الطوب الخرسانية غير المدعمة باستخدام طبقات الملاط (SFRM) المُقَوَّى بألياف حديدية ومخلوط بمادة الميكروسيليكا. ونظراً للتطوَّر الواضح في استخدام المعادن بحجم الميكرو كإضافة للإسمنت، فقد تم إضافة مادة الميكروسيليكا لملاط (SFRM)، حيث تعمل الميكروسيليكا على تحسين قوة الملاط وزيادة كثافته وتقليل المسامات والنفاذية، لكنها لا تحسن مقاومة الملاط لإجهاد الشد. لذلك، تم استخدام الياف الحديد في الملاط (SFRM) لزيادة مقاومته لإجهاد الشد وتطوير درجة قابليته للسحب.

تم اعداد جدران غير مدعمة باستخدام الطوب الخرساني المجوف بمقاييس كبيرة وصغيرة وتم طلائها بملاط (SFRM) من جهة وجهتين، كما تم استخدام الملاط كغراء بين الطوب لدراسة أدائها في مقاومة الاجهاد الافقي والرأسي. كما تم أيضا تصميم نماذج (FEM) باستخدام (CDP) المتوفرة في برنامج (ABAQUS). وقد أجريت الاختبارات المعملية للخواص الميكانيكية لمكونات الجدار من أجل استخدامها كبيانات لنموذج (FEM) ومعايرته الفعلية مع نتائج التجارب المعملية.

أثبتت نتائج الاختبارات المعملية لهذا العمل أن هناك زيادة ملحوظة في مقاومة قوة القص لجدران الطوب غير المدعمة والمعدلة باستخدام (SFRM). وأظهرت مخرجات المحاكاة (FEM) اتفاق جيد مع النتائج التجريبية للجدران المدروسة من حيث نمط الفشل والصلابة وقوة التحمل.

CHAPTER 1

INTRODUCTION

1.1 General

A masonry wall is one of the oldest and common types of structural component, which is constructed from hand-placed units of natural or manufactured material such as clay brick, concrete block, etc., and one stacked atop another and joined to each other with mortar. In general, masonry building can be found in regions like India, Middle East, Eastern Europe and some parts of Asia [1]. Because of easy installing, low cost and availability in different types (clay, concrete, stone etc.), people keep using masonry wall and it represents the majority of the residential buildings in the developing countries [2].

Unreinforced masonry walls (URM) are mainly built for partition walls, structural walls, retaining walls which can be made nowadays using concrete masonry units. Concrete composed of Portland cement and aggregate (usually sand and fine gravel) is used to make concrete blocks. Concrete blocks come in many sizes and may be produced with hollow centers in order to reduce weight and improve insulation.

URM walls can act as a compressive element with magnificent capacity, but it shows bad performance in resisting in-plane lateral loads such as wind and earthquake [2]. As a result, a catastrophe takes place, causing a big loss in terms of lives and economy [3]. Elastic properties, as well as failure criteria of URM, are regarded as anisotropic. Orthogonal

planes of weakness are attributed to the mortar joints. Failure modes for URM components comprise of compressive crushing, the diagonal tensile splitting of units, tensile cracking along the bed and head joints, and the sliding shear failure of bed joints [4].

In recent years, considering environmental, technical and sustainability requirement of the output product, the use of micro-mineral additions to cement as cementitious materials has been increased. These micro-materials have the ability to modify the fresh and hardened, physical and chemical properties when they are added as a partial replacement of cement. There are 3 major advantages of using micro-materials. The first advantage is the construction of high-strength concrete. The second advantage is lowering the construction times as they are capable of producing concrete with reduced curing time. The third advantage is to obtain similar strengths with less cement needed which decreases the cost and environmental impact of producing construction materials [5, 6].

Recently, micro-materials, such as microsilica (also called silica fume) is showing potential because of its ability to improve the performance of concrete compared with traditional mineral admixtures. The advantages of microsilica include the production of very high strength mortar concrete, increased density and reduced permeability and porosity.

Fibers had been used as reinforcement since prehistoric times. At that time, straws were used in mud bricks and horsehair was used in mortar. In the 1900s, fibers of asbestos were used in concrete. The idea of composite materials came in the 1950s and fiber reinforced concrete was one of the topics of interest [7]. Steel fiber is one kind of fiber reinforcement system, which increases structural integrity, tensile strength, and ductility. The key

advantage of using steel fibers in mortar or concrete is: steel fibers are useful as multi-directional reinforcement, which helps to improve the crack resistance [1].

Finite element model (FEM) is a convenient method to understand and predict the nonlinearity behavior of URM structures. ABAQUS software provides a suitable environment to simulate the URM structures due to the availability of Concrete Damage Plasticity (CDP) model. CDP is based on constitutive models which describe the fracture behavior of masonry units and mortar joints in order to model the failure mechanisms mentioned above with this tool [8]. The brittle behavior of masonry units under tension/compression introduces a motivating challenge in the modeling aspect.

As any country, the Kingdom of Saudi Arabia possesses buildings with concrete masonry walls all around the area and they mostly consist of URM walls. Since most of these buildings are located in regions prone to low seismic activity, there is a movement by some private and governmental sectors in the Kingdom to strengthen structural elements.

Therefore, the aim of this research was to develop a strengthening procedure for the existing concrete masonry wall using steel fiber reinforced mortar admixed with microsilica (SFRM) as plasters. A number of trial mixes for SFRM had been prepared in order to choose an appropriate mix based on strength and workability. Then, the URM was plastered using this high strength mortar and tested under cyclic loading. FEM simulation was calibrated with the experimental results.

1.2 Need for Research

Most of the old concrete masonry structures had not been originally designed to resist lateral loading, such as seismic loading. The wall systems constructed in Saudi Arabia are mostly considered as a load bearing type, designed only to sustain gravity loading. Since the Kingdom of Saudi Arabia region is exposed to the risks of earthquake hazards [9], there is a need for an investigation to gain knowledge about the performance of such structures subjected to seismic loading and to propose suitable strengthening methods for enhancement of their lateral resistance.

1.3 Objectives

The fundamental objective of this research was to evaluate the performance of URM concrete walls plastered with steel fiber reinforced high strength mortar admixed with microsilica (SFRM) including the enhancement of lateral resistance and the effect of plastering thickness on the strength and ductility.

The specific objectives of the research were:

1. To evaluate the performance of normal concrete masonry wall (NCMWR) retrofitted using high-performance mortar for plastering based on indices of strength and ductility under cyclic loading.
2. To evaluate the performance of normal concrete masonry wall (NCMWJ), using SFRM in joints, based on strength and ductility under cyclic loading.
3. To develop a mechanistic model to predict the shear capacity of plastered walls including the influence of plastering thickness.

4. To analyze the above concrete masonry walls using finite element modeling in the ABAQUS environment.

1.4 Thesis Outline

The thesis consists of 6 chapters as follows: Chapter 1 contains the introduction, description of the need for this research and stating of the objectives. Chapter 2 gives a comprehensive literature review about previous research related to URM wall and retrofitted methods. The review also includes the effect of microsilica and steel fiber on the concrete properties.

Chapter 3 includes a detailed description of all experimental work related to mix design of SFRM and mechanical properties all masonry components. Then, Chapter 4 includes the experimental investigation of prism compression test and lateral cyclic test. All specimens' preparation, tests setup and tests results were analyzed and discussed in this chapter.

Chapter 5 contains the numerical investigation (consists of both FEM and mechanistic models) which describes the models methodology, input, and analysis of the output results. Comparison of the experimental results and the numerical investigation is shown also in this Chapter.

The thesis is concluded with Chapter 6 which contains conclusions and recommendations followed by references and appendices.

CHAPTER 2

LITERATURE REVIEW

Several investigations on masonry structures have been carried out in order to understand the behavior of URM walls before and after retrofitting process. There are different retrofitting methodologies that have been studied in order to enhance the performance of concrete masonry structures. In this research, the surface treatment (SFRM plaster) is the retrofitting method used to enhance the performance of unreinforced masonry (URM) walls. Therefore, this Chapter focuses on the review of masonry structure behavior subjected to lateral loading before and after retrofitting. Also, a literature search was conducted on the compressive capacity of concrete masonry walls, the effect of microsilica and steel fibers on concrete properties and numerical studies of masonry behavior will.

2.1 Review on Masonry Wall

Masonry walls can act as a compressive element with magnificent capacity, but when it comes to resist in-plane lateral loads, such as wind and earthquake, it exhibits bad performance [2]. Several studies on strengthening techniques were conducted over the years in an attempt to make enhancement in reducing the damage from in-plane horizontal loadings. The application of the surface treatment using mortar was proposed by many researchers [10].

Bhattacharya et al. [1] introduced different types of retrofitting methods either early implementation or under research. These methods are external reinforcement, surface treatments (ferrocement, shotcrete, etc.), grout/epoxy injection (re-pointing), seismic wallpaper (GFRP & CFRP), confinement, post-tensioning (rubber tyres), mesh reinforcement (polymer and steel) and L-shaped reinforcement. Moreover, these methods were categorized and analyzed to be compared based on buildability, sustainability and economy as well as providing a useful insight. This study also highlighted the advantages and disadvantages of many retrofitting methods. However, there is still no much researches have been conducted on retrofitting URM using high strength mortar admixed with steel fiber as plaster.

Haach et al. [11] proposed the seismic behavior of masonry walls reinforced by a combination of horizontal and vertical reinforcement. A total of eight panels were constructed with an aspect ratio of 0.67 and subjected in-plane cyclic test which started by applying constant axial pre-compression load followed by lateral cyclic loading. The in-plane cyclic performance of concrete masonry walls is affected by the pre-compression, masonry bond and horizontal reinforcement. The authors concluded that the stiffness and ductility of the masonry walls are affected by the pre-compression level. As the pre-compression increases, the masonry walls will be stiffer and more brittle under lateral load. Moreover, the initial flexural cracking is limited when vertical reinforcement is present, which leads to diagonal crack development based on the experimental test [11]. Consequently, the horizontal reinforcements improve and control the distribution of cracking with only a small increase of lateral strength.

Mosallam & Banerjee [12] carried out an experimental study on the evaluation of the performance of URM walls and the improvement of in- plane shear capacity by retrofitting URM walls using FRP composites. They tested six identical wall specimens of 1:1 aspect ratio (height/length) under in-plane cyclic lateral load accompanied with a constant axial load. Four of these specimens were externally strengthened using different composite retrofitting systems. The authors reported that an improvement in the ultimate capacity of the walls was achieved due to the effect of fiber reinforced polymer [12]. Also, they proved that the wall ultimate failure modes were improved from brittle failure mode to ductile failure due to the effect of FRP. Furthermore, they executed a comprehensive analytical investigation (whether a code-based or research-based) and validate it with experimental findings. As a result of this investigation, they concluded that analytical models generally will not provide a precise prediction of the shear capacity for different retrofit structures. Therefore, they recommended that extensive research on analytical models should be taken place in near future in order to develop applicable analytical models to be used in wide range of URM walls retrofitted with FRPs.

Bischof et al. [13] had carried out research on retrofitting of URM wall with carbon mesh and tested it under in-plane cyclic lateral load and tensile load. In this study, they used high-quality spray mortar below and above the carbon fiber reinforced polymer sheets on the wall in different schemes. Test results revealed that this system of retrofitting reached similar strength and higher ductility than being retrofitted by means of bonded CFRP sheets. The authors suggested that carbon mesh with high-quality mortar is a good option for static or seismic retrofits for a masonry wall.

Vasconcelos et al. [14] studied unreinforced masonry walls retrofitted by textile reinforced mortar. In their research, they retrofitted masonry wall using new reinforcing material based on braided fibrous structures which were developed through braiding of polyester yarns around a core made of either glass or carbon fiber or without any core. Researchers fabricated URM walls by placing these braided materials on the surface of clay brick walls in a mesh-like configuration and coating with a mortar layer in out-of-plane loading. They also studied the flexural behavior of developed masonry walls. The test results revealed that, due to the application of textile reinforced mortar, the ultimate deformation capacity increased by 322% and damage resistance capacity increased by 17.5% compared with the control specimen.

Basaran et al. [15] constructed 24 walls with dimensions of 400 mm length, 400 mm width and 100 mm thickness. Four walls were used as reference specimens while the others were plastered with different types of reinforced plaster mortar (2%, 3% polypropylene and 5% steel fiber). The load was applied to the samples at an angle of 30, 40, 60 and 90 degrees. According to the tests results, the load bearing capacity has been increased significantly after using particular reinforced plaster on both sides of the walls compared to the control samples. Also, the stiffness of the walls has been improved notably by such a unique coating. The test results revealed that steel fiber increases the ductility of the sample better than polypropylene.

Interesting research was carried out by Elgawady et al. [16] on half-scale brick clay masonry walls retrofitted using steel bars mesh coated by shotcrete layer. Three walls were tested and classified as one control, one retrofitted by steel mesh and coated with shotcrete mortar on one side by 40 mm and the last was coated on two sides by 20 mm for each face.

The results showed that the lateral capacity was increased significantly by 3.5 times the control sample capacity.

Only a few people use the idea of using high strength mortar with steel fiber as a surface treatment to retrofit URM walls. The use of steel fiber facilitates the application of the mortar layer utilizing the common trowel because it holds the mortar together. In addition, steel fiber has the ability to improve the ductility behavior as well as increasing the energy dissipation of the wall. Facconi et al. [17] used mortar reinforced with nano-silica and short high strength steel fibers as a surface treatment technique. Four walls were tested; one as a reference specimen, two strengthened with 25 mm thickness layer with different types of steel dowel connection to improve the bond, the last was the first specimen after it was tested and repaired with 25 mm thickness layer to be tested again. The results revealed improvement in the shear capacity by 30% higher than the reference sample, also enhancement in the stiffness by 60% in the elastic level of the experiment.

2.2 Review on Masonry Prism

Prism test method is one of two methods that are preferred by the researchers and designers to evaluate the compressive strength of URM wall, while the other method, which is unit (masonry brick) strength method, depends only on block and mortar strength, and it does not take into consideration the effect of workmanship and curing [18].

Mohamad et al. [19] studied the deformability, strength and failure mode of concrete masonry wall subjected to axial load. A tensile stress test was adopted for seven block specimens resulting in an average tensile strength of 2.3 MPa. The compressive strength of the block and mortar was recorded to be 23 MPa and 8.3 MPa, respectively. A total of

10 LVDTs were connected horizontally and vertically on the masonry wall for recording the deformability and to study the effect of joints mortar. The compressive capacity of the wall reached a value of 11 MPa. The researchers concluded that the non-linearity behavior and failure mode of the wall were controlled by the head-joint, which is the weakest point in their experimental work [19].

Casali et al. [20] studied the influence of both hollow concrete block geometry and joint mortar type on the prism/unit ratio, deformation and failure behavior of structural masonry prisms. This study was adopted for four mortar types (two packaged-dry mortars and two cement-lime mortars) and two concrete block geometries (face-shell thickness of 25 mm and 32 mm) with different compressive strengths. The results obtained showed that concrete block geometry influenced prism compressive capacity where it was recorded to have a lower level for prisms made with packaged-dry mortar and concrete blocks with the smallest thickness. However, prisms with this same geometry but built with cement-lime mortar produced better overall results. Concrete block geometry and type of mortar also influenced mechanical behavior. The highest prism/unit ratio was achieved in prisms with cement-lime mortar. The prisms made with packaged-dry mortar showed higher deformation and crushing of the mortar joint (with 50% of rupture force).

Interesting research was carried out by Oliveira & Hanai [21]. They tested eight models of a unit concrete prism with two samples of every model. The first model was a reference while the second and the third were retrofitted by weak mortar and strong mortar, respectively. Strong mortar with welded meshes and another strong mortar with welded meshes using two different types of connectors, to enhance the bond, used for the fourth, fifth and sixth models, respectively. The last two models were reinforced by strong mortar

with steel fibers and weak mortar with polypropylene. The test results revealed that unit concrete prism reinforced with strong mortar plus welded meshes increased the ultimate load capacity by a factor of about 1.44. The efficiency of strengthening with mortar overlays was affected by the mechanism failure of the prism.

Shah [22] carried out a research on the application of ferrocement in the strengthening of unreinforced masonry columns. He investigated unreinforced masonry column retrofitted with mortar as plaster subjected to axial load. The experimental study revealed that an increasing by 119% of the first crack load and 121% of the ultimate load of a ferrocement encased masonry column. Well distributed and finer cracks were developed in ferrocement coated column compared to the plain specimen. He also suggested that the poor bond between brick masonry column and ferrocement is leading to premature failure. There is an expectation of severe spalling and delamination at higher reinforcement ratio.

Sarangapani et al. [23] used different types of bricks and mortars to study the shear bond and flexural strength of URM walls. A modified bond wrench test was used to determine the flexural bond strength, and shear bond strength was determined with a triplet test. In order to investigate the increase in compressive strength as increasing the bond strength, bond-enhancing techniques have been applied. The authors found that the bond strength is increased by using either a strong mortar, a mortar with plasticizing additives, cement slurry or epoxy coatings. Accordingly, an increase in bond strength leads to increase in the compressive and flexural strength of masonry prism.

Nagarajan et al. [24] presented in their research the effect of different mortar ratios on the material properties, shear and compressive behavior of brick masonry. Brick prism triplets

were subjected to compression and shear load to evaluate and compare their compressive, bond strength and interface behavior. In the results of this research, the shear strength was increased more for small mortar ratio (cement/sand) of (1:2 > 1:3 > 1:4). Also, the shear bond strength of brick prisms cast with pre-wetted bricks is high compared to dry bricks.

2.3 Review on Microsilica and Steel Fibers in Concrete

Toutanji [25] had undertaken a study of the influence of silica fume on the compressive strength of cement paste and mortar. He worked with 5 different water-binder ratios (0.34, 0.31, 0.28, 0.25 and 0.22) and two different percentage (25% and 16%) silica fume addition by weight of cement. To ensure no segregation, superplasticizer content was adjusted. The test results showed that the silica fume contributes to strengthening the bond between the aggregate and cement paste, in a consequence of that compressive strength of mortar had increased. However, there was no influence on the strength of cement paste. From past research, he reported that the optimum silica fume content should be 15%.

Duval et al [26] investigated the influence of silica fume on the workability and the compressive strength. He used low water-cementitious materials ratios (0.25, 0.3, 0.35, 0.4 and 0.45) with naphthalene sulphonate superplasticizer. This research revealed that up to 10% silica fume addition, workability was not reduced. It was observed that at low water-cementitious ratios, slump loss with time increased with high replacement level. The test result showed that there was higher compressive strength gain (less than 15%) at 20% silica fume addition as a replacement of cement. Then, the authors proposed a model relating the water-cementitious ratio and silica fume content to estimate the compressive strength. It

was reported that this model can estimate compressive strength with an accuracy of better than 5%.

Mazlooma [27] studied the mechanical properties of high-strength concrete affected by silica fume. The researcher studied the short and long-term influence on mechanical properties of high strength concrete with different levels of addition (0, 6, 10 and 15%) of silica fume having water/binder ratio as 0.35 where the total binder content was 500 kg/m^3. The author conducted his study based on the compressive strength, secant modulus of elasticity, strain due to creep, shrinkage, swelling and moisture movement. The test results revealed that higher percentage of silica fume addition decreased the workability but improved the short time mechanical properties (compressive strength and secant modulus of elasticity).

Bhanja [28] investigated the influence of isolated contribution of silica fume on the tensile strength of concrete. Water-binder ratios were taken ranging from 0.26 to 0.42 and silica fume-binder ratios from 0.0 to 0.3 and 28 day compressive, flexural and split tensile strengths were examined. The test results showed that flexural strength had greater improvements (15-25%) than split tensile strength than the control specimen with silica fume addition from 5 to 10%. It was established that microparticles can be used to fill the capillary pores of concrete in order to reduce porosity and increase the strength of the concrete.

Lee et al. [29] studied the mechanical properties of mortar admixed with microsilica and steel fiber. Mortars with water/binder ratio of (0.3 and 0.5) were prepared with and without 10% microsilica of cement weight and (0, 0.3 and 1 vol. %) steel fiber. The researchers

studied slump, yield stress and plastic viscosity of fresh mortars where they found that the fresh mortars required more superplasticizer to maintain the slump flow close to that without silica fume for two different w/b ratios. Also, a 4% and 10% improvement in the cohesiveness of fresh plain mortars when admixed by 10% microsilica for w/b 0.3 and 0.5, respectively was observed. It was found that silica fume increased the compressive strength but showed no obvious effect on the bending strength for both w/b either with or without silica fume. The mortar with 0.3 vol% steel fiber recorded a great decrease in the flowability with w/b 0.3 without silica fume, but only slightly for those with silica fume but the effect for w/b 0.5 was the same either with or without microsilica. It did not give a consistent positive effect on compressive strength of mortar for both w/b ratios, however, it gave a slight increase in 28-day flexural strength.

2.4 Review on FEM Simulation of URM Walls

In the last two decades, numerical procedures in engineering have been developed tremendously and more attention has been given by researchers to develop numerical methods to simulate the real behavior of masonry structures [30]. However, a number of factors influence the structural behavior of masonry walls, such as geometry, anisotropy of the units, bond properties, material properties of units and mortar, and workmanship, which make the numerical simulation of masonry extremely difficult [8]. Nevertheless, masonry researchers have attempted to model masonry behavior through numerical trials and they were successful to get the real behavior of masonry to acceptable levels.

In accordance with the research conducted by Bolhassani et al. [31], the masonry modeling technique is either micro or macro. The macro modeling endeavors to define the masonry

based on the homogeneous material and it can provide an approximate response only equivalent to a single material, which is an assemblage of units and mortar with average properties. Micro model represents the actual pattern of masonry and considers the masonry units, mortar and interface separately and each is characterized by distinct properties. The micro modeling studies are required to get a better understanding of the local behavior of masonry structures. The necessary parameters for modeling have to be extracted from small-scale laboratory tests. On the other hand, macro modeling is relevant for the global analysis of masonry structures, where the structure is composed of walls with sufficiently large dimension. Bolhassani et al. [31] also modeled masonry walls subjected to uniaxial and diagonal compression load in ABAQUS environment. Hollow and partially grouted masonry were modeled using detailed micro-modeling. Mortar joints and units were smeared into one homogeneous material, and they were modeled using Concrete Damage Plasticity (CDP) model available in ABAQUS library [32]. The joint was modeled as interface cohesive element with traction–separation behavior. Based on the concluded results, the more accurate response of masonry can be represented by the detailed micro modeling which showed good agreement to the experimental tests in the difference of behavior and strength of partially and fully grouted masonry.

To simulate the nonlinear response of the masonry components individually, the CDP model available in ABAQUS need to be used [8]. CDP model has been developed to predict the behavior of concrete and other quasi-brittle materials such as rock and mortar under cyclic loading. Cracks in tension or crushing in compression are the main failure modes of this model. The model is based on primary models started by Lubliner et al. [33] and developed by Lee and Fenves [34]. The masonry components can be modeled discretely

where the tension and compression damage from micro to macro cracking can be employed individually. CDP model assumes that the uniaxial compressive and tensile response of concrete is characterized by damaged plasticity. Concrete damage plasticity is oriented for analysis of concrete elements and the brittle behavior of masonry, together with the cracks development, can be simulated with good accuracy [35].

Vindhyashree et al. [36] simulated prisms in ANSYS and ABAQUS environment. These prisms were tested experimentally in their laboratory and others from literature tests results. In ABAQUS modeling, the stress-strain characteristics of block and mortar were input to the software and C3D8R elements were used to model the masonry components. The model was meshed using an 8-noded element having three degrees of freedom (DOF) at each node. The research concluded that there is a good agreement between FEM and experimental tests in terms of compressive strength values and crack patterns.

CHAPTER 3

PROPERTIES OF MASONRY COMPONENTS

3.1 Introduction

In this study, several experimental tests on masonry components have been carried out starting by mix trials of steel fiber reinforced mortar admixed with microsilica (SFRM) in order to select the appropriate mix in terms of strength and workability. In order to carry out the nonlinear simulation, some mechanical properties of masonry components were tested such as uniaxial compression and tensile strength. The mechanical properties of masonry components play a role in understanding the experimental behavior of URM hollow concrete block wall exposed to axial and lateral loading. In addition, the results of tested properties were used in the FEM simulation in order to calibrate it with the experimental results. This Chapter can be divided into the following sections:

- Mix design and preparation of SFRM.
- Mechanical properties tests of masonry components.

Flow chart of the experimental and numerical programs is shown in Figure 3-1

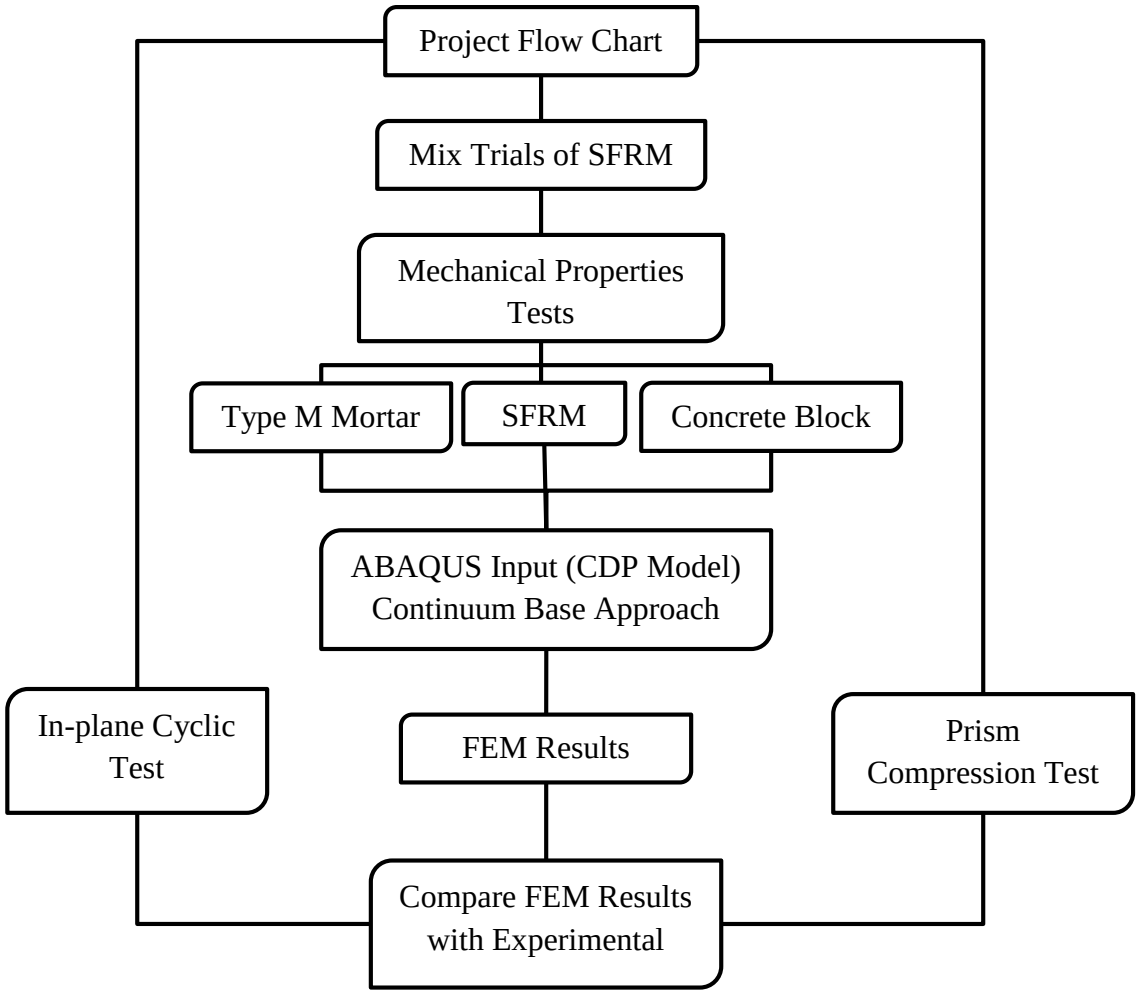

Figure 3-1: Project Flow Chart

3.2 Mix Design and Preparation of SFRM

This task contains the detailed processes of mixing, testing and selecting the SFRM to be used as plaster. Based on literature review, some researchers reported that the optimum amount of micro silica is 10% of cement weight and 15% by others. Therefore, three mixes were prepared in this research with 10%, 15% and 20% microsilica while fixing the amount of all others ingredients. For the amount of steel fiber, 2% by mix weight (0.6% by volume) was used which is the minimum amount that can be used to develop the properties of the concrete as reported by ACI 544.3R-08 and suggested by some researchers [28, 29]. Table

3-1 shows the specifications of steel fiber used in the mixes and Table 3-2 shows the ingredients distribution for each mix.

Table 3-1: Specifications of Steel Fibers

Steel Fiber	Business Name	Length (mm)	Diameter (mm)	Tensile Strength (MPa)
Micro Steel Fiber	WSF0213	13± 1	0.2± 0.05	> 2500
Brass Coated Hooked Ends Steel Fiber	GSD03525	25± 1	0.25± 0.05	> 2500

Table 3-2: Mix Proportion of SFRM for 1 m^3

Mix	SFRM100	SFRM102	SFRM150	SFRM152	SFRM200	SFRM202
w/b (by mass)	0.35	0.35	0.35	0.35	0.35	0.35
Cement (kg)	500	500	500	500	500	500
Microsilica (kg)	50	50	75	75	100	100
Water (kg)	192.50	192.50	201.25	201.25	210.00	210.00
SP = 3% (kg)	16.50	16.50	17.25	17.25	18.00	18.00
Fiber = 2% by mass (kg)	0	50	0	50	0	50
Sand (kg)	1547	1531	1495	1479	1443	1427
Density kg/m^3	2306	2334	2289	2322	2271	2305

Mixing of SFRM was implemented using special equipment and procedure to develop consistency in batching, casting and curing. The casting of SFRM was carried out in Civil and Environmental Engineering Department's laboratory, using horizontal pan mixer.

The measured quantities of cement, fine sand, microsilica were mixed at low speed for about 3 minutes. Water and superplasticizer were mixed separately for 30 minutes before the starting of the dry mix. Then, the mixed liquid of water and superplasticizer was added slowly to the dry mix in a course of 4 to 6 minutes. After putting all the liquid, the mix was transformed into a flowable paste. Finally, steel fibers were added to the mix at a very slow rate to ensure uniform dispersion of steel fiber in the mix. The total mixing time of SFRM is approximately 15 to 20 minutes. In accordance with ASTM C 109 & C 307, compressive strength cubes and briquettes test samples were prepared for each mix and put into oven heat curing at 90ºC for 48 hours. Also, the flow table test (ASTM C 1437) was conducted in order to obtain the required workability (Figure 3-2 to Figure 3-5). Figure 3-2 shows the flow table tests and Figure 3-3 shows the cubes and briquettes prepared for compression and tensile strength. Figure 3-4 and Figure 3-5 compare the damage of cubes and briquettes after testing with and without steel fibers. It is clearly shown that the samples with steel fibers kept sticky together after the failure due to the effect of steel fibers in improving the behavior of the mortar.

Figure 3-2: Flow Table Test

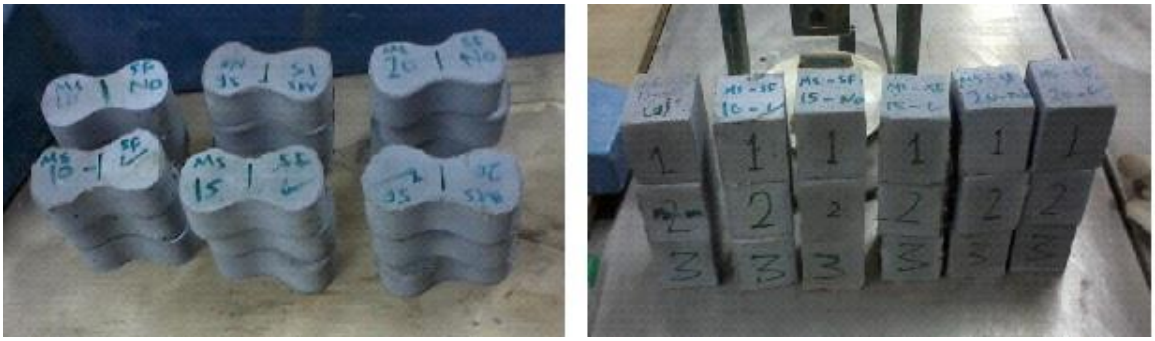

Figure 3-3: Cubes and Briquettes Prepared for Testing

Figure 3-4: Failure of Cubic Compressive Strength

Figure 3-5: Briquettes Tensile Strength Damage

Table 3-3 shows the results of tested cubes and briquettes as well as flow table test of each mix trial. Where SFRM is referring to steel fiber reinforced mortar admixed with microsilica and followed by three numbers; the first two numbers for the percentage dosage of microsilica and the third number represents the percentage of steel fibers by mix weight

Table 3-3: Properties of SFRM with and without Fibers

Sample	Compressive Strength (MPa)	Mortar briquette (MPa)	Flow (mm)
SFRM100	56	5.1	210
SFRM102	58	5.1	200
SFRM150	70	6.5	230
SFRM152	70	6.6	220
SFRM200	75	7.1	250
SFRM202	76	7.3	240

The mix containing 15% microsilica content was selected to be the plaster material used in retrofitting the wall due to the required compressive, tensile strength and workability. Regarding the economical point of view, a thin layer of mortar with high strength is required to enhance the performance of URM wall resulting in lower amounts of plaster materials affecting the cost of plaster.

3.3 Mechanical Properties Tests of Masonry Components

In order to understand the behavior of URM walls experimentally as well as numerically, some mechanical properties need to be tested individually for masonry components. These tests are:

- Uniaxial Compression Stress Test.
- Tensile Stress Test.
- Triplet Test.

The tests procedures and details are described below.

3.3.1 Uniaxial Compression Stress Test

This test was conducted for type M mortar (mortar according to ASTM C 270 was used as head-bed joints when constructing the walls), SFRM and concrete blocks individually.

The detailed procedures are described below:

- **Type M Mortar and SFRM**

In order to find the compressive behavior of type M mortar and SFRM, cylindrical specimens of 150 mm length x 75 mm diameter were prepared and tested according to ASTM C 39. The average of three samples was taken and one cylindrical specimen was subjected to a cyclic uniaxial compression load. The cyclic loading test results are important to capture the stress-inelastic strain curve which used in ABAQUS input. Also, cubes of 50 mm were used to measure the compressive strength of both mortar types according to ASTM C 109 to ensure the uniformity of the mix for each patch. Figure 3-6 shows the experimental setup and instrumentations details of uniaxial compression test.

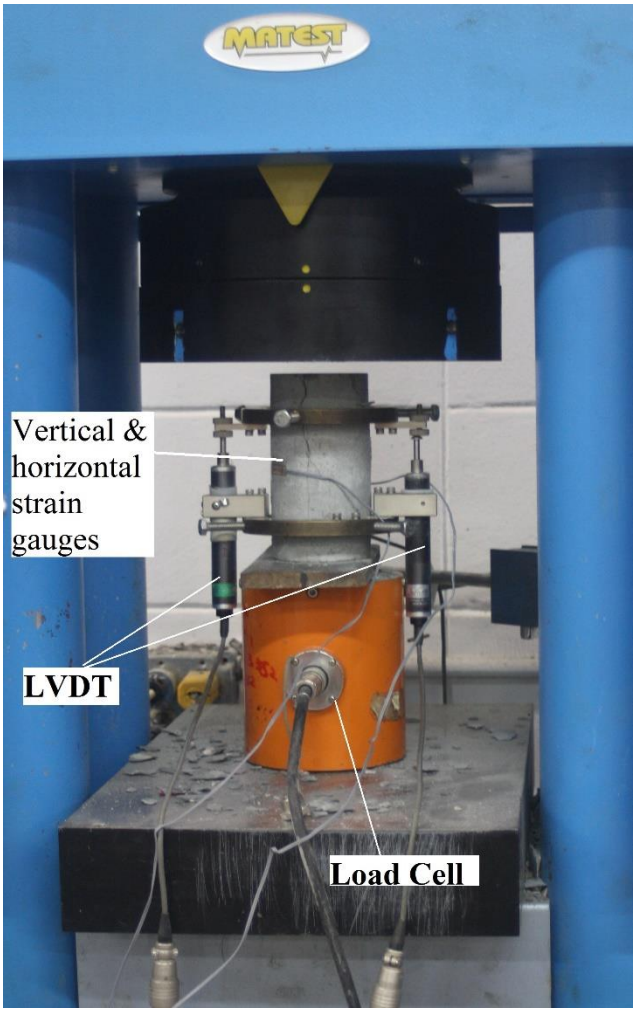

Figure 3-6: Uniaxial Compression Test Details

Type M mortar was prepared according to ASTM C 270 (1 cement: 3 sand; 0.6 w/c ratio) and specimens were cured for 28 days. Two LVDTs, one PLC-60-11 cross type strain gauge and load cell were connected to the cylinders of type M mortar and SFRM, as shown in Figure 3-6 to efficiently capture the behavior of the cylinders under test and to find Young's modulus and Poisson's ratio. The specimen was placed and subjected to axial loading in a progressive manner under displacement control with slow loading rate and readings were taken for each 0.005 mm. The load cell, strain gauges and LVDTs data were picked up using TOKYO SOKKI data logger. Then, the envelope of cyclic stress-strain

curve was plotted and the Young modulus was calculated from the plot. The Poisson's ratio was calculated based on the reading of cross-strain gauge. Table 3-4 shows the mechanical properties of both SFRM and type M mortar. Stress-strain curves were plotted as shown in Figure 3-7 and Figure 3-8 for both type M mortar and SFRM, respectively.

Table 3-4: Mechanical properties of the selected mortar.

Mechanical Property	Type M Mortar	SFRM Mortar
Cylindrical Compressive Strength [MPa]	24	60
Cubic Compressive Strength [MPa]	30	72
Elastic Modulus [GPa]	20	28
Poisson's Ratio	0.20	0.25

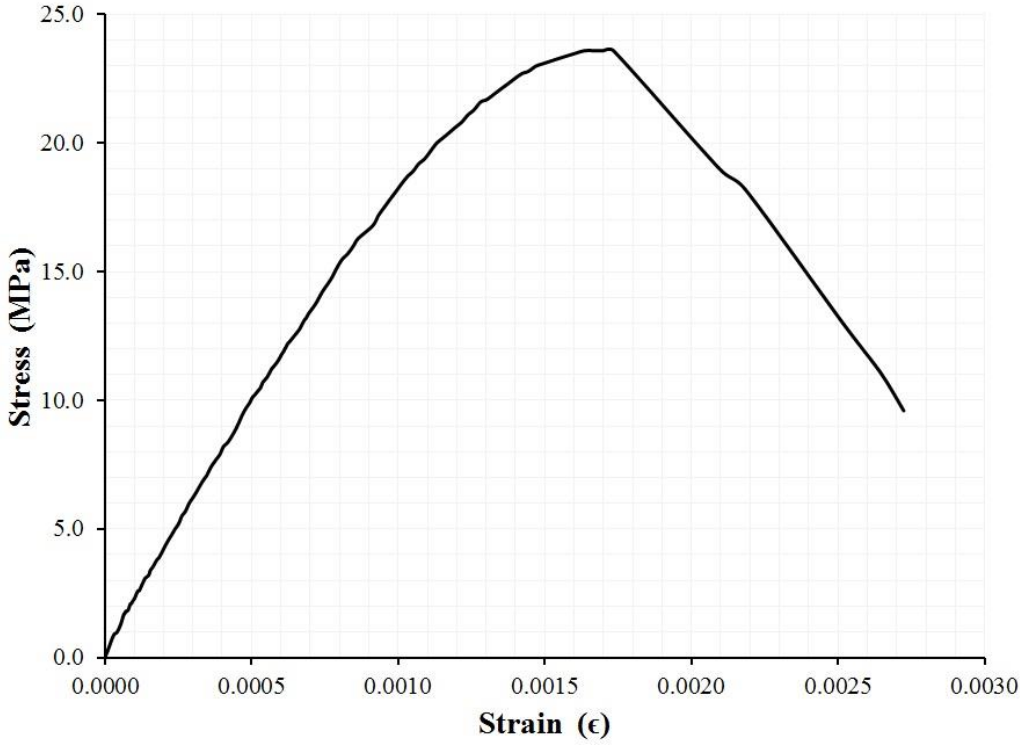

Figure 3-7: Stress-Strain Curve of Type M Mortar in Compression (Envelope)

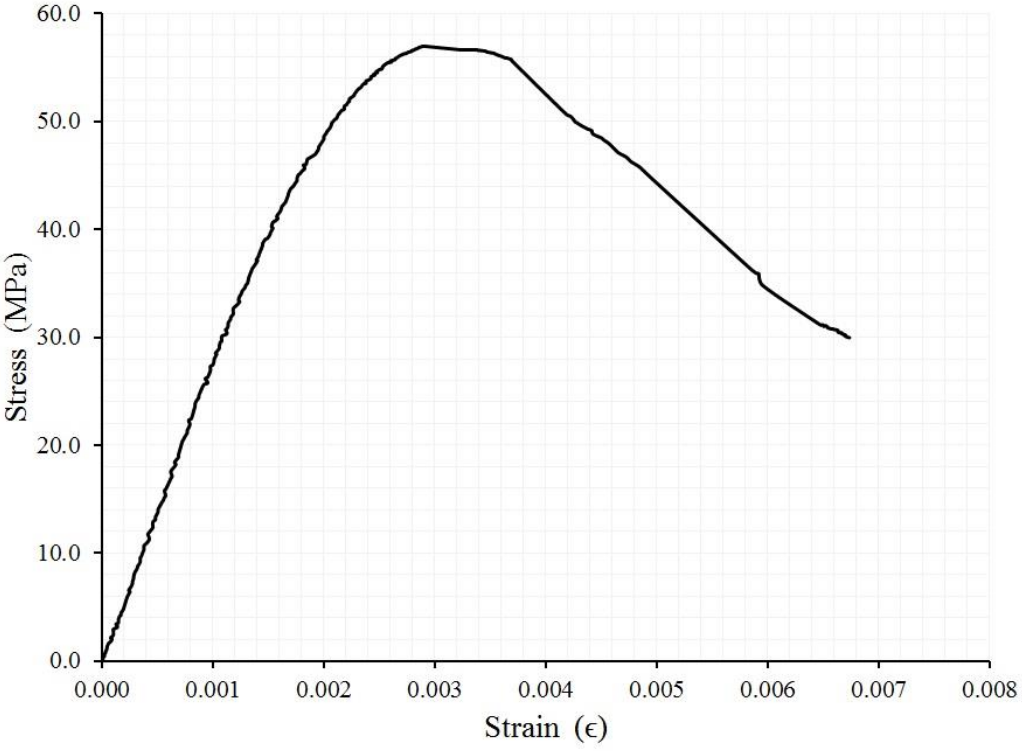

Figure 3-8: Stress-Strain Curve of SFRM in Compression (Envelope)

- **Hollow Concrete Block**

In order to ensure that the load was distributed uniformly, each block unit of (400 mm x 200 mm x 100 mm); (length, height, width) was capped by a high strength mortar (EMACO S88 CT provided by BASF) layer of 5 mm thickness. The compressive strength of the masonry concrete block can be determined by testing full-size block according to ASTM C140-11a [37]. PLC-60-11 cross type strain gauges were connected to the block unit on both sides using epoxy to level the surface and LVDTs to capture the axial displacement and load cell were fixed on the moving plate of the testing machine. Three units were tested under monatomic compression tests in order to find the ultimate compressive strength which found to be an average of 14 MPa. The failure was a middle vertical crack in the web of the hollow concrete block followed by crushing of the block from the top, as shown in Figure 3-9.

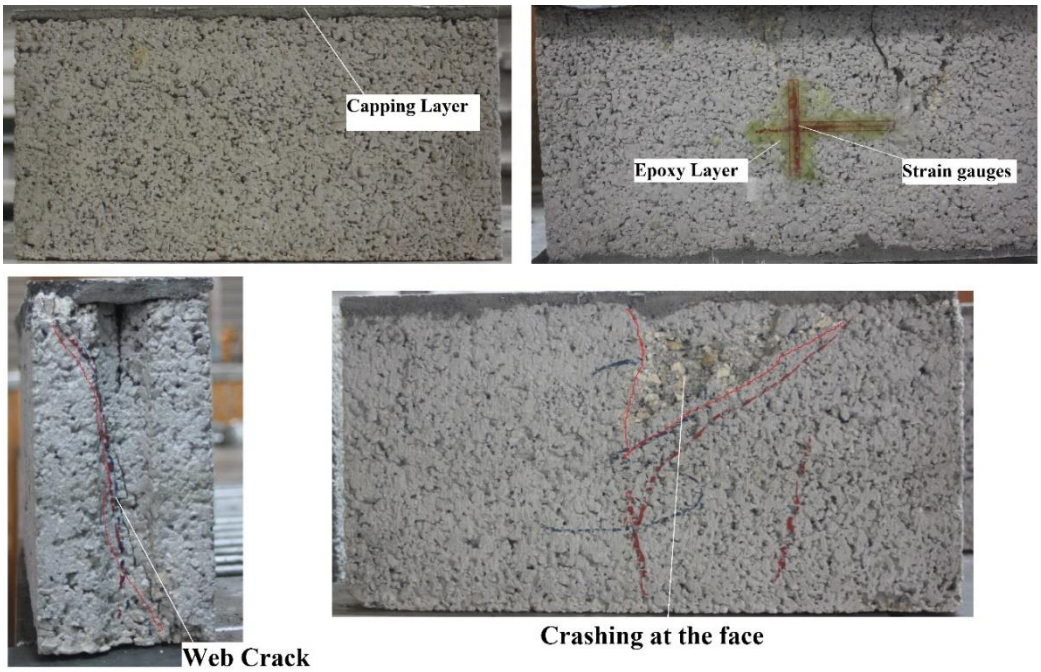

Figure 3-9: Concrete Hollow Block Test Preparation and Failure Mode

A hollow concrete block was tested under cyclic compression load using the same rate that was used in testing the mortar cylinders. The envelope of the stress-strain curve was plotted in Figure 3-10 and then Young's modulus and Poisson ratio were calculated to be 16.5 GPa and 0.18, respectively.

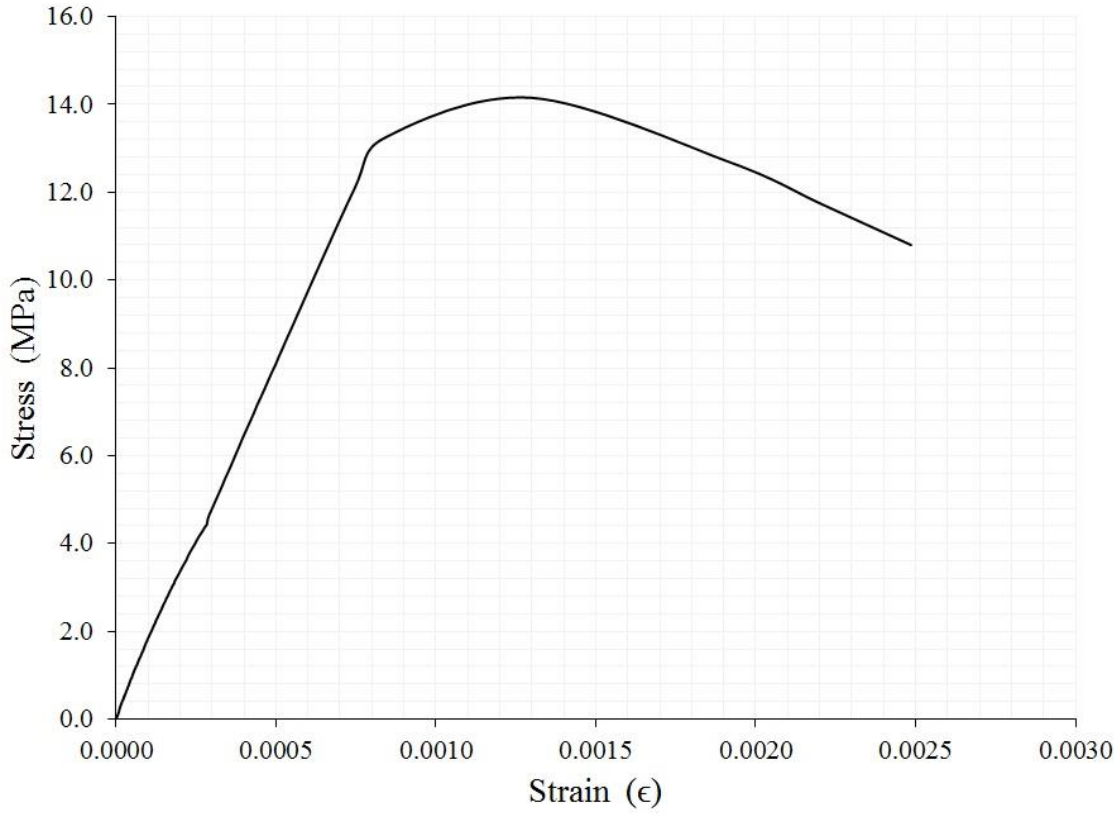

Figure 3-10: Stress-Strain Curve of Hollow Concrete Block in Compression (Envelope)

3.3.2 Tensile Stress Test

In order to understand the behavior of URM wall exposed to tensile stress, it is important to know the tensile strength of individual masonry components. The tensile strength of concrete hollow block and type M mortar was determined in this research by flexural test while the SFRM tensile strength was determined by dog bone test.

- **Dog Bone Test of SFRM**

Dog bone test is a convenient method to determine and capture the behavior of the SFRM. Therefore, the specimen was prepared to be subjected to direct tensile stress according to ASTM D 638-02a. Specimen was first cast with SFRM and cured in a water tank for 28 days. Then, the specimen was retrofitted with CFRP in order to prevent the failure at the neck of the dog-bone, as shown in Figure 3-11. First, one sample was tested under monatomic direct tension to determine the tensile capacity. Thereafter, a progressive cyclic loading was applied on another specimen to catch elastic, strain hardening and softening zone. Two strain gauges were connected against to each other. The experimental setup is shown in Figure 3-12. Then the envelope of cyclic stress-strain curve was plotted, as shown in Figure 3-13.

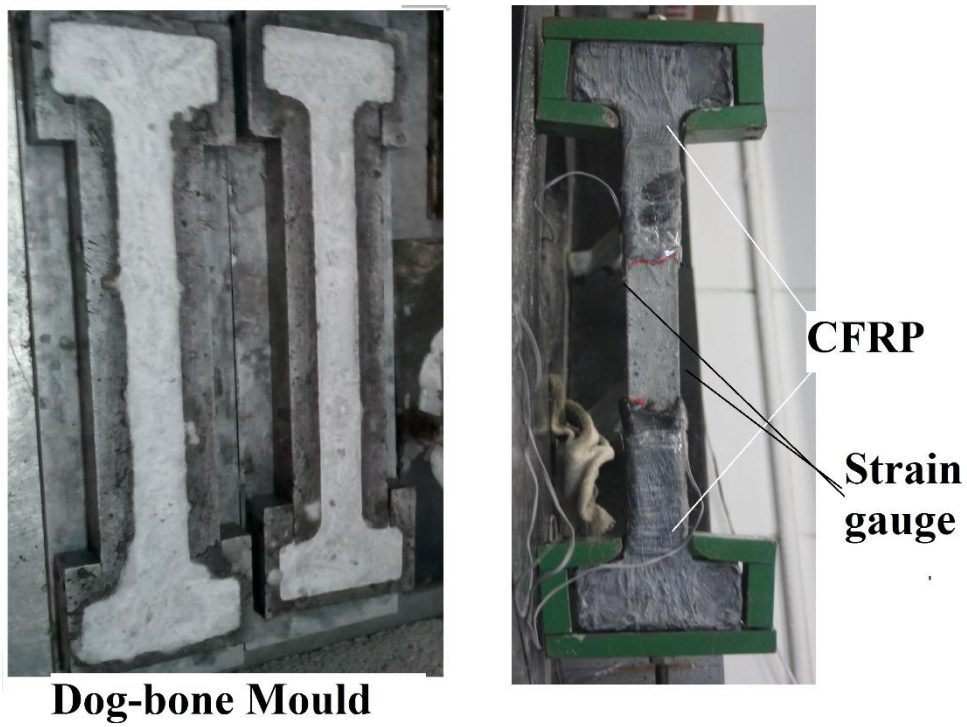

Figure 3-11: Dog-bone Specimens

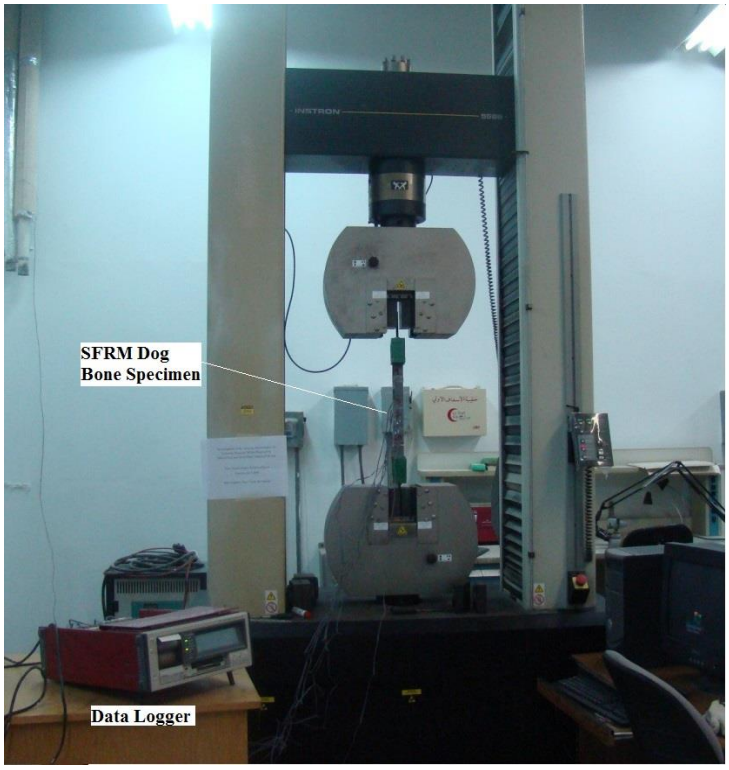

Figure 3-12: Experimental Setup of SFRM Dog Bone Test

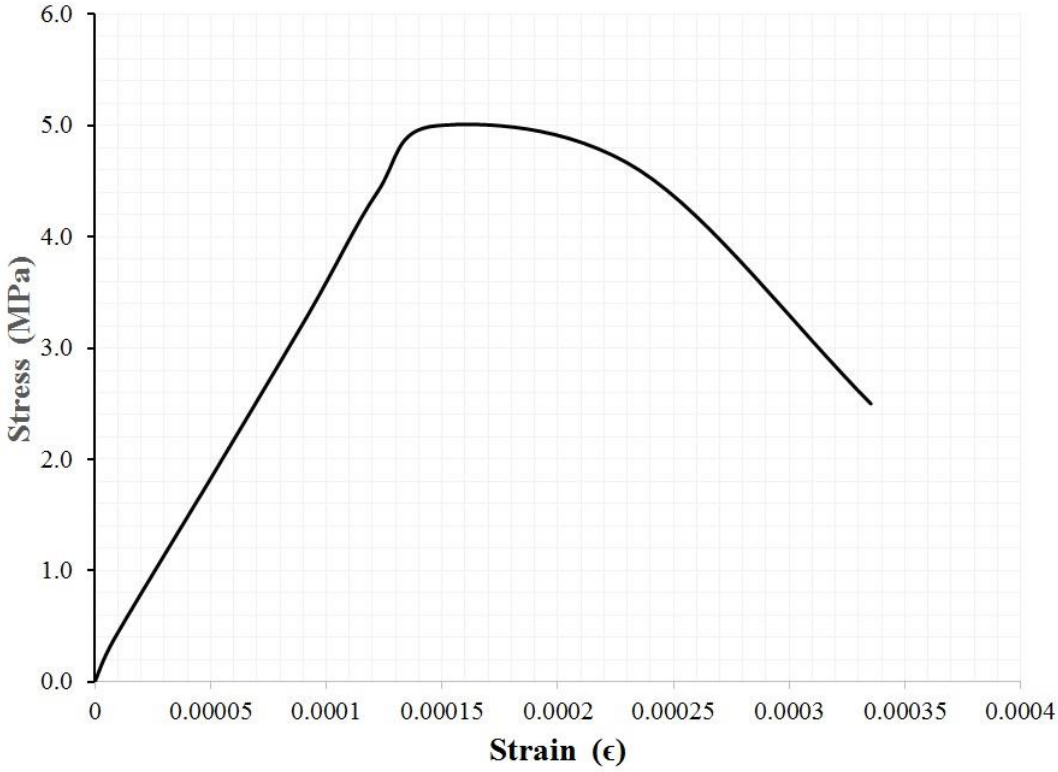

Figure 3-13: Stress-Strain Curve of SFRM in Tension

- **Flexural Test of Type M Mortar**

A beam with dimensions of 750 mm × 75 mm × 150 mm was subjected to a four-point flexural load. The beam was cast and cured in a water tank for 28 days. After curing, a 2.5 cm notch was created in the middle of the beam along the width (75mm side) for localizing the failure. Four strain gages were placed, two in each side, in the maximum moment region. Two metal bars were placed in a L/3 distance of the span. The load was applied in a cyclic manner to catch the elastic portion, strain hardening portion and softening portion. The test setup is shown in Figure 3-14. The stress-strain curve is shown in Figure 3-15.

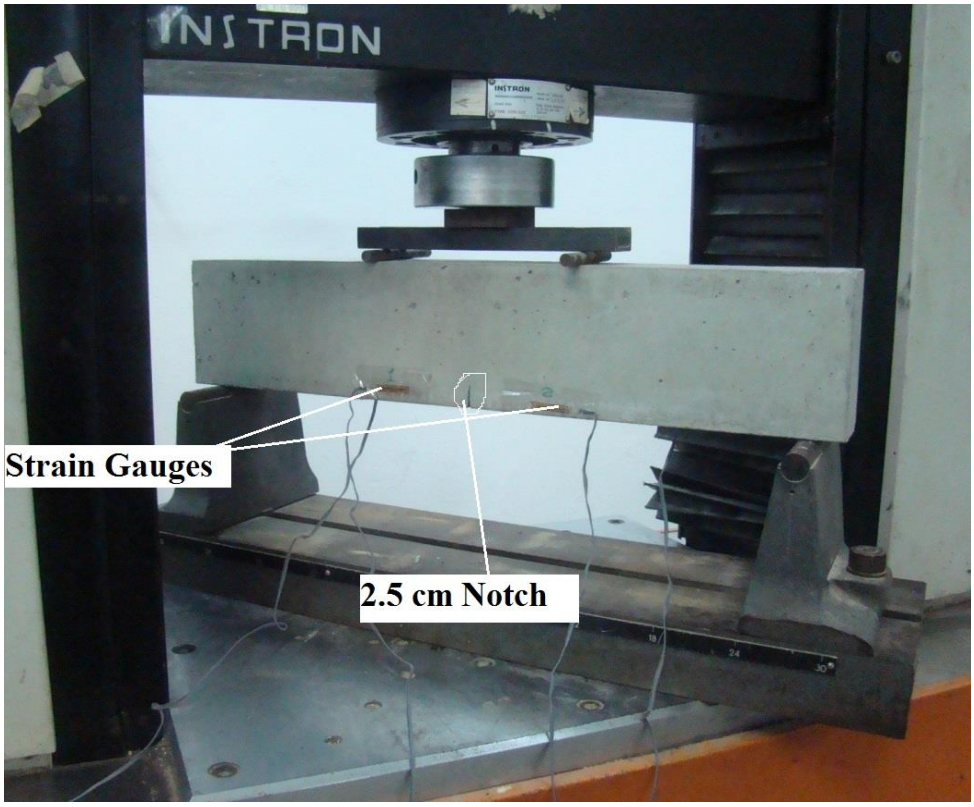

Figure 3-14: Type M Mortar Flexural Test Setup

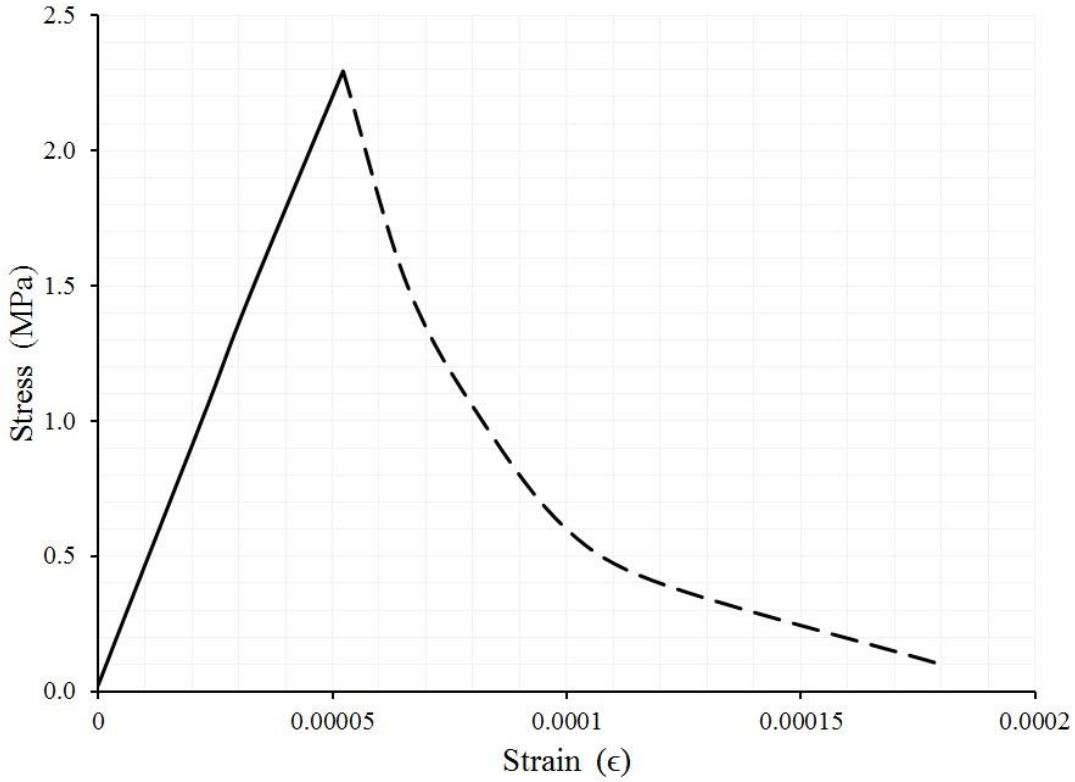

Figure 3-15: Stress-Strain Curve of Type M Mortar in Tension

- **Flexural Test of Hollow Concrete Block**

Similar to type M mortar beam, one-unit block (400 mm x 100 mm x 200 mm) was subjected to a four-point flexural load. The maximum moment region in this test was 20 cm long where two plates (100 mm x 20 mm x 10 mm) is placed under the load on the top of the block at 8 cm from the support's edges. The supports were placed at 3 cm from the edge of the block and the width of the plates under the load was 20 mm in order to prevent the local failure. Therefore, failure was expected to be at the maximum moment region. First, an average tensile strength of three masonry block was found to be 1.8 MPa. Then, cyclic loading was applied on one concrete block with strain gauges placed at the maximum moment regions. The experimental setup with failure mode are shown in Figure 3-16 and the stress-strain curve is plotted in Figure 3-17.

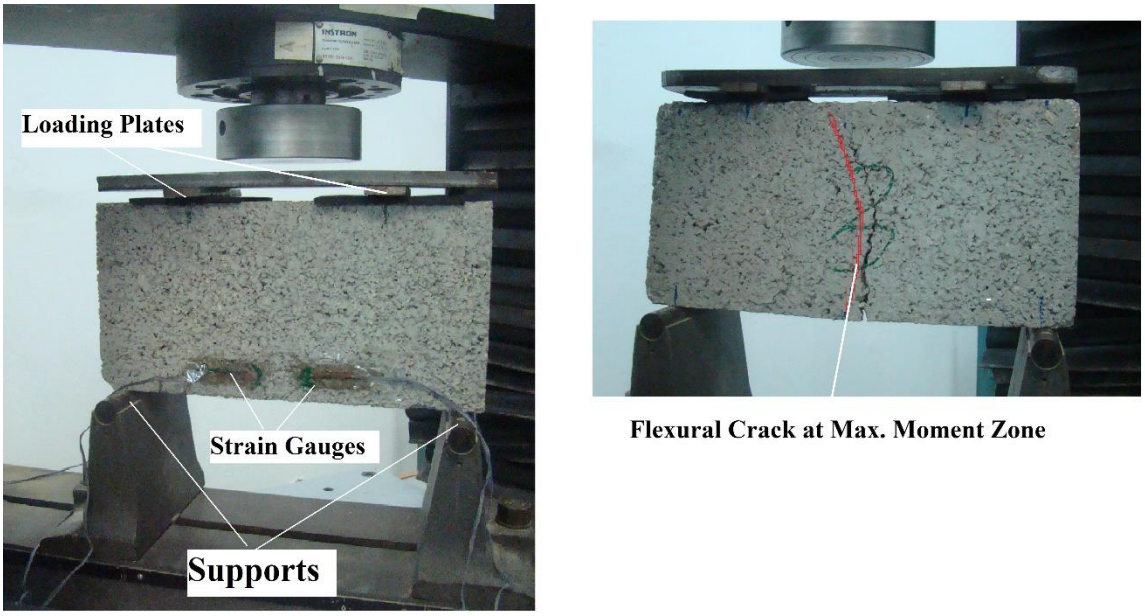

Figure 3-16: Flexural Test Setup and Failure of Concrete Block

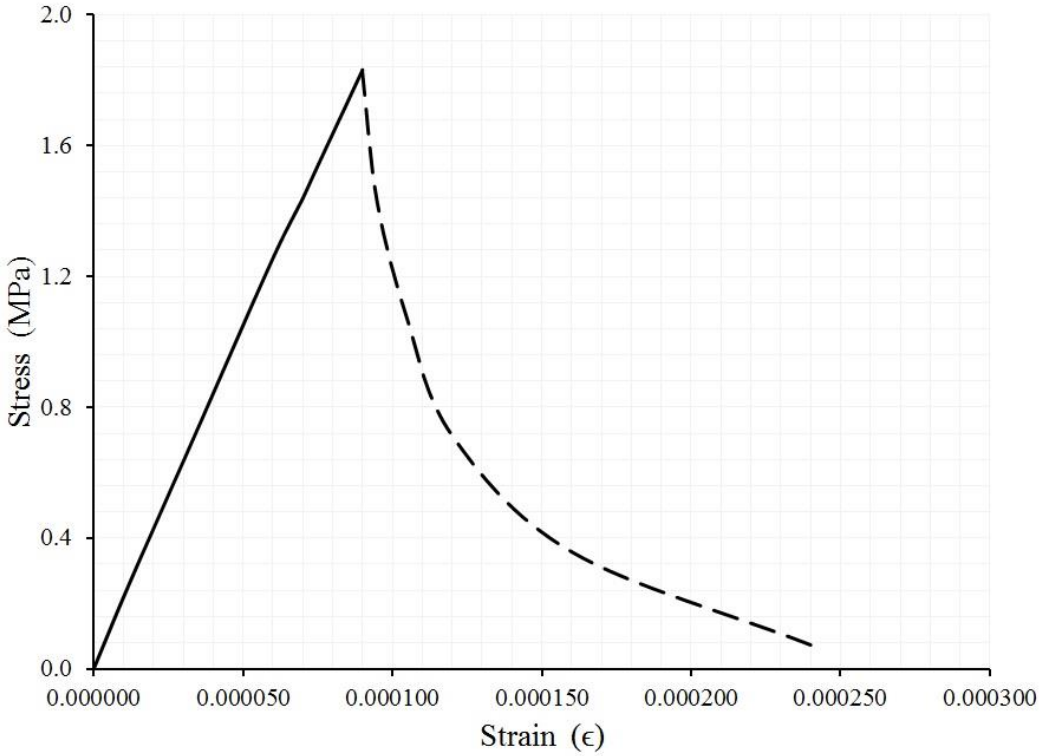

Figure 3-17: Stress-Strain Curve of Concrete Hollow Block in Tension

3.3.3 Triplet Test

A triplet test was adopted in this work according to European Standard (EN 1052-3:2002) in order to understand the interface behavior between the concrete masonry blocks and SFRM plaster. A triplet specimen consisting of three half concrete blocks (200 mm x 200 mm x 100 mm) were gathered using SFRM mortar with 10 mm thickness. After that, the triplet was cured for 28 days and then subjected to direct shear load, as shown in Figure 3-18. The hollow concrete block is weak at the holes resulting in cracks at the middle block before any occurrence of de-bonding between the block and joint mortar. Nevertheless, the captured data up to the block's crack was captured and plotted in Figure 3-19. The shear stiffness (K_{ss}) was calculated to be 24 N/mm^3 from the plotted data. The K_{ss} value can be helpful in the calibration of surface-to-surface cohesive element parameters in the FEM simulation [38].

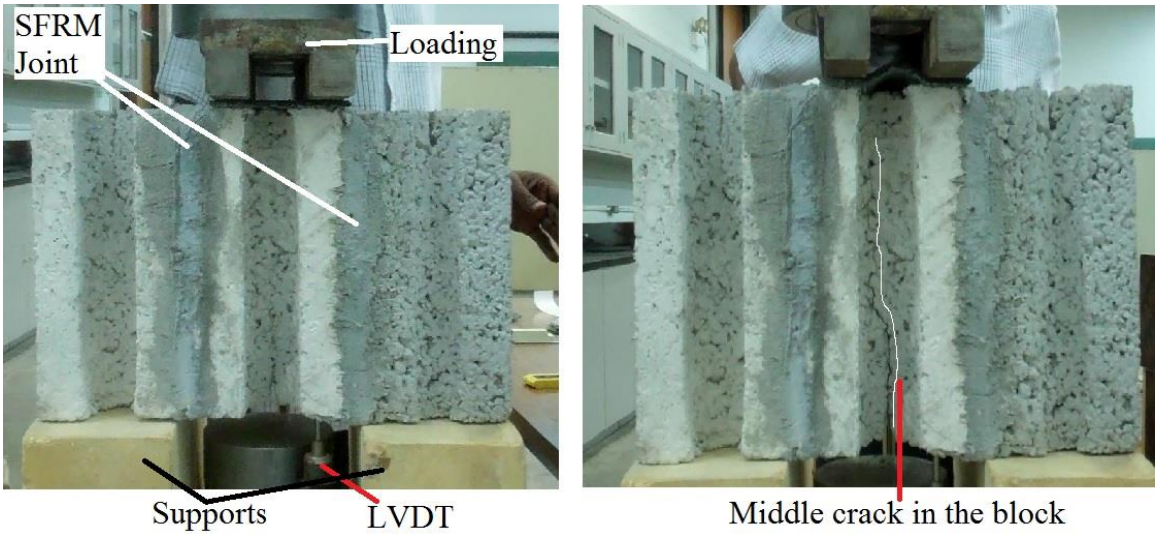

Figure 3-18: Triplet Test Setup

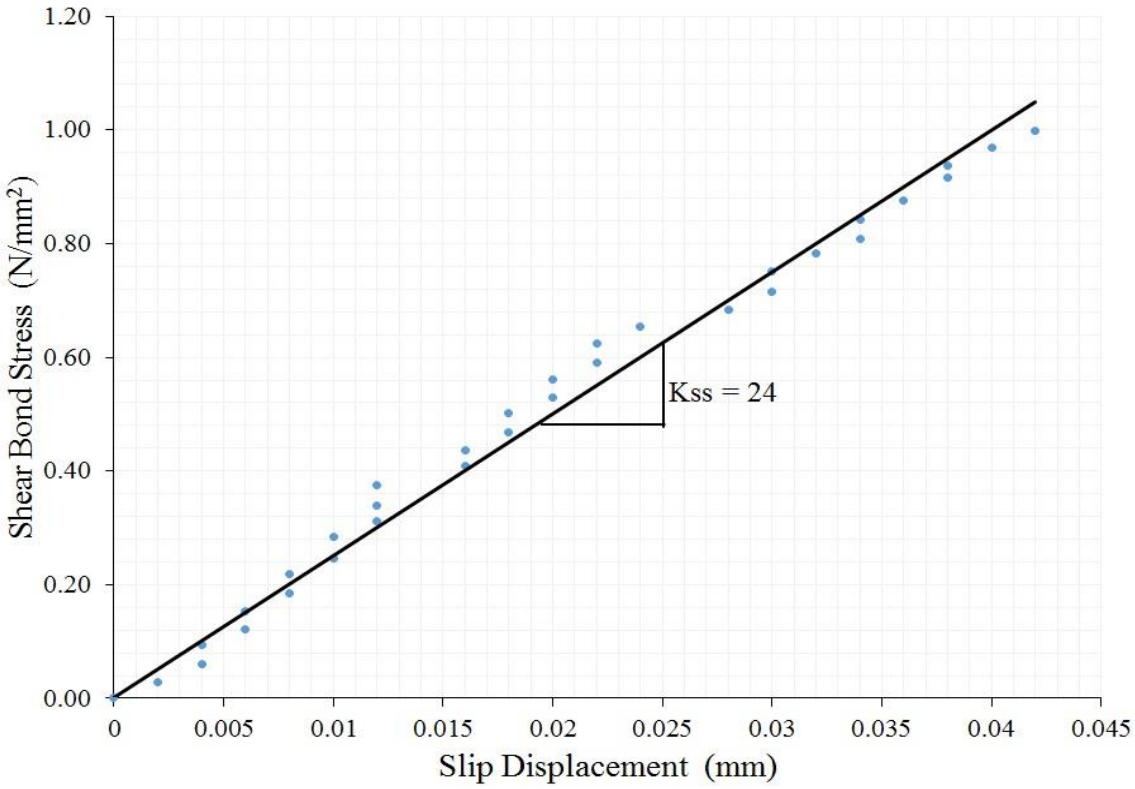

Figure 3-19: Shear Bond Stress vs. Slip Displacement Curve

CHAPTER 4

EXPERIMENTAL TESTS OF PRISMS AND WALLS

4.1 Introduction

Several researchers studied the behavior of URM walls when subjected to both axial and lateral cyclic loading as mentioned previously. The purpose of all experimental programs is to achieve a better understanding of the behavior of walls under such loading and then develop sufficient resistance of masonry structures against any hazard that may cause catastrophic damage. Prisms compression tests were conducted in order to identify the required axial load to be applied when the full URM wall subjected to in-plane cyclic loading. Four concrete masonry walls with eight prisms were tested, with their description as given in Table 4-1.

Table 4-1: Specimens Description.

Specimen Name	Type of Blocks	Type of Joint Mortar	Type of Plastering	No. of Wall Specimens	No. of Prism Specimens
NCMW[(1)]	Normal Concrete Blocks	Mortar Type M[(4)]	None	1	3
NCMWR[(2)]	Normal Concrete Blocks	Mortar Type M	SFRM	1 One side 1 Two sides	1 one side 10 mm 1 two sides 10 mm 1 two sides 20 mm 1 two sides 30 mm
NCMWJ[(3)]	Normal Concrete Blocks	SFRM	None	1	1

[(1)] Normal Concrete Masonry Wall.
[(2)] Normal Concrete Masonry Wall Retrofitted.
[(3)] Normal Concrete Masonry Wall with SFRM in Joint.
[(4)] Mortar According To ASTM C270 (1 Cement : 3 Sand; 0.5-0.6 W/C ratio)

4.2 Prism Compression Test

The importance of prism compression test is to determine the compressive capacity of full wall scale. The results of this test can be used to identify the required compression stress to be applied during the lateral in-plane cyclic test of a full wall. ASTM C 1314 reports that there should be at least two courses (layers of masonry units) and the European Standard EN1052-1 (1999) specifies that there should be at least one head-bed joint. Therefore, all prism specimens were constructed by two half hollow concrete blocks as the first layer joined by head joint and one full block joined to the first layer by bed joint. The prepared prisms can be classified as following:

- Normal Concrete Masonry Wall (NCMW), Control Prism.
- Normal Concrete Masonry Wall with SFRM as Head-bed Joints (NCMWJ Prism)
- Normal Concrete Masonry Wall Retrofitted with SFRM (NCMWR Prism)

4.2.1 Specimens Preparation

All prisms were prepared according to ASTM C 1314 and EN1052-1:1999 with an aspect ratio of 1:1 and dimension of 410 mm x 410 mm 100 mm (Length x Height x Thickness). First, seven prisms (NCMW) were prepared with type M mortar in head-bed joint and another one with SFRM in head-bed joint (NCMWJ). Then, three of the NCMW prisms were plastered using SFRM with thicknesses of 10 mm, 20 mm and 30 mm on both sides and one with 10 mm thickness on one side only. For balanced surface level, a top and bottom capping by high strength mortar (EMACO S88 CT) was put for all prisms. All specimens were cured for 28 days using burlap blankets. In order to attain a good quality control, the prisms were covered by plastic bags to keep the burlap blankets moist. Figure 4-1 shows the prepared specimens with curing processes.

Figure 4-1: Prisms Preparation Processes

4.2.2 Experimental Setup

All the specimens were tested inside steel frame which is closed from the top and bottom to act as supports. A vertical hydraulic jack inside the steel frame was used to exert axial pressure on the specimen. Two steel plates were put in the steel frame to transfer the vertical load from the hydraulic jack to the specimens; one plate under the specimen, the other above the specimen. Figure 4-2 shows the details of the experimental setup.

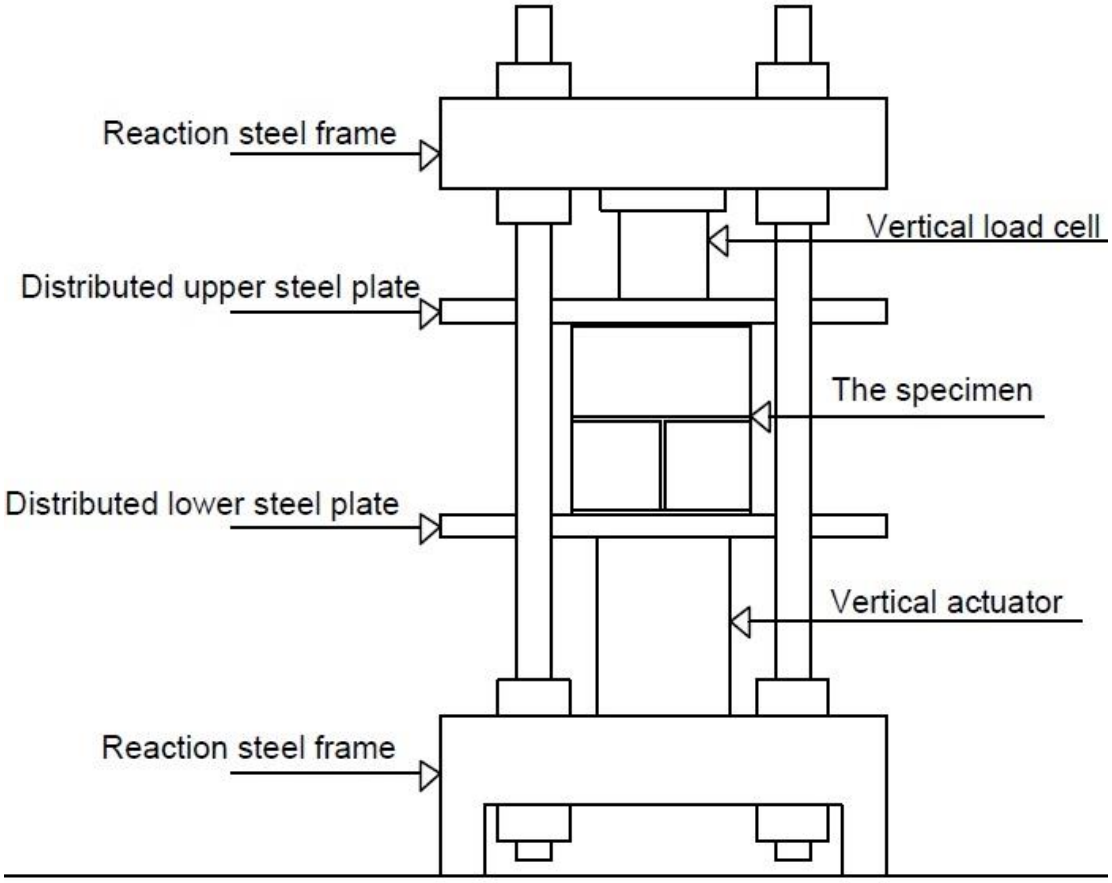

Figure 4-2: Experimental Setup Details

One load cell was attached to the hydraulic jack to measure the vertically applied load while three linear variables differential transducers (LVDTs) were utilized to measure displacements; one to measure horizontal displacement, the other two to measure vertical

displacement. In addition, four strain gauges were placed on top corners of the prism to check the eccentricity. All of the strain gauges, LVDTs and the load cell were connected to data logger device to collect and monitor the data. Instrumentation setup is shown in Figure 4-3 where V.L, H.L and S.G referred to vertical LVDT, horizontal LVDT and strain gauges, respectively.

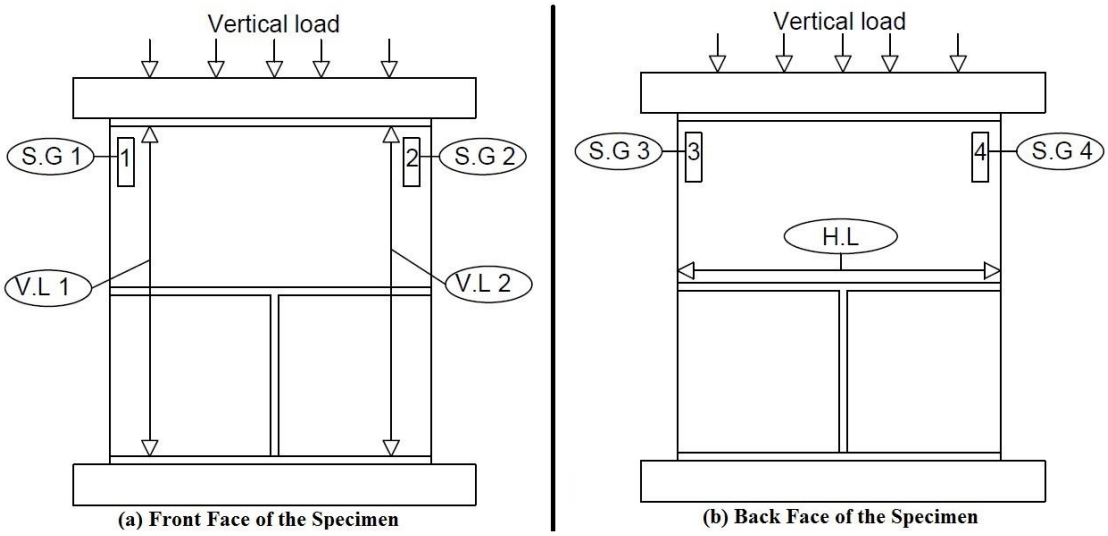

Figure 4-3: Instrumentation Setup Details of Prisms

To ensure that the axial loading is distributed uniformly, a laser leveler was used to place the prism in an accurate alignment vertically and horizontally. In addition, every specimen was tested in three cycles; the first cycle was up to 50 kN, the second cycle was up to 100 kN, the last one was up to failure. The purpose of the first and second cycles was to check the eccentricity of the specimen through the means of four strain gauges installed on the top corners of each prism. Figure 4-4 shows the alignment preparation of prism test.

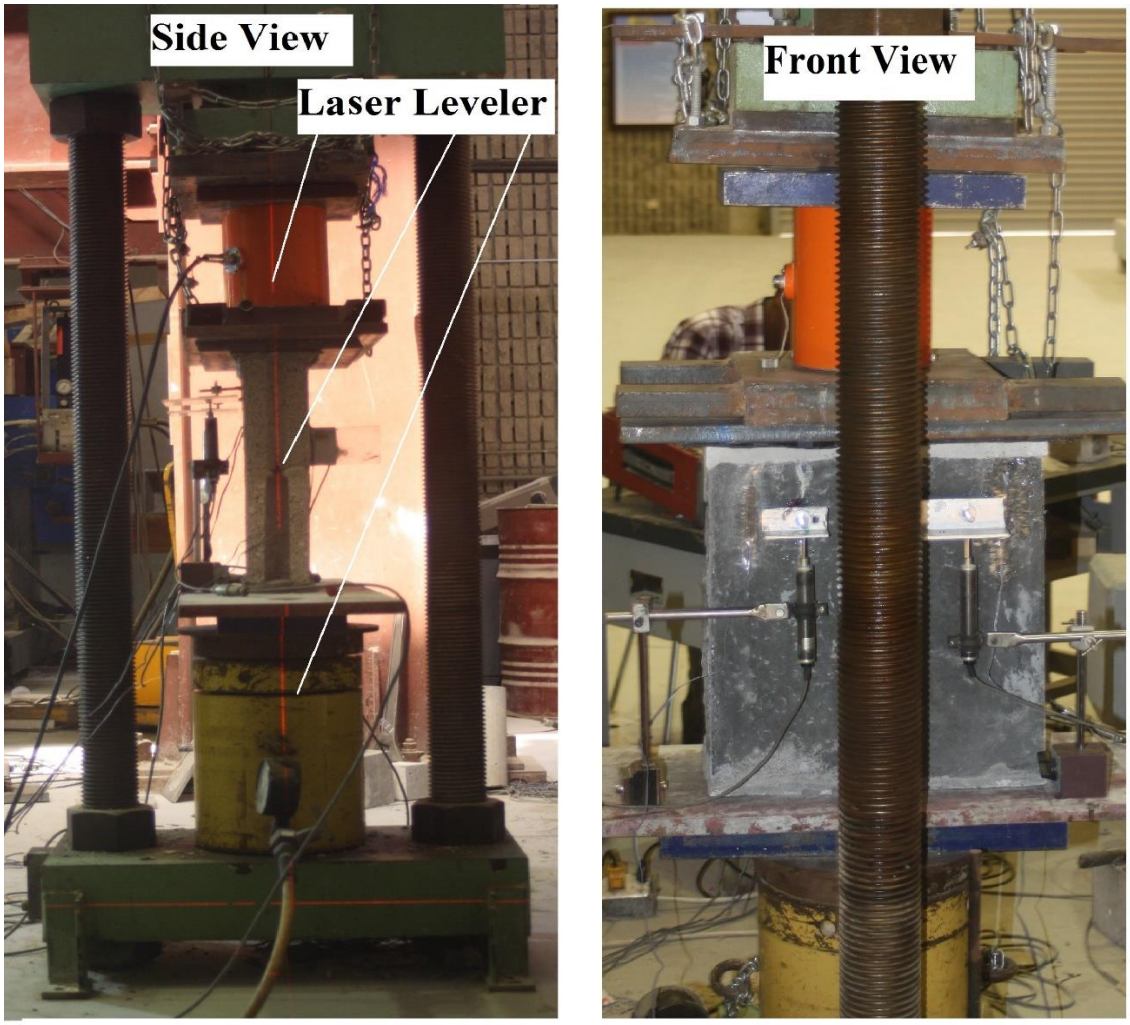

Figure 4-4: Prism Alignment

All the prepared prisms followed the explained setup during testing. The experimental results and failure modes are detailed in the following section.

4.2.3 Failure and Test Results

- **NCMW Prisms (Control)**

Three NCMW's were tested as control specimens in order to ensure that the experimental setup was performing well. A vertical crack in the web of the hollow concrete block occurred at a vertical load of 260 kN corresponding to a vertical displacement of 0.25 mm.

After this crack took place, the specimen developed a vertical crack at the middle face of the block for one specimen and crushing then fail immediately. The maximum axial load was recorded during the test for each specimen to be 260 kN, 295 kN and 295 kN. Hence, the average strength of the three specimens was calculated to be 9.7 MPa corresponding to an axial displacement of 0.3 mm. Figure 4-5 shows the axial load vs axial displacement curves of the three control specimens. The failure mode is shown in Figure 4-6.

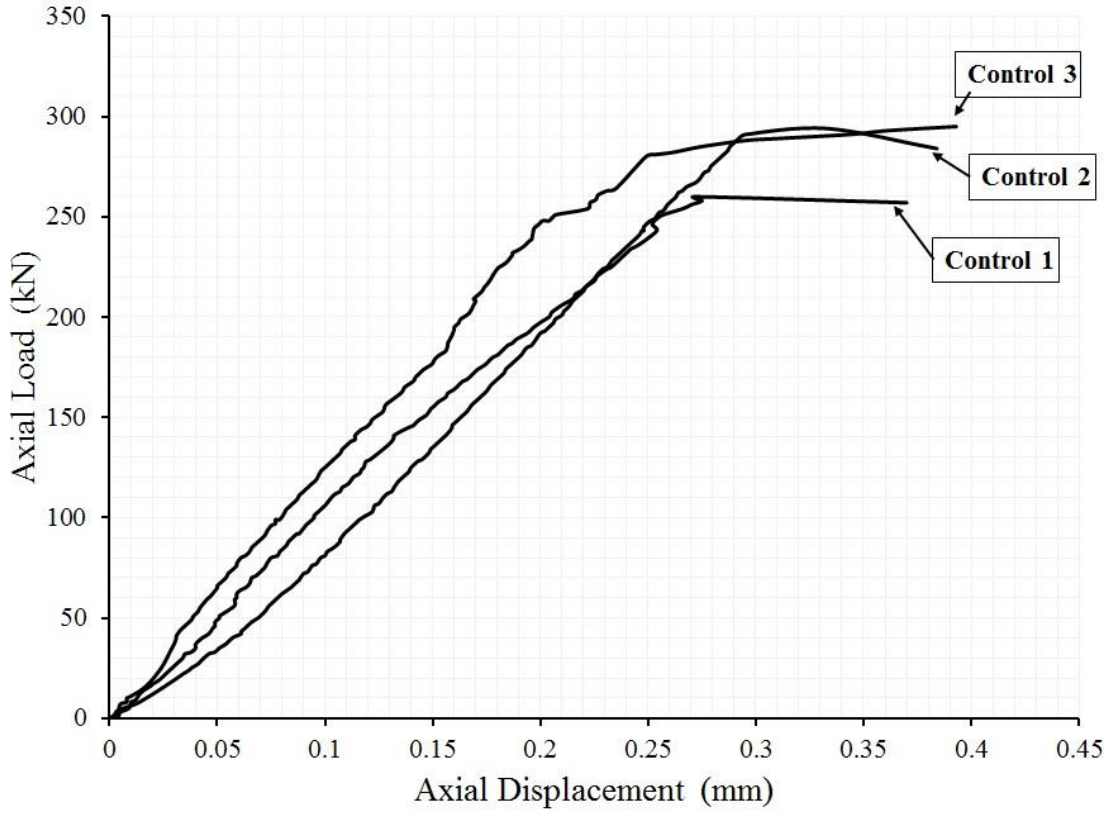

Figure 4-5: Axial Load vs. Axial Displacement Curve of NCMW Control Specimens

Figure 4-6: Failure Mode of NCMW Control Specimens

- **NCMWJ Prism (SFRM Joint)**

In this specimen, the only difference is the bed-head joint's mortar, where type M mortar was replaced by SFRM. The behavior of this prism is similar to the control one in crack patterns starting by splitting of block's web at 270 kN axial load corresponding to 0.25 mm axial displacement. Then, the web cracked was followed by a vertical middle crack at the face of the prism. Compared with the control specimen, the NCMWJ prism shows a good stability after the occurrence of cracks and crushing of the blocks where SFRM holds the parts together, as shown in Figure 4-7. The recorded maximum axial load was 295 kN (10.2 MPa) at 0.35 mm axial displacement. The axial load vs. axial displacement diagram of NCMWJ with NCMW is shown in Figure 4-8.

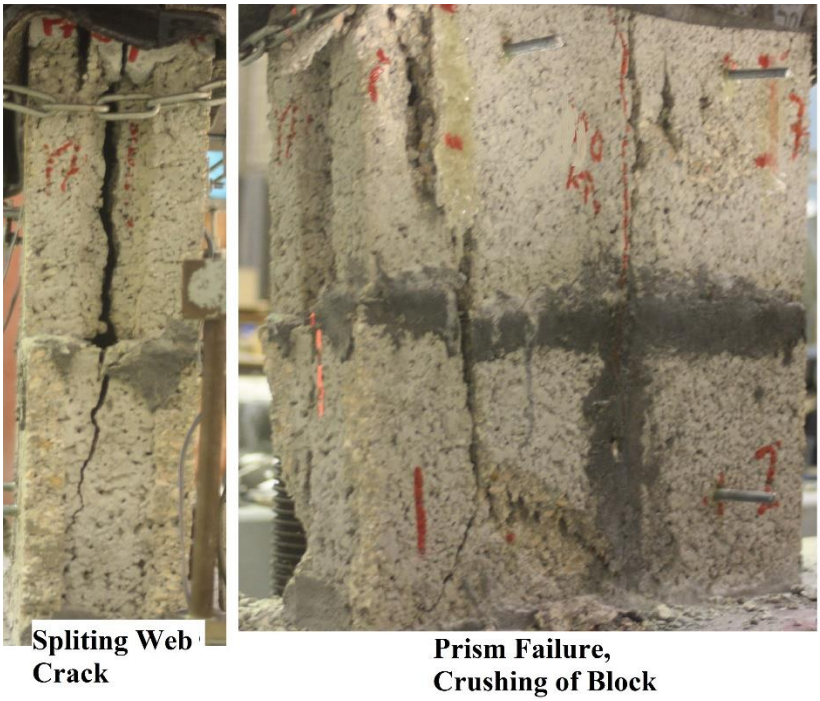

Figure 4-7: Failure Mode of NCMWJ Prism

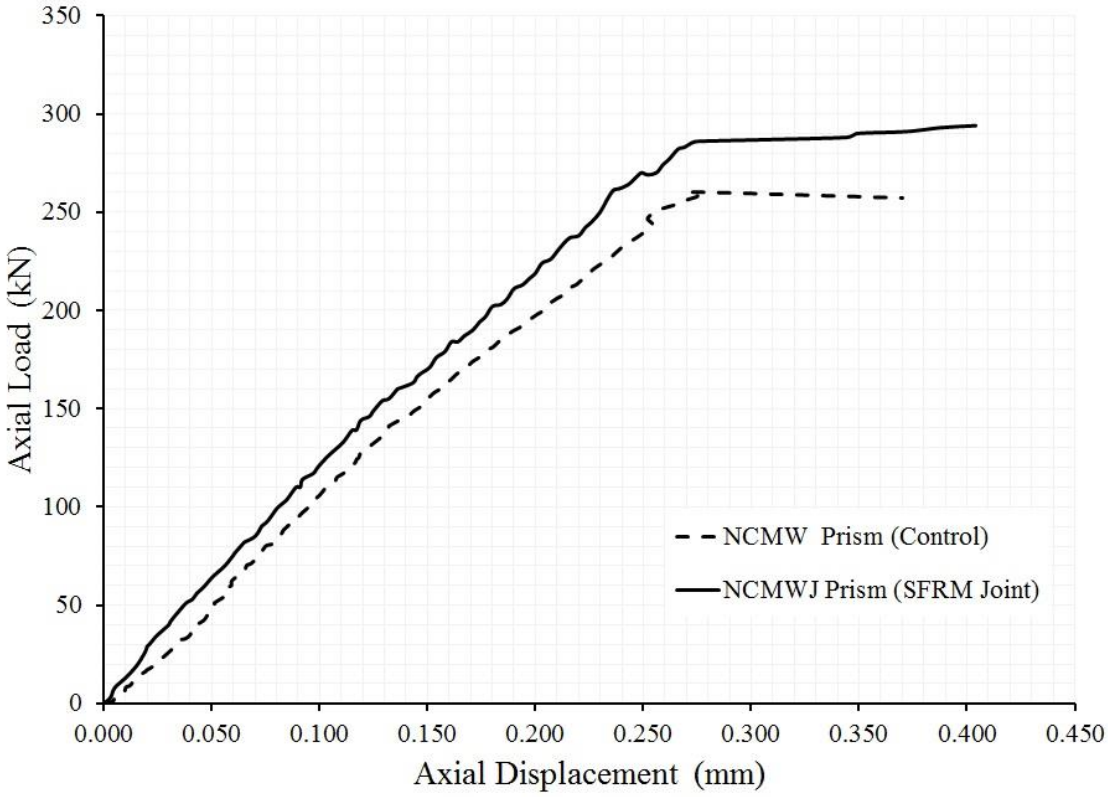

Figure 4-8: Axial Load vs. Axial Displacement Curve of NCMWJ

- **NCMWR Prism (Retrofitted with SFRM)**

This group consisted of four specimens; one is with one side plaster of 10 mm thickness, three with 10 mm, 20 mm and 30 mm thick plaster on both sides.

For one side retrofitted specimen, the first crack was a splitting of block's web by a vertical crack occurred at 308 kN axial load and 0.25 mm vertical displacement similar to the control specimens. However, it developed a small strength after the first crack took place where it reached a maximum axial load of 395 kN (12.0 MPa) with an axial displacement of 0.5 mm. The failure of this specimen was mainly controlled by the failure of the un-retrofitted side without of plane failure due to the stiffness difference between both sides. The failure mode of this specimen is shown in Figure 4-9.

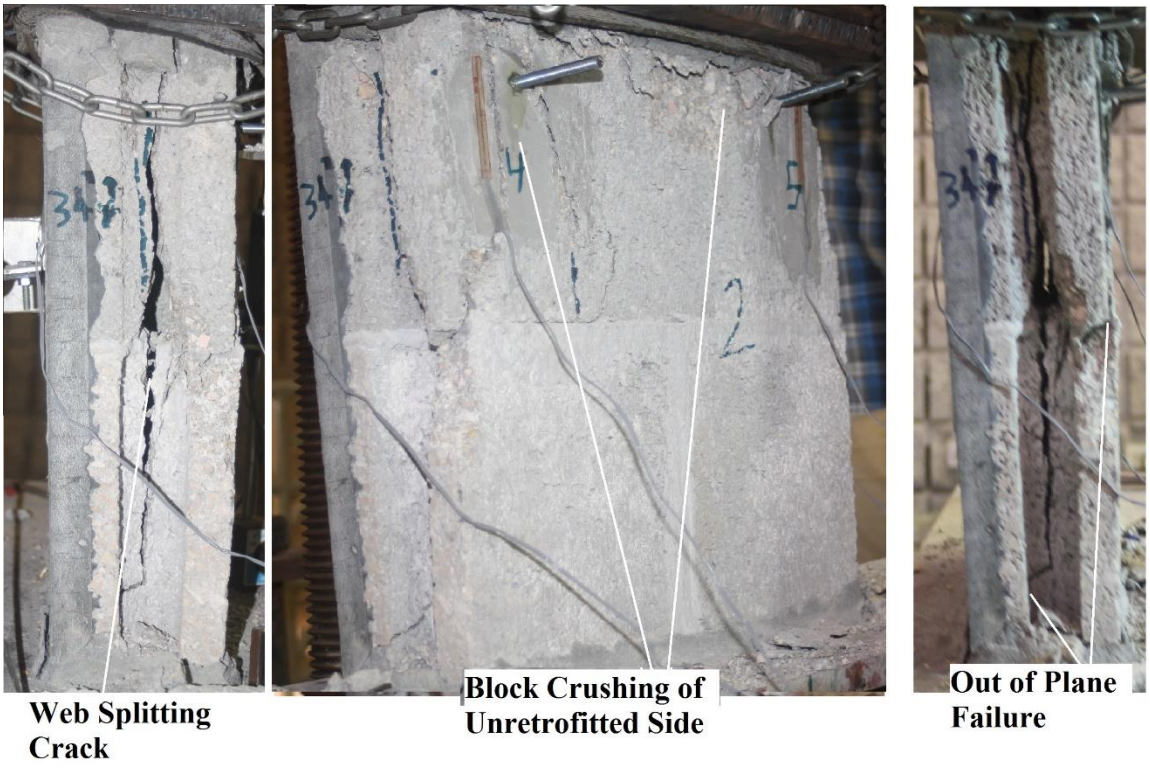

Figure 4-9: Failure Mode of NCMWR Prism One Side Retrofitting

For all other three specimens retrofitted on both sides, they followed the same behavior of crack patterns and propagation. A vertical crack split the web of hollow concrete blocks was initiated at axial loads of 307 kN, 450 kN and 550 kN for retrofitted specimens by10 mm, 20 mm and 30 mm thickness, respectively. The corresponding displacement to the splitting crack was 0.2-0.25 mm which is close to the control specimen. The difference in the load of first crack initiation is reasonable due to the plaster thickness increase resulting in increasing the specimen's stiffness. The failure of those specimens was mainly controlled by crushing of the concrete block while the plaster layers kept the prisms standing and carrying more load till complete block's crush. The failure mode is shown in Figure 4-10.

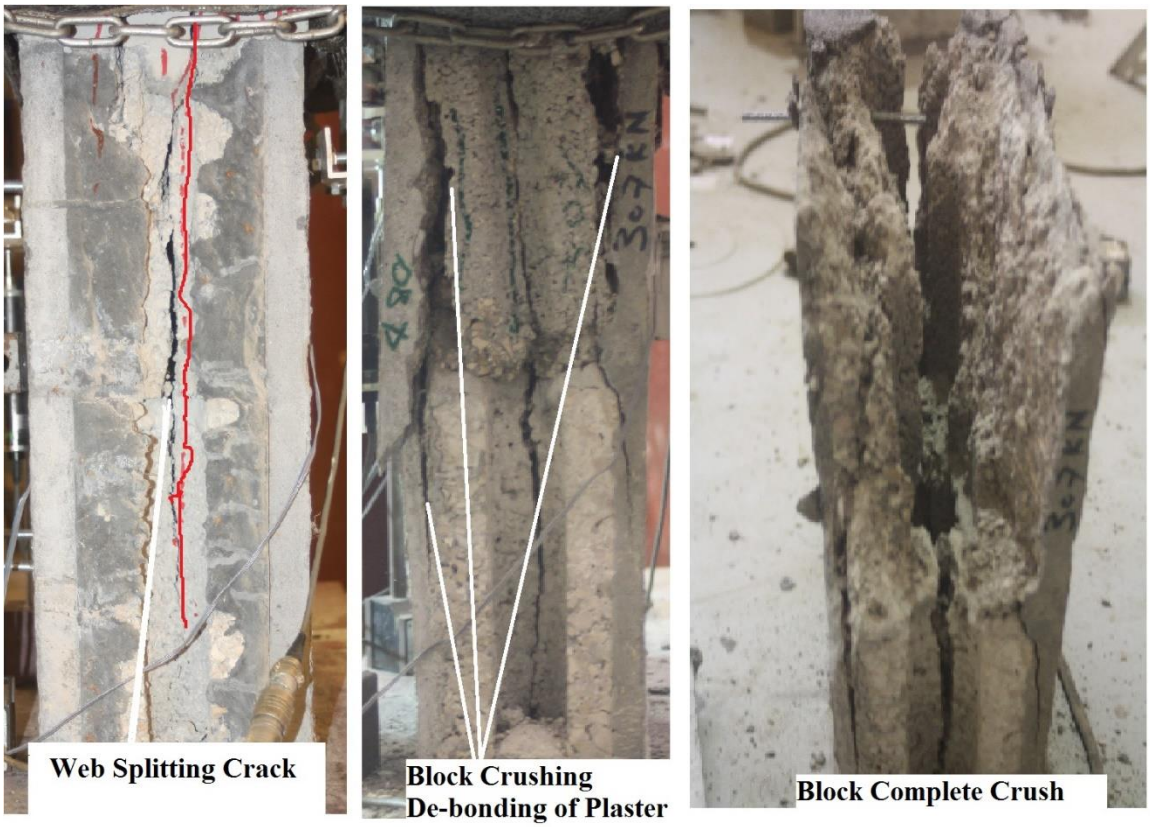

Figure 4-10: Failure Mode of NCMWR Prism Two Sides Retrofitting

The maximum axial load and corresponding axial displacement reached by 10 mm, 20 mm and 30 mm plaster's thickness specimens were 510 kN (14.0 MPa) with 0.55 mm, 890 kN (20.0 MPa) with 0.64 mm and 1160 kN (22.0 MPa) with 0.8 mm, respectively. The specimen stiffness increased by increasing the plaster thickness. Also, each specimen showed an increase in the ultimate axial displacement due to the ductility development by SFRM. In order to illustrate the strength, stiffness and displacement development, axial load vs. axial displacement curve was plotted for all retrofitted specimens with the control one in Figure 4-11.

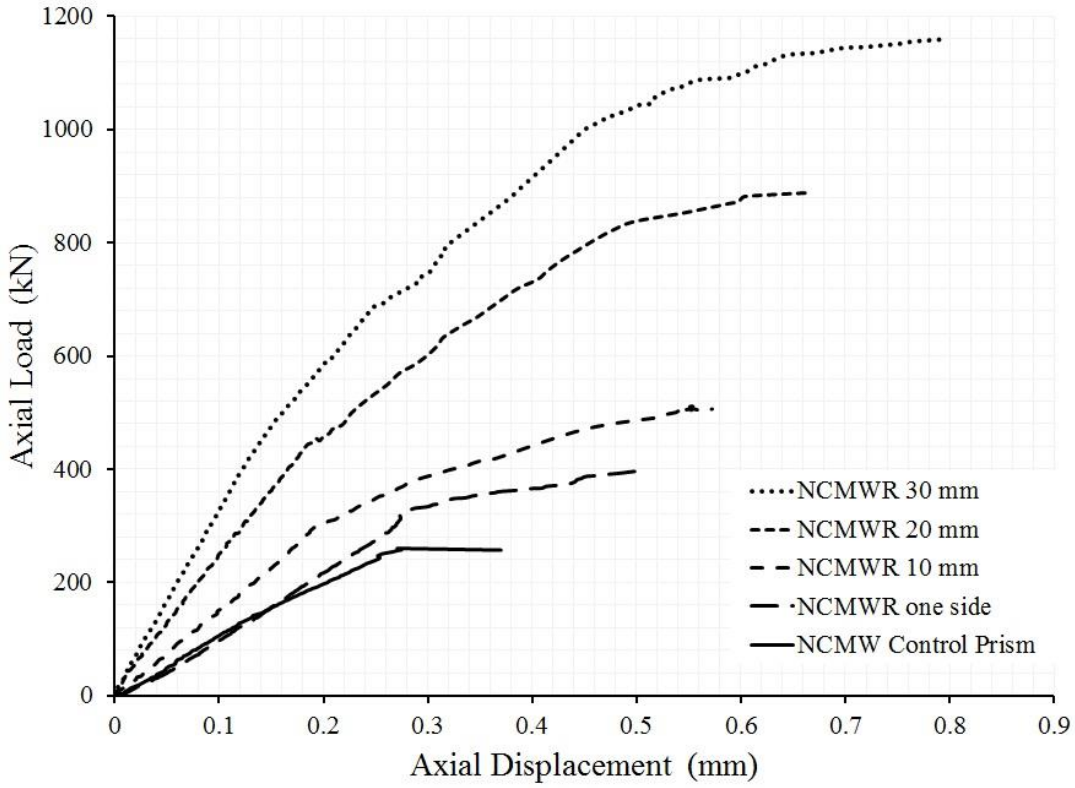

Figure 4-11: Axial Load vs. Axial Displacement Curve of NCMWR Prisms with Control one

4.2.4 Summary of Prism Compression Test

The compressive strength capacity of URM walls is very important to determine the required stress to be applied during the cyclic lateral test. In this study, a compression test on NCMW, NCMWJ and NCMWR prisms was carried out in order to investigate the effect of plaster material and thickness on the prism capacity.

For the NCMW control and NCMWJ (SFRM Joint) prisms, the compression strength was less than the strength of the concrete masonry block. Truthfully, the uniaxial strength of the masonry prism in comparison to the uniaxial strength of the masonry unit is affected by the availability of head-bed joints and the large scale of prism compared to concrete masonry block. Regarding the effect of large scale, this phenomenon has been observed by several researchers in which the increase in the size of prism or wall leads to a reduction of compression strength [20, 21] . Therefore, this influence was reduced in this study by using only two layers with height/length ratio of 1.0 in accordance with ASTM C 1314.

Noticeably, the retrofitting using SFRM plaster increased the strength capacity, stiffness and behavior of the prisms experimentally. The retrofitted prisms exhibited more ductility compared with the control specimen. The stiffness of the NCMWJ and NCMWR (one side) is close to the control specimen because of that, concrete block is the main material can affect the stiffness in these two specimens. However, for the NCMWR (one side), the plastered side is stiffer than the uncoated side resulting in the out of plane failure, as shown in Figure 4-9. The values of load, at the first crack occurrence, prism axial capacity and initial stiffness are presented in Table 4-2.

Table 4-2: Comparison Results of the Prisms Compression Tests

Prism's Name	1st crack Load (kN)	Axial Load			Stiffness	
		Ultimate (kN)	Strength MPa	Increase %	kN/ mm	Increase %
NCMW Control	260	280(*)	9.7	0.0	1060	0.0
NCMWJ SFRM Joint	270	295	10.2	5.2	1200	13.3
NCMWR one side	308	395	12.0	23.7	1190	12.3
NCMWR 10 mm	307	510	14.0	43.3	1500	41.5
NCMWR 20 mm	450	890	20.0	105.0	2480	134.0
NCMWR 30 mm	550	1160	22.0	126.8	3280	209.4
Increase %: the percentage increase in the control specimen value. (*) the average of the three control prisms.						

As shown in Table 4-2, the web crack occurred at higher load for prisms with higher SFRM plaster thickness. Also, the ultimate load was increased by 40% for each 10 mm increase in the SFRM plaster thickness. It is important to mention that, 20 mm of SFRM plaster layer takes and an extra axial load of about 290 kN equivalent to the capacity of control specimen which has an effective thickness of 72 mm. Furthermore, the stiffness of the retrofitted prisms developed as the SFRM plaster thickness increased where it found to be 1.4, 2.3 and 3 times the control for two side plaster with a thickness of 10 mm, 20 mm and 30 mm, respectively. The improvement in the retrofitted prisms stiffness with the plaster thickness is clearly shown in Figure 4-12.

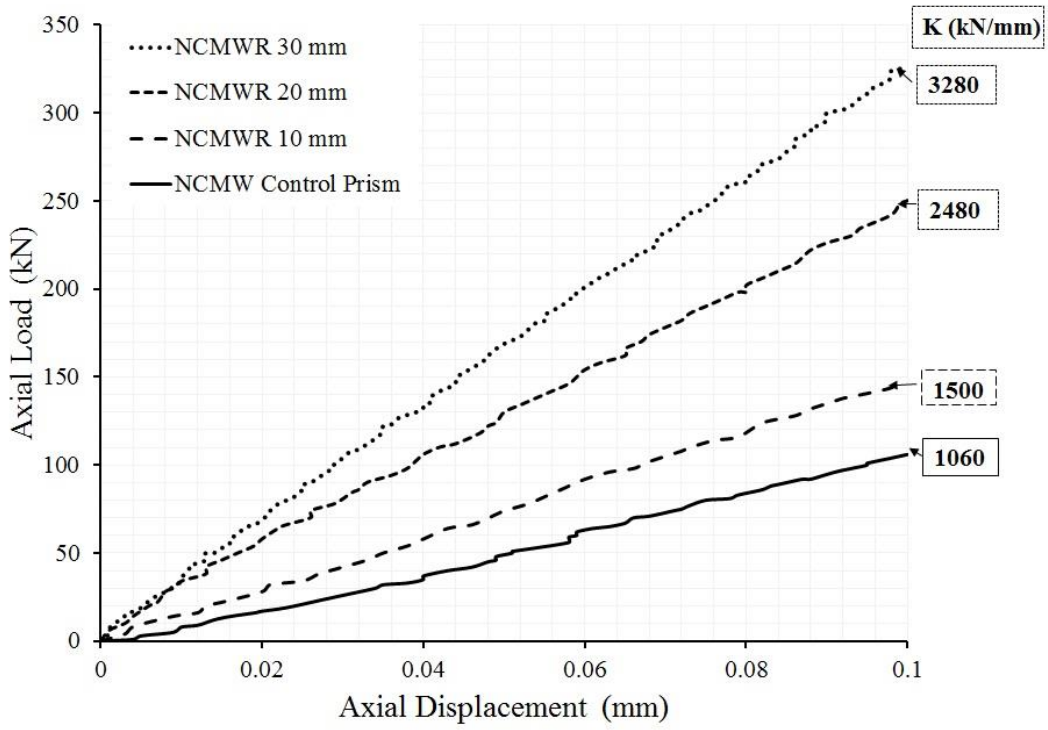

Figure 4-12: Stiffness Development of the Retrofitted Prisms

4.3 Lateral In-Plane Cyclic Test

This test was made in order to achieve the main objectives of this study, investigating the behavior of URM walls subjected to in-plane cyclic loading. Therefore, three wall samples (NCMW) were built using hollow concrete blocks of dimensions 400 mm x 200 mm x 100 mm (L x H x W) and a 10 mm thickness type M mortar at head-bed joints and one using SFRM at head-bed joints (NCMWJ). One of the NCMW walls was a control specimen and the other two were retrofitted using SFRM plaster of 10 mm thickness on one and both sides (NCMWR). The prepared URM walls can be classified as following:

- NCMW Wall (Control)
- NCMWJ Wall (SFRM Joint)
- NCMWR Wall (SFRM Plaster one and both sides)

4.3.1 Specimens Preparation

First, the walls were built with dimensions of 810 mm x 830 mm x 100 mm (Length x Height x Width). Then, the curing process was performed for about three days using burlap blankets with continuous water curing. After that, two walls were plastered using SFRM one on one side and the other on both sides. Thereafter, all the walls were leveled from the top and fixed from bottom in a U steel channel using high strength mortar (EMACO S88 CT provided by BASF). Then, the curing process was continued for 28 days using burlap blankets with continuous water curing and covered by the plastic cover for quality control. Finally, the walls were placed in the proper position within a steel frame fabricated for the purpose of testing the wall under cyclic loading in the reaction floor at KFUPM Civil Engineering laboratories. The dimensions and preparation processes of wall specimens are shown in Figure 4-13.

Figure 4-13: URM Wall Specimens Preparation

4.3.2 Experimental Setup

In order to apply the required loading for testing, the steel frame was constructed on the reaction floor. This frame was used to exert the axial load as well as the lateral loading on the wall. The axial and lateral stresses were exerted on the wall using special equipment fabricated for this test and it consisted of two hydraulic jacks and controller. One of the hydraulic jacks exerts only compression force and the other exerts both compression and tension forces for lateral loading. The two hydraulic jacks were designed so that the applied force on the walls is slow. The slow loading is helpful for capturing more data resulting in precise hysteresis diagram relates the load to displacement.

The axial force was exerted on walls using Enerpac hydraulic jack which has a capacity of 2000 kN. First, the URM walls were placed on top of built-up steel section attached firmly to the reaction floor through two high 5 cm diameter strength big bolts. The wall was then firmly attached to this built-up section using two high strength bolts.

Each wall was loaded horizontally and vertically through concrete reinforced beam of 300 mm wide and 400 mm high. This beam was put over each wall to transfer the loads from two hydraulic jacks (one was vertical and the other was horizontal). The axial force was applied by the vertical hydraulic jack and distributed to the top area of the wall through two beams. One of these two beams was the fabricated concrete beam. The other is stiff I-section steel beam.

During the lateral loading of the wall, the top side of the wall, as well as the attached concrete beam, had to move freely so that the desired lateral load exerted on the wall could be achieved. The vertical hydraulic jack and the steel beam were stationary in which movements (in-plane and out of plane) were prevented using a set of in-plane and out of

plane supports. To allow the lateral movement of the stiff concrete beam, as well as the top of the wall attached to the concrete beam, a set of cylindrical round bars, were placed between the steel beam and the concrete beam. To prevent the damage of the top side of the concrete beam and also to facilitate the rotation of the round bars, the thick steel plate was used to cover the top side of the concrete beam. This steel plate was firmly attached to the beam using previously prepared bolt attached to the inside of the concrete beam at the time of casting. As mentioned before, the wall was attached firmly to the built-up steel section. This was achieved by attaching the U wall support to the built-up steel section using two high strength bolts. To prevent the wall from sliding in the first course, two angle steel section were used at the two bottom ends of the wall. This two angle sections were attached to the U-section using the same bolts used to attach the U wall support section to the built-up section. The gaps between the steel angles and the wall were then filled using high strength mortar (EMACO S88 CT).

The horizontal load was transmitted to the wall through the concrete beam that was attached to the horizontal jack. One side of the horizontal jack was attached to the end of the concrete beam and the other side to a strong vertical reaction wall. Unfortunately, the horizontal jack was not designed for recording the exerted load. Due to this limitation, a fabricated setup was prepared and attached to the tip of the horizontal jack from one side and to the end of the stiff concrete beam on the other side. This fabricated setup allowed recording the lateral load exerted on the wall using only one load cell. The horizontal jack was then attached to the reaction wall through a thick steel plate and a strong hinge that allowed only vertical rotation of the horizontal jack. Figure 4-14 and Figure 4-15 illustrate the schematic laboratory set-up.

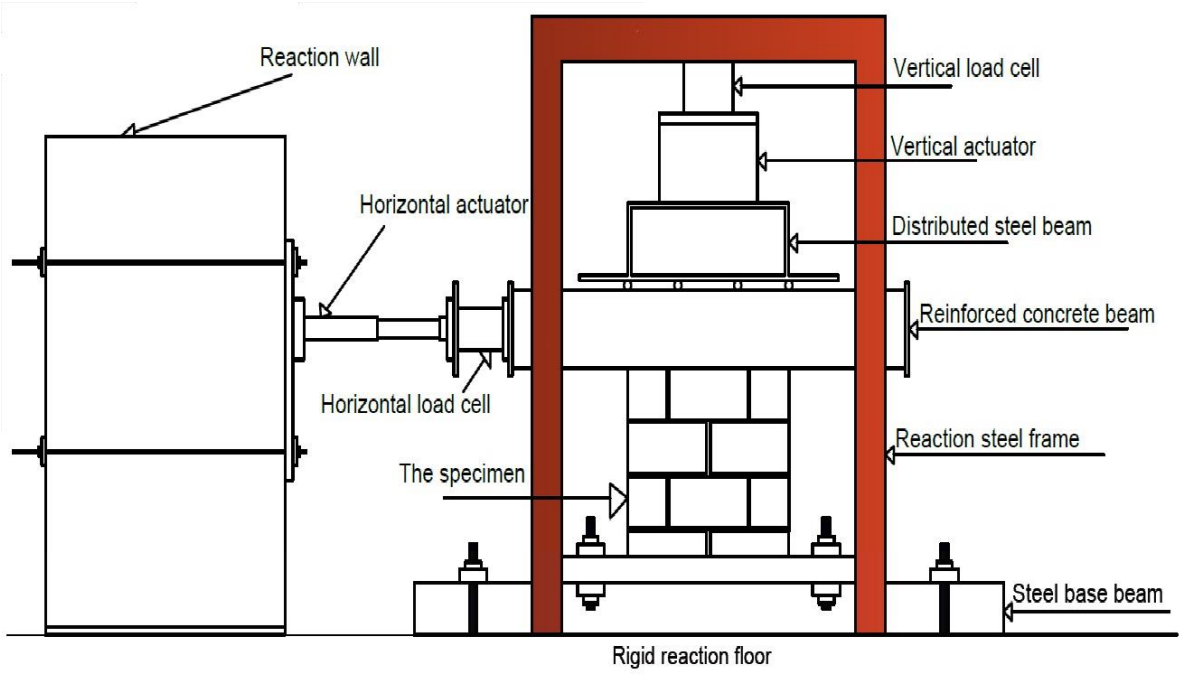

Figure 4-14: URM Wall Cyclic Test Schematic Laboratory Set-up

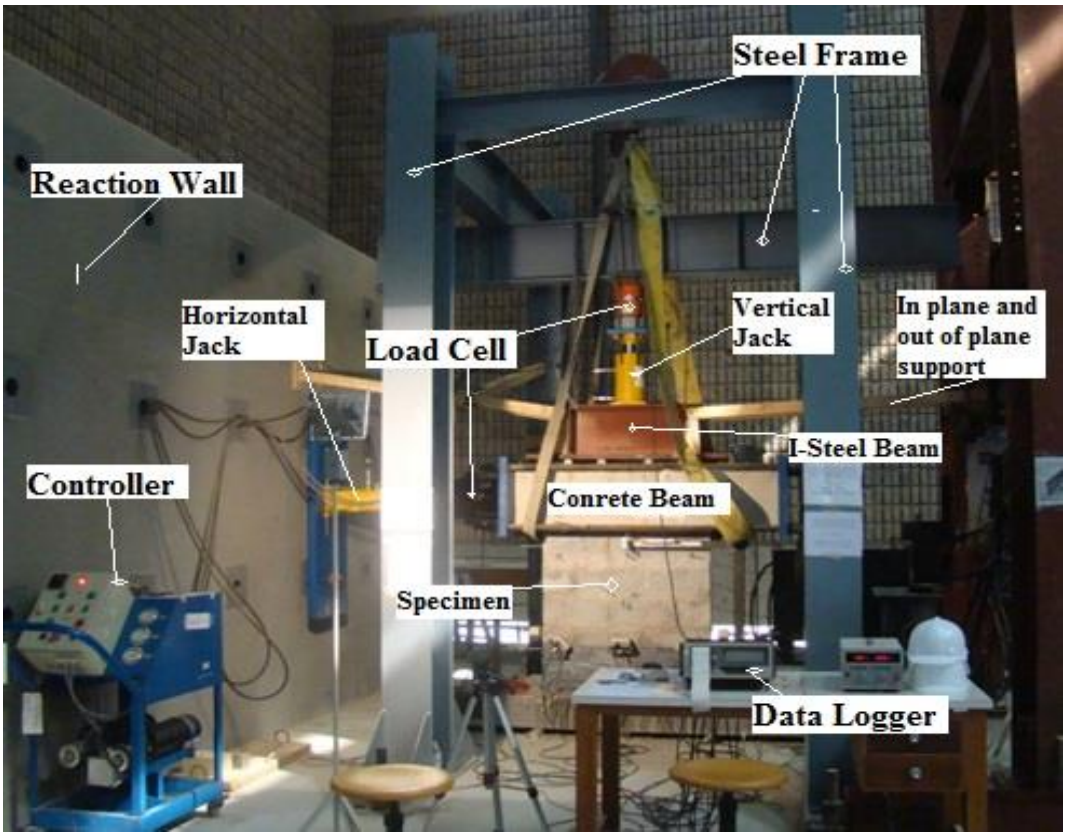

Figure 4-15: Photo of the URM Wall Cyclic Test Laboratory Set-up

In order to understand the lateral behavior of the URM wall, some data were captured and recorded. Therefore, two load cells were attached to each hydraulic jack to measure the applied loads, while three linear variables differential transducers (LVDT's) were utilized to measure displacements. One LVDT was to control and measure horizontal displacement and the other two were used to measure the vertical displacement. In addition, two strain gauges were placed diagonally on the walls to observe the elongation of the wall in the direction of diagonal crack. All of the load cells, LVDT's and strain gauges were connected to data logger device through which the data were monitored and collected. Instrumentation setup is shown in Figure 4-16 where V.L, H.L and S.G referred to vertical LVDT, horizontal LVDT and strain gauges, respectively.

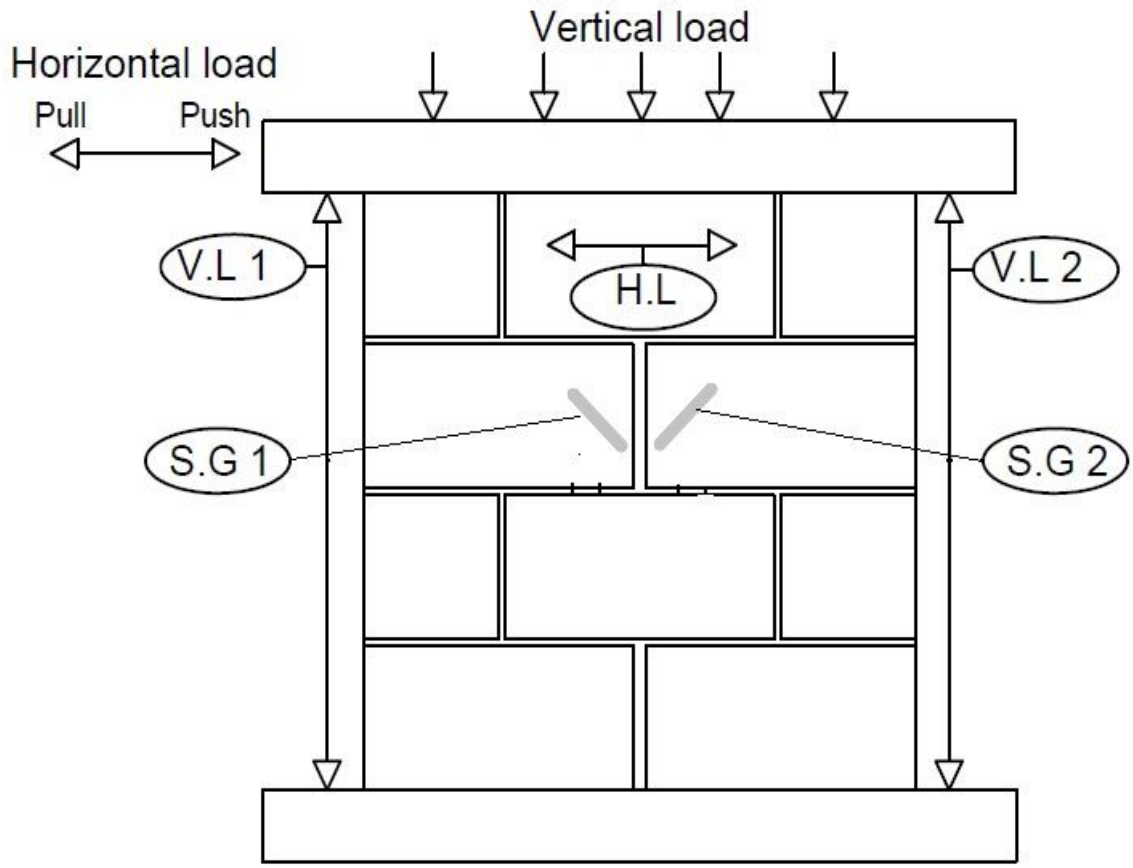

Figure 4-16: URM Wall Cyclic Test Instrumentation Setup

For all the URM wall specimens, a vertical stress of 45% of the prism maximum stress capacity was applied first through the vertical hydraulic jack and kept constant. Then, the wall was subjected to a cyclic loading using a displacement control load. The horizontal displacement load was controlled by means of the horizontal LVDT connected to the top center of the wall. The displacement-regime, which was adopted in this experiment, is shown in Figure 4-17. Each wall followed this system of displacement-regime until they failed.

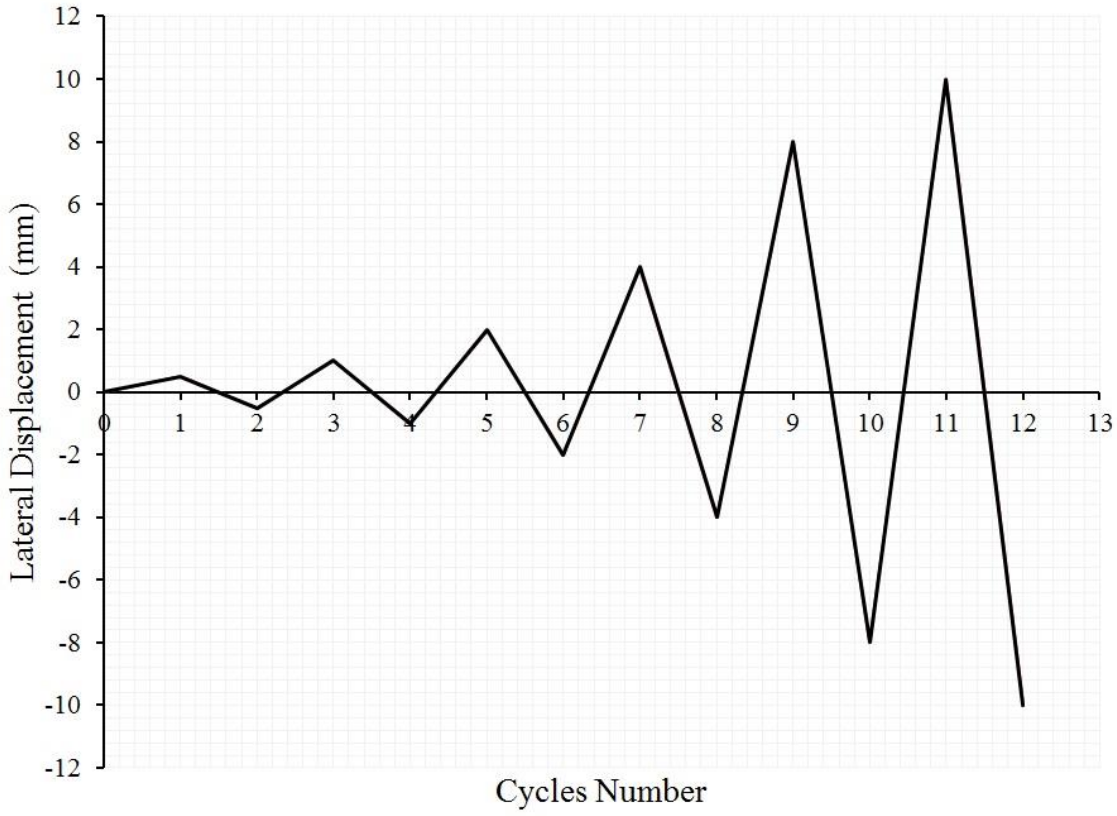

Figure 4-17: Lateral Displacement Regime

All the walls specimens followed the testing processes described in this section. Therefore, the experimental observations and results are described in the following sections.

4.3.3 Failure and Test Results

- **NCMW Wall (Control Specimen)**

The wall was tested under cyclic loading to evaluate the tensile capacity and use it as a reference to observe the increase in the retrofitted specimens. An axial load of 260 kN (4.5 MPa) was applied, which was approximately corresponding to 45% of the NCMW prism's capacity. A splitting crack was initiated at the top middle of the wall towards the bottom compressed corner and propagated through the concrete blocks with an angle of 15^{o}. This crack was occurred during the third cycle in the positive (Push) direction at 82 kN lateral force and 1.63 mm lateral displacement (crack1 in Fig. 4.18a, b). For the same cycle in the negative direction (Pull), another crack symmetrical to Crack1 was observed at a lateral load of 75 kN and lateral displacement of 1.9 mm (crack2 in Fig. 4.18a, b). Then, the loading was continued as pull till diagonal cracks took place by an angle of 30^{o} at 102 kN lateral force and 6.4 mm lateral displacement (crack3 in Fig. 4.18a, b).

It is important to mention that the no de-bonding of head-bed joint during the test except at the head joints of the last layer, which was an extension of the cracks occurred first, as shown in Figure 4-18. The lateral shear capacity of this wall was calculated to be 1.75 MPa. In addition, the wall after releasing the loads and all experimental instrumentation setup is shown in Figure 4-19. The relationship between the lateral load and lateral displacement was observed to be almost linear. The linearity started to change slightly before the occurrence of cracks. NCMW control specimen showed a brittle behavior whereby it failed immediately after reaching its full capacity without showing any sign of non-linear behavior. The captured data of lateral load and lateral displacement was plotted up to the

occurrence of first cracks in Figure 4-20 in order to understand the hysteretic response of NCMW wall.

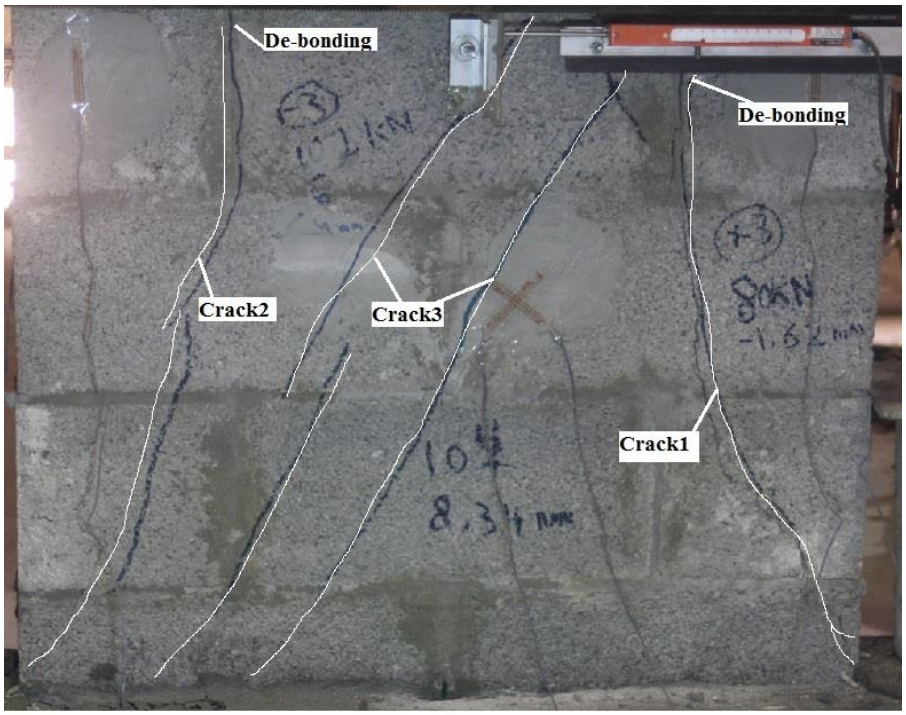

(a) NCMW Wall Front Veiw

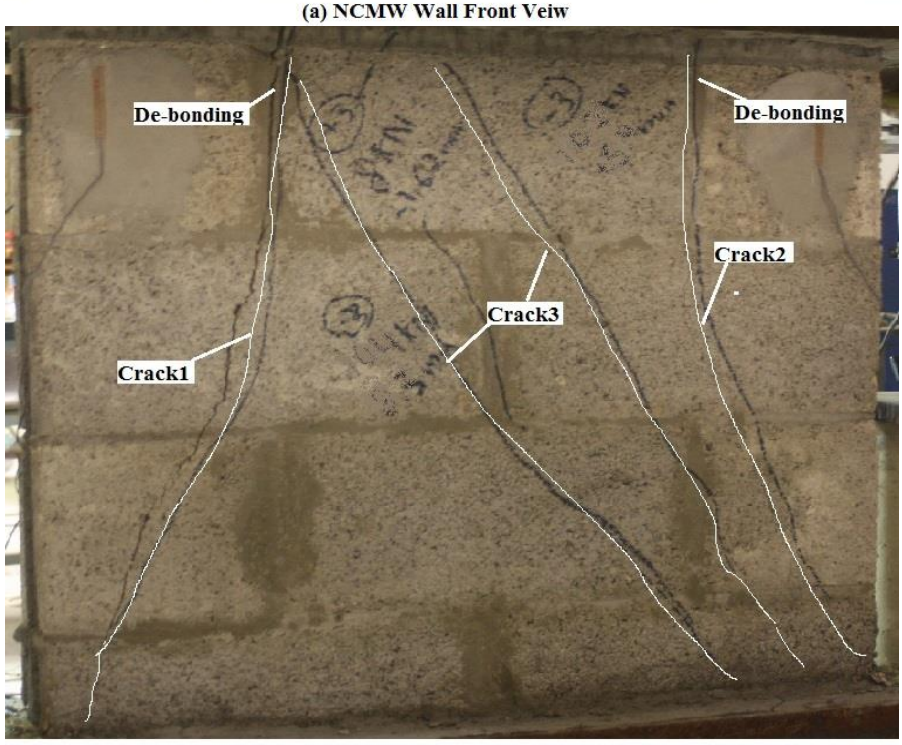

(b) NCMW Wall Back Facw

Figure 4-18: NCMW Wall Cracks Pattern

Figure 4-19: NCMW Wall after Releasing Instrumentation Setup

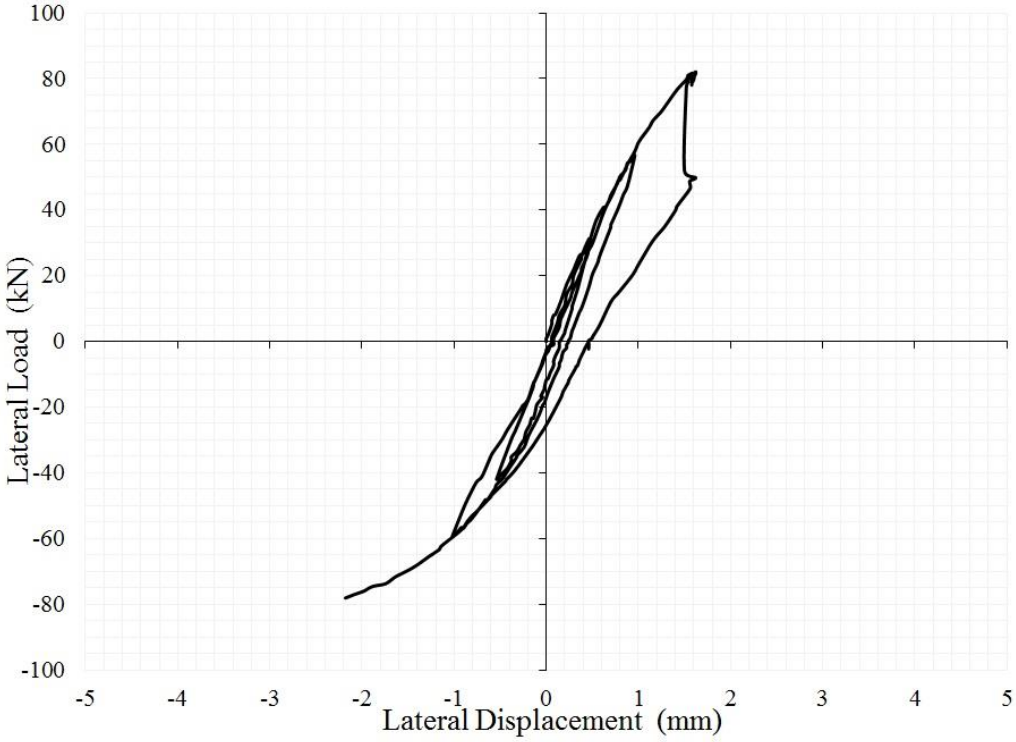

Figure 4-20: Lateral Load Displacement Hysteresis of NCMW Wall

- **NCMWJ Wall (SFRM Joint)**

The same applied axial load on the control specimen was also exerted in this test corresponding to 45% of the ultimate compressive strength of the prism. The wall was also tested under cyclic load to observe the increase in shear capacity using SFRM joints instead of type M mortar joints. The first crack occurred by an angle of 20^{o} at 96 kN lateral force and 2.1 mm lateral displacement during the fourth cycle in the positive direction (Push) (crack1 in Figure 4-21a, b). Then, two cracks took place at 90 kN lateral force and 3.18 mm lateral displacement during the fourth cycle in the negative direction (Pull) (crack2 in Figure 4-21a, b). One of these two cracks occurred by an angle of 31^{o}, which is the one crossed crack1 and the other occurred by an angle of 15^{o} which is similar to crack2 of NCMW wall.

It is important to mention that the no de-bonding of bed-head joint occurred during the test due to the effect of SFRM which worked as a good binder between the blocks keeping them sticky together. The lateral shear capacity of this wall was calculated to be 2.0 MPa. Also, the wall after releasing the loads and all experimental instrumentation setup is shown in Figure 4-22. The relationship between the lateral load and lateral displacement was observed to be linear till the occurrence of the cracks. Compared with NCMW specimen, NCMWJ wall showed a slight non-linearity behavior where it attained an additional lateral displacement at the ultimate load before failure. Also, it was noticed that the NCMWJ wall parts kept sticky together after removing experimental instrumentation setup. The captured data of lateral load and lateral displacement was plotted up to first cracks occurrence in Figure 4-23 in order to understand the hysteretic response of NCMWJ wall.

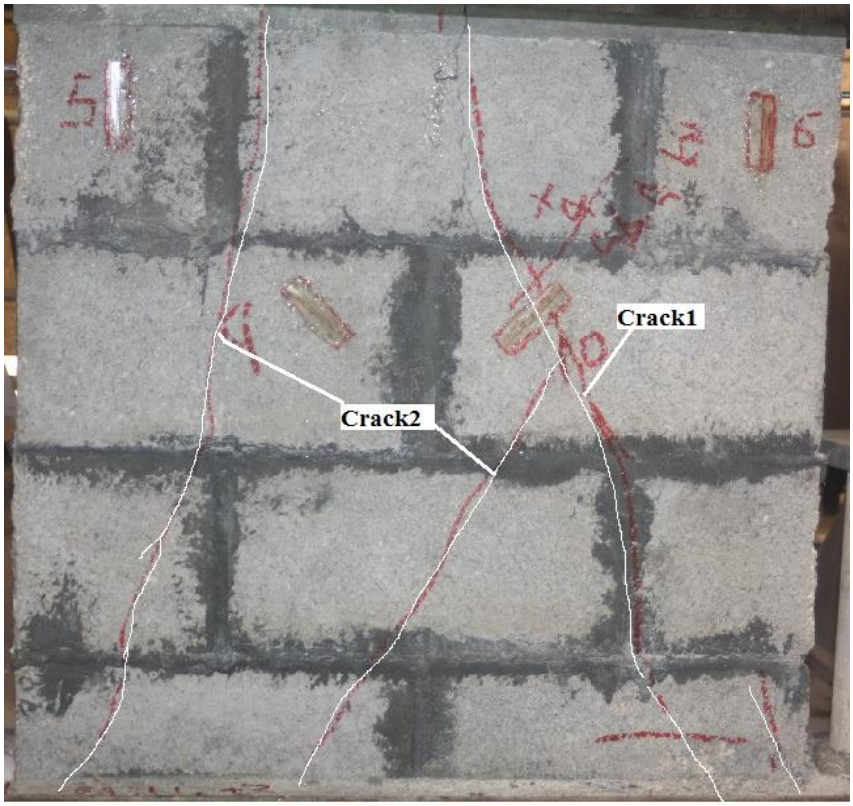

(a)NCMWJ Wall Front Veiw

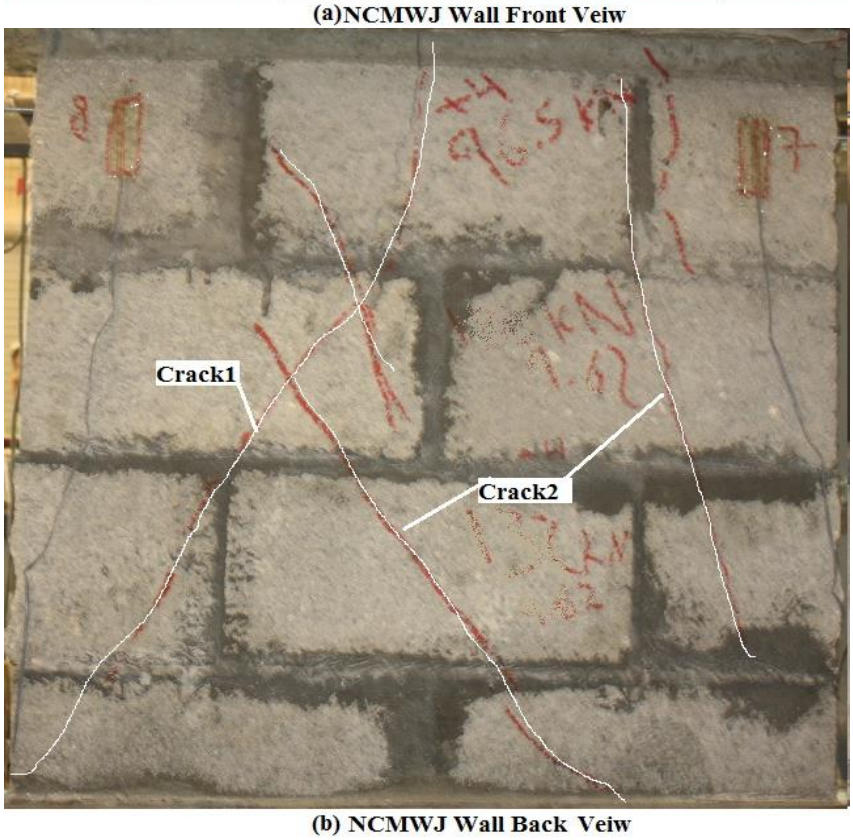

(b) NCMWJ Wall Back Veiw

Figure 4-21: NCMWJ Wall Cracks Pattern

Figure 4-22: NCMWJ Wall after Releasing Instrumentation Setup

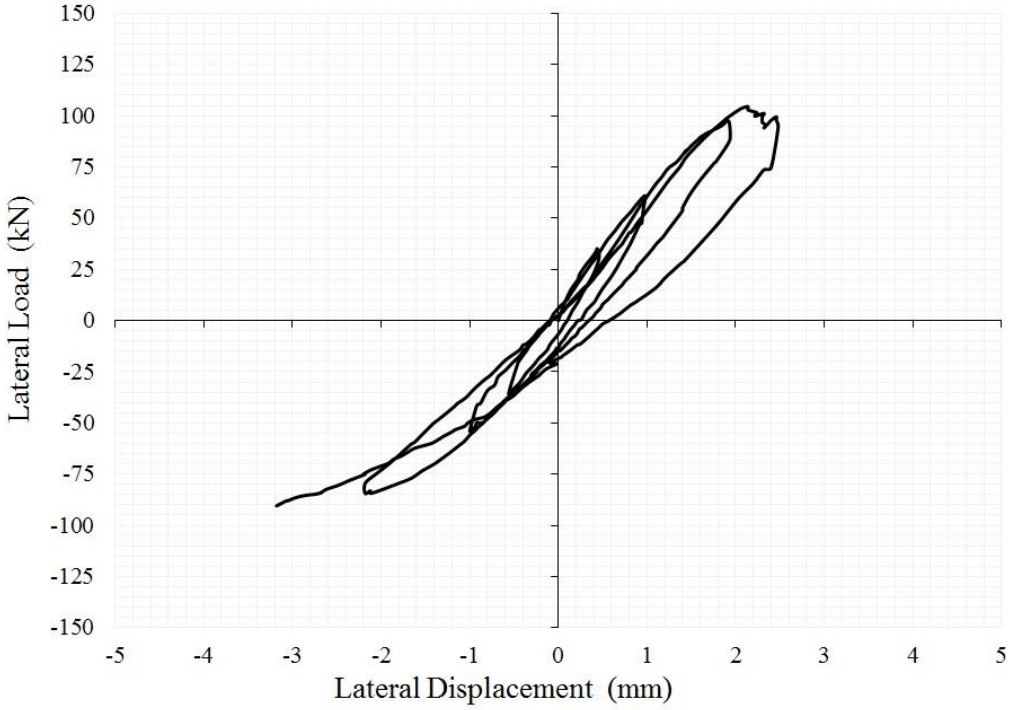

Figure 4-23: Lateral Load Displacement Hysteresis of NCMWJ Wall

- **NCMWR Wall (Plastered on One Side)**

As described in Section 3.5.1, this specimen was prepared as NCMW wall and plastered by SFRM 10 mm layer on one side. An axial load of 300 kN (4.5 MPa) was exerted in this test corresponding to 40 % of the ultimate compressive strength of the NCMWR one side plastered prism. The wall was also tested under cyclic load to observe the development of shear capacity using SFRM as retrofitted material from one side only. The first crack occurred by an angle of 20^{o} at 110 kN lateral force and 2.5 mm lateral displacement during the fourth cycle in the positive direction (Push) (crack1 in Figure 4-24a, b). Then, another crack took place by an angle of 25^{o} at 98 kN lateral force and 2.5 mm lateral displacement during the fourth cycle in the negative direction (Pull) (crack2 in Figure 4-24a, b). The third crack started with mini-cracks occurred with increasing lateral force in the negative direction. Theses cracks connected together at a load of 133 kN and lateral displacement 8 mm (crack3 in Figure 4-24a, b).

It is important to mention that SFRM one side plaster clearly affected the behavior and capacity of URM wall. The plaster saved the wall from complete damage and separation of concrete block parts. The lateral shear capacity of this wall was calculated to be 2.0 MPa including plaster area. The wall after releasing the loads and all experimental instrumentation setup is shown in Figure 4-25. The relationship between the lateral load and lateral displacement was observed to be linear till the load corresponding to the capacity of the control specimen (82 kN). Then, NCMWR wall (one side) showed a non-linearity behavior till occurrence of the first crack. Also, it was noticed that the steel fiber of the plaster kept the cracked parts saved from separation during the test and after removing experimental instrumentation setup. The captured data of lateral load and lateral

displacement was plotted up to first cracks occurrence in Figure 4-26 in order to understand the hysteretic response of NCMWR one side wall.

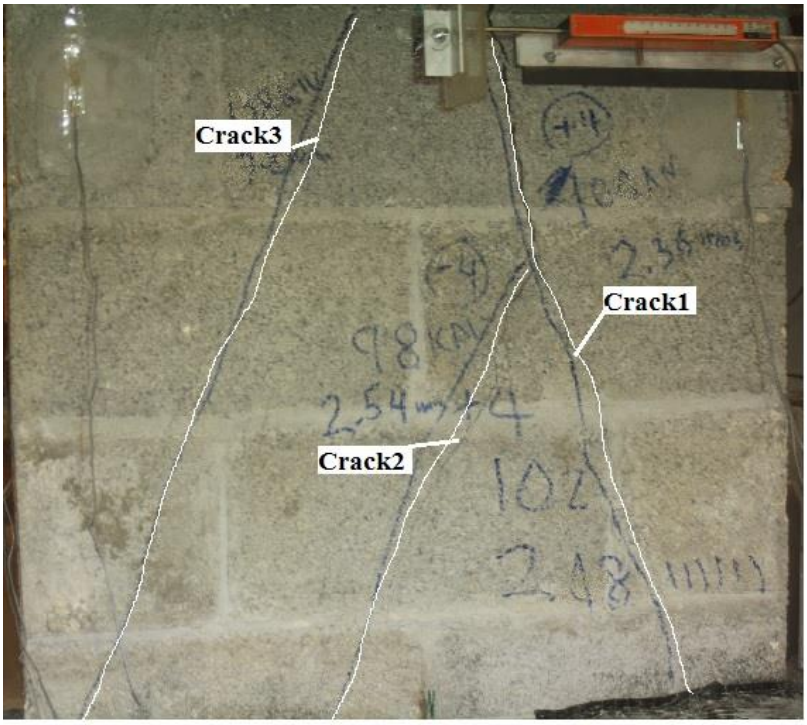

(a) Un-retrofitted Face NCMWR Wall One Side

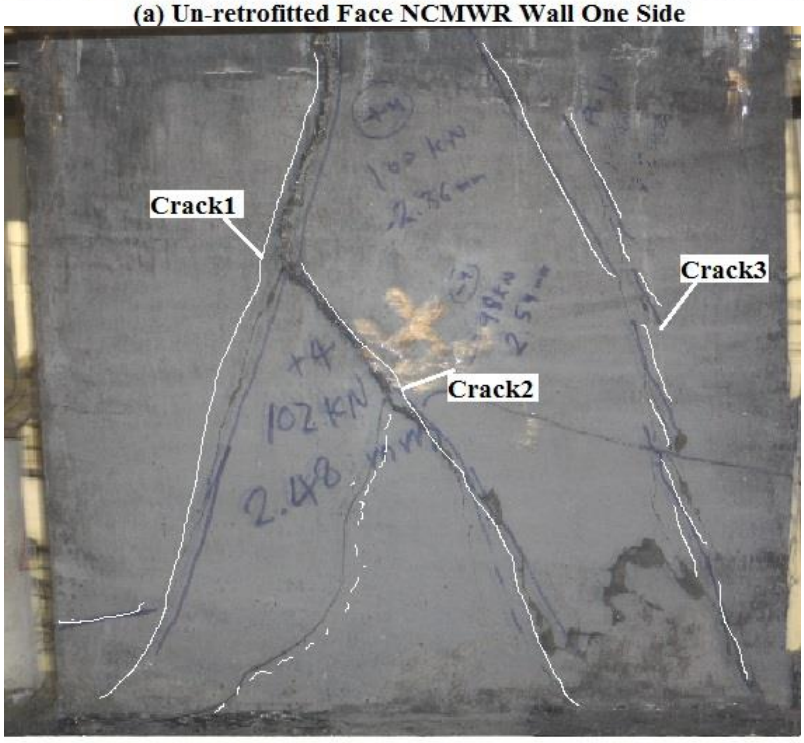

(b) Retrofitted Face of NCMWR Wall One Side

Figure 4-24: NCMWR Wall (One Side) Cracks Pattern

Figure 4-25: NCMWR Wall (One Side) after Releasing Instrumentation Setup

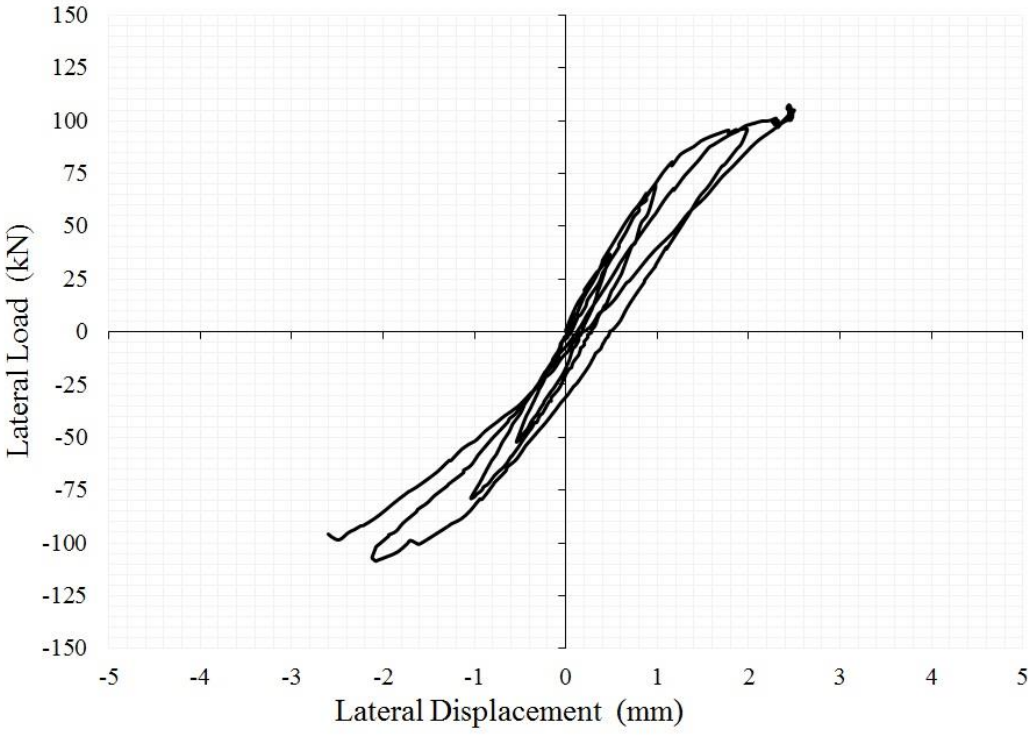

Figure 4-26: Lateral Load Displacement Hysteresis of NCMWR Wall (One Side)

- **NCMWR Wall (Plastered on Two Sides)**

This specimen was plastered on both sides by 10 mm layer of SFRM mortar as a retrofitted material. An axial load of 400 kN (5.4 MPa) was exerted in this test corresponding to 35% of the ultimate compressive strength of the NCMWR two side plastered prism. The wall was also tested under cyclic load to observe the development of shear capacity using SFRM as retrofitted material on two sides.

Unlike the control, NCMWJ and NCMWR one side specimens, this wall was dominated by rocking failure at 163 kN lateral force during the fourth cycle in the positive direction (push), as shown in Figure 4-27. Also, a crack at the base occurred resulting in the uplifting of the wall from the base during the test, which prevented the load to be increased furthermore. This crack was due to the low level of applied axial load. Therefore, the axial load then increased up to 500 kN. It was noticed that the lateral load increased up to 200 kN without any crack.

The relationship between the lateral force and lateral displacement was almost linear up to 140 kN horizontal force and then the stiffness began to deteriorate because of the rocking mode failure. The SFRM layer worked as confinement thereby preventing the diagonal crack through the concrete bricks from occurring. Retrofitted URM wall by a 10 mm SFRM layer on both sides developed the shear capacity and hysteresis behavior of the wall. The captured data of lateral load and lateral displacement was plotted up to rocking crack occurrence in Figure 4-28 in order to understand the hysteretic response of NCMWR two sides wall.

Figure 4-27: NCMWR Wall (Two Sides) Cracks Pattern

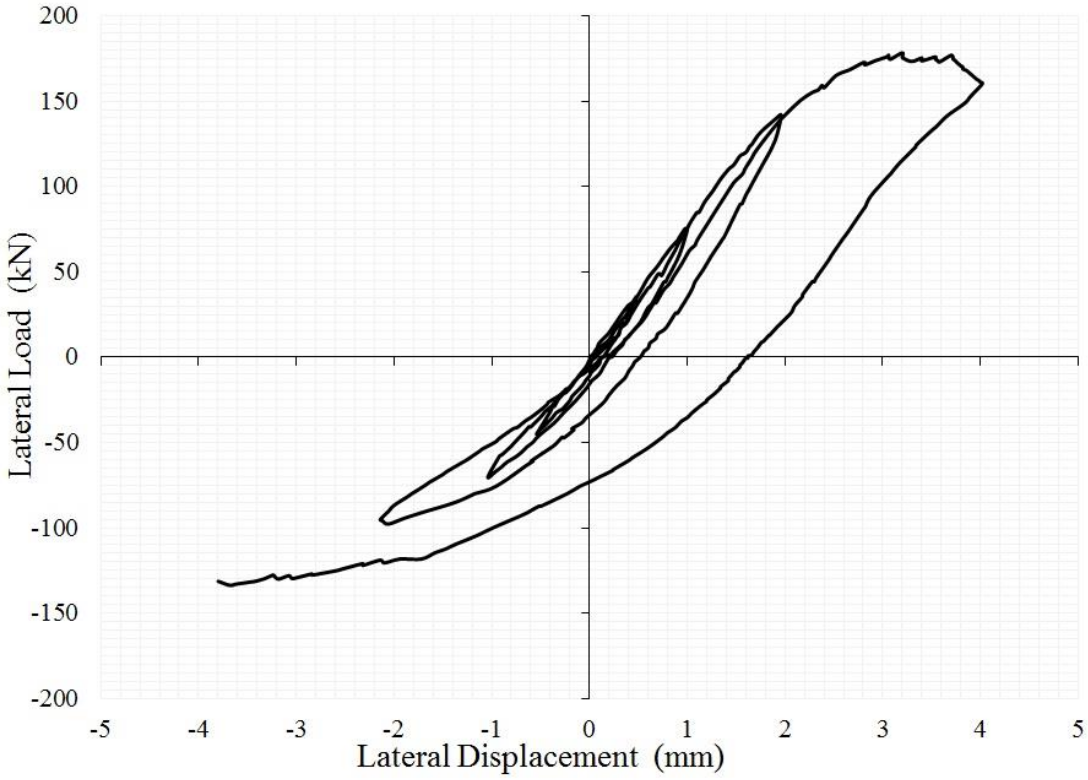

Figure 4-28: Lateral Load Displacement Hysteresis of NCMWR Wall (Two Sides)

4.3.4 Summary of Lateral In-Plane Cyclic Test

This section is to summarize and discuss the behavior of the walls under cyclic load. Based on the experimental and FEM observations, the level of axial force and material strength are highly affecting the wall response to lateral load. Therefore, a pre-compression stress of 45% of the wall compressive capacity was applied resulting in a tension stress at a certain lateral load. This tension stress causes the diagonal cracks described in Section 4.3.3. The material strengths clearly affect the URM wall behavior which can be noticed from the superior performance of the retrofitted specimens.

It has been noticed that the diagonal crack occurred through the concrete blocks passing through the bed joints and de-bonding in the head joint of the top layer only in the case of control wall. On the other hand, the crack pattern in the NCMWJ was initiated through the block only without any de-bonding in the head joints. The use of SFRM as a retrofitting material enhanced the behavior, stiffness and lateral capacity of the URM wall. The stiffness was increased by 17% and 26% for NCMWR on one and both sides, respectively. Also, the improvement in the shear capacity of URM was 17%, 34% and 117% for NCMWJ, NCMWR on one side and NCMWR on two sides, respectively.

Regarding the cyclic behavior of all investigated walls, the relationship between the lateral load and the lateral displacement was almost linear. The linearity started to change after the beginning of cracks and failure. Nonlinear behavior of the retrofitted walls started at the third cycle and accompanied with the lateral capacity of the control wall. In order to show the results clearly, the envelope of the load-displacement curve is plotted for the experimental test results in Figure 4-29. Also from a design point of view, the load capacity is represented by the load at the first crack occurrence in a push. The initial stiffness was

calculated as the slope between 0 and 1.0 mm displacement and the lateral capacity of all walls are shown in Table 4-3.

Table 4-3: Comparison Results of the Wall Lateral Tests

Wall's Name	Stiffness (0 – 1 mm)		Exp. Lateral Capacity		Mode of Failure
	kN/mm	Increase %	kN	Increase %	
NCMW Control	60.6	0.0	82.0	0.0	Diagonal Cracks
NCMWJ	62.2	2.6	96.0	17.1	Diagonal Cracks
NCMWR (one side)	71.7	17.3	110.0	34.1	Diagonal Cracks
NCMWR (two side)	76.2	25.7	178.0	117.1	Rocking Failure
Increase %: the percentage increase in the control specimen value.					

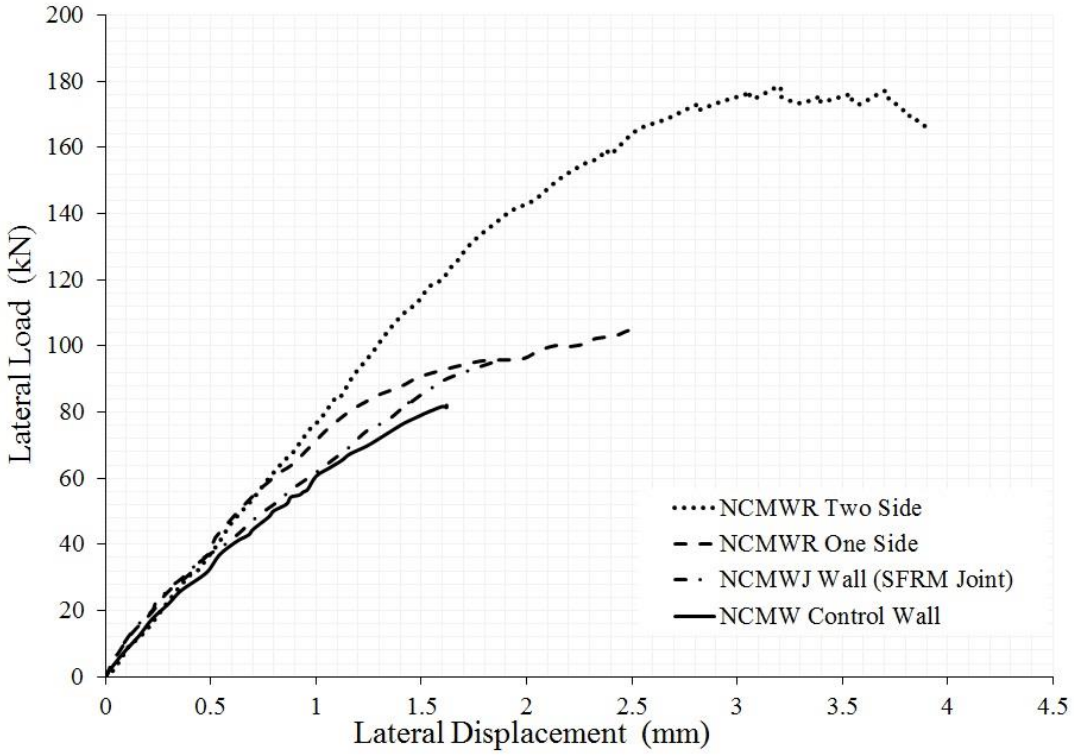

Figure 4-29: Envelope Diagram of All Tested Walls.

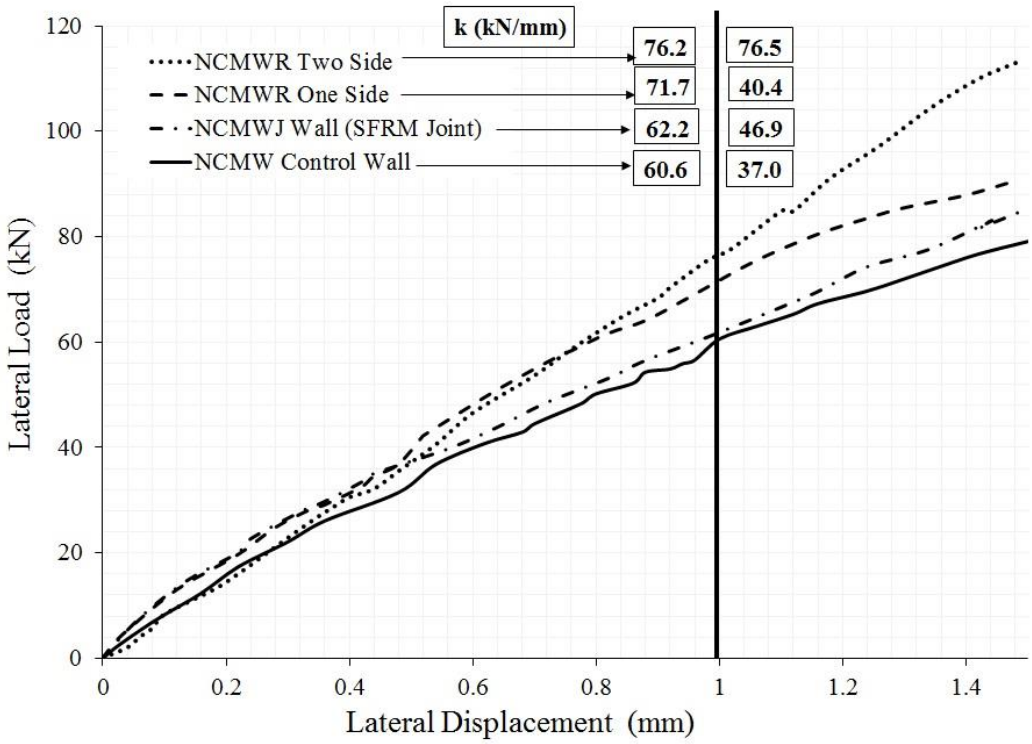

Figure 4-30: Stiffness Development of the Walls

One of the things that were observed about using SFRM as the retrofitting material is the ability to improve the stiffness of the wall. Figure 4-30 illustrates how the stiffness was improved. The data in this figure is taken between 0 and 1.5 mm lateral displacement. The figure is divided into two stages, for the first stage, the average secant stiffness was calculated in a range of (0.0-1.0) mm while the second stage the average secant stiffness was calculated in a range of (1.0-1.5) mm.

The NCMW and NCMWJ walls have almost the same initial stiffness but the decrease in the stiffness in the second stage is 38% and 24.6% for NCMW and NCMWJ, respectively. It is clear that the initial stiffness of NCMWR one and two side specimens improved by 18.3% and 25.7% higher than the control specimen. The stiffness of the NCMWR one side in the second stage decreased by 43.7% while remained the same for the two side retrofitted wall.

CHAPTER 5

NUMERICAL INVESTIGATION

5.1 Introduction

Finite element method (FEM) is a convenience technique to understand and predict the non-linearity behavior of masonry structures. As described in the literature, there are many ways of simulating the URM walls. In this study, an FEM simulation for prism and full wall tests of the tested specimens was adapted in an ABAQUS environment [32] using concrete damage plasticity (CDP), which was originally developed by Lubliner and his colleagues [33] and further extended by Lee and Fenves [34]. A detailed micro-modeling analysis level was used in which concrete blocks, mortar and plaster are modeled using continuum approach as an elastoplastic damage. In order to employ the CDP model, specific material parameters need to be input in carrying out the simulation. Some of these parameters were based on actual experimental data, such as modulus of elasticity, Poison's ratio and stress-plastic strain data from uniaxial compression and tensile tests. For these properties, all required mechanical properties were discussed in Chapter 3. Also, some needed properties were assumed based on ABAQUS default values and previous researches [8, 38]. The model was constructed to be similar to the real specimens in terms of wall details, boundary conditions and loading process. The model construction is illustrated in Figure 5-1, where the mortar and block were modeled as the actual used in the experimental parts in terms of dimensions, block's opening area and connecting order.

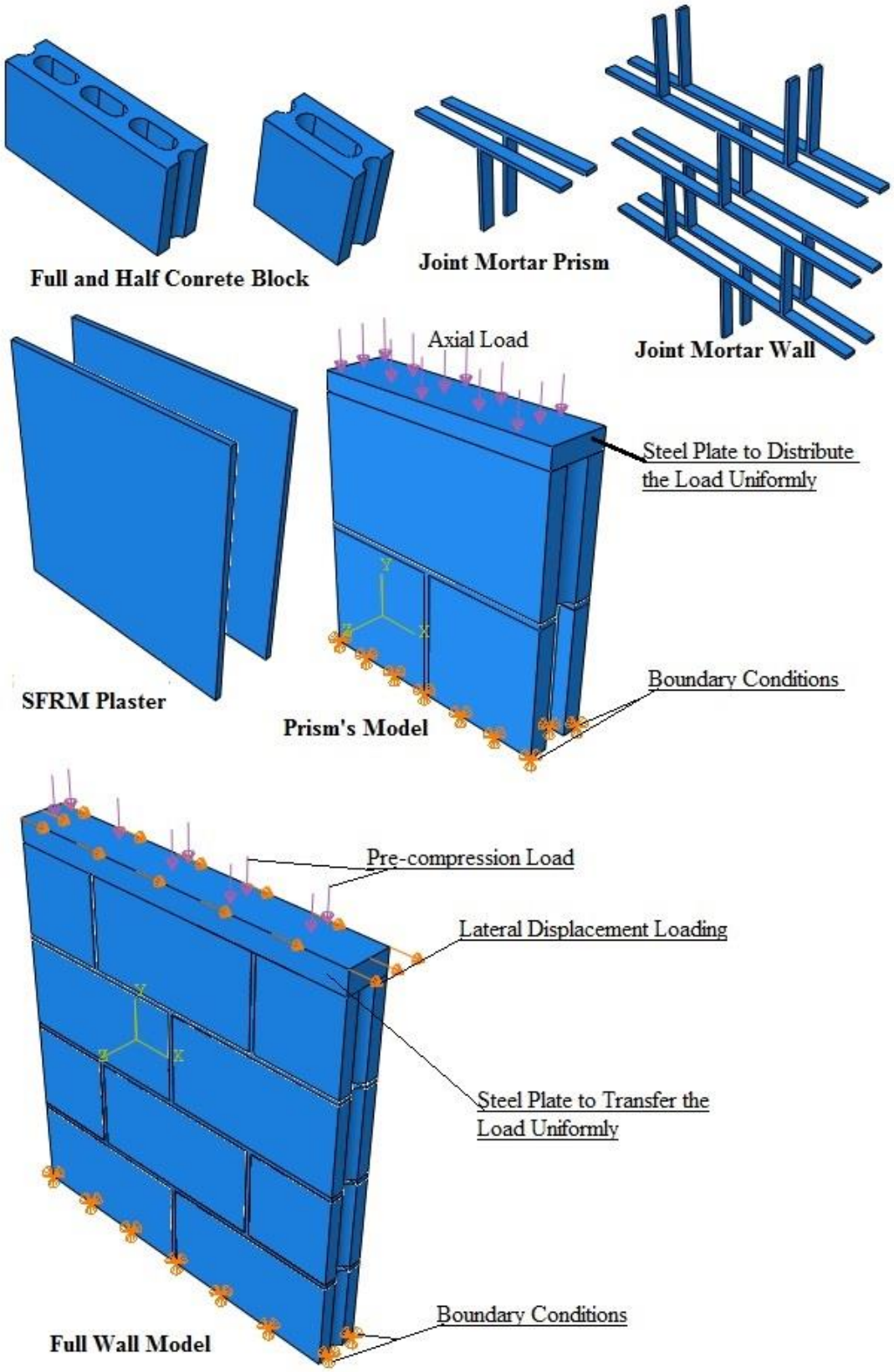

Figure 5-1: Masonry Components Details of FEM

5.2 Simulation Parameters

5.2.1 Material Properties of Masonry Components

In order to come up with an accurate simulation, FEM mesh and element types should be adequate for the problem. Therefore, the mesh size was chosen based on different runs till no change in the results was observed with increasing the number of elements. Also, using a possible small elements number is important for time and memory consuming during the analysis.

In this study, hollow concrete blocks, joint mortar and overly mortar meshed with element type of 3D stress linear, hex shaped with reduced integration elements (C3D8R) and element length of 10 mm for prisms and 25 mm for walls. For prism simulation, the finite element simulation was under load control where axial pressure was applied on the top of the connected steel plate. For the cyclic simulation of a full wall, the FEM was studied under displacement control where the axial pressure was applied first as in the experimental test then cyclic in-plane (push-pull) displacements were applied up to the first crack was observed in the experimental test. Conforming to the experiential setup, to distribute the load uniformly, the steel plate was connected to the top of the model with the perfect contact element.

To simulate masonry prisms using CDP model, stress–plastic strain behavior of concrete block, mortar and plaster need to be employed as well as damage factor and the contact element. Uniaxial compression and tensile stress-strain curves were employed based on the laboratory tests results discussed in Chapter 3 for the concrete masonry components. Figure 5-2 and Figure 5-3 show the stress-plastic strain data of masonry components in

compression and tension, respectively. Also, the parameters used in the CDP model are shown in Table 5-1.

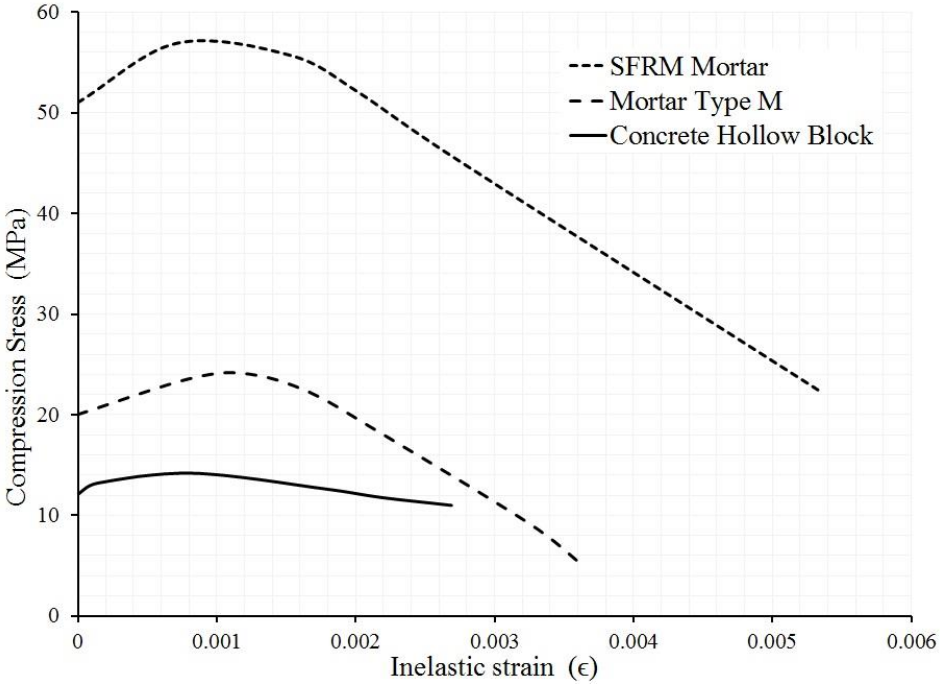

Figure 5-2: Compression Stress-Inelastic Strain Curve of Masonry Components.

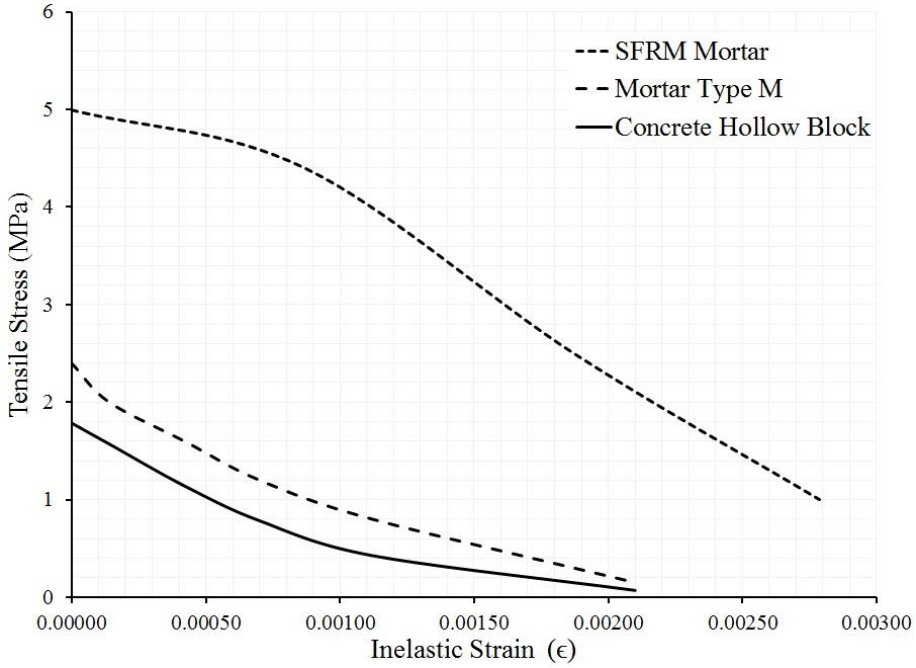

Figure 5-3: Tensile Stress-Inelastic Strain Curve of Masonry Components.

Table 5-1: Parameters Used in Concrete Damage Plasticity (CDP) Model.

Masonry Component	Mass Density (Kg/mm^3)	Young's Modulus (GPa)	Poisson's Ratio	Dilation Angle ψ	Eccentricity ϵ	fbo/fco	K	Viscosity Parameter
Concrete Block	2000	16.5	0.18	26^o	0.1	1.16	0.67	0.0
Type M Mortar	2200	20	0.2	36^o	0.1	1.16	0.67	0.0
SFRM Plaster	2500	28	0.25					

As shown in Table 5-1, density, Young's modulus and Poisson's ratio were calculated from the laboratory tests results. The other parameters in the table are based on previous research and ABAQUS default. It is important to mention that the Young's modulus in full wall model was reduced till capturing the same stiffness of the experimental results. This reduction is due to the nature of material when studying the lateral behavior where the values of 8.0 GPa, 9.0 GPa and 10 GPa were used for the block, type M mortar and SFRM, respectively.

5.2.2 Interface Contact Element

For interaction contact between masonry components, a friction contact element with a coefficient of 0.85 was used to be the general contact between the concrete block and joint mortar. The contact between the wall surfaces and SFRM plaster was defined as a surface-to-surface cohesive contact, where the surface based cohesive behavior is primarily intended for situations in which the interface thickness is negligibly small. In the surface-to-surface based behavior adopted in this model, the contacted surfaces are the inner surfaces of the SFRM plaster and the outer surfaces of the constructed masonry wall. It means that the thickness of the cohesive element was assumed to be 1.0 as defaulted according to ABAQUS library of the surface-to-surface based cohesive behavior.

A constitutive law accounting for the traction-separation of the interface was adopted for this purpose. The traction-separation model assumes initially linear elastic behavior of interface followed by the initiation and evolution of interface damage. The elastic behavior is written in terms of an elastic constitutive matrix as (Eq.5.1) that relates the traction stress vector to the separation vector through a full-populated stiffens matrix in the coupled low behavior. However, an uncoupled behavior is represented by setting the off-diagonal terms to be zero, as shown in Eq.5.2.

$$\begin{Bmatrix} \vec{t}_n \\ \vec{t}_s \\ \vec{t}_t \end{Bmatrix} = \begin{bmatrix} K_{nn} & K_{sn} & K_{tn} \\ K_{ns} & K_{ss} & K_{ts} \\ K_{nt} & K_{st} & K_{tt} \end{bmatrix} \begin{Bmatrix} \vec{\delta}_n \\ \vec{\delta}_s \\ \vec{\delta}_t \end{Bmatrix} = \boldsymbol{K}\vec{\boldsymbol{\delta}} \qquad (5.1)$$

$$\begin{Bmatrix} \vec{t}_n \\ \vec{t}_s \\ \vec{t}_t \end{Bmatrix} = \begin{bmatrix} K_{nn} & 0 & 0 \\ 0 & K_{ss} & 0 \\ 0 & 0 & K_{tt} \end{bmatrix} \begin{Bmatrix} \vec{\delta}_n \\ \vec{\delta}_s \\ \vec{\delta}_t \end{Bmatrix} = \boldsymbol{K}\vec{\boldsymbol{\delta}} \qquad (5.2)$$

The interface traction stress vector $\vec{t}$ consists of three components that are $\vec{t}_n, \vec{t}_s \; and \; \vec{t}_t$ the corresponding separations (displacements) are denoted by $\vec{\delta}_n, \vec{\delta}_s \; and \; \vec{\delta}_t$, respectively. To define the linear elastic behavior of uncoupled traction-separation behavior, the terms $K_{nn}, K_{ss} \; and \; K_{tt}$ which are normal and tangential stiffnesses as required. The values of 18.0 N/mm^3, 20.0 N/mm^3 and 20.0 N/mm^3 were used for $K_{nn}, K_{ss} \; and \; K_{tt}$ respectively. These values were calibrated according to the conducted triplet test discussed in Chapter 3 and previous research related to concrete block and mortar [38].

Once the elastic interface stress limit was reached, the interface damage behavior was defined to simulate the interface degradation and eventual failure of the interface. The failure mechanism consists of two ingredients: the interface damage initiation criterion and interface damage evolution law. The initial response is assumed to be linear elastic as discussed above.

However, once a damage initiation criterion is met, the damage will occur according to a user defined damage evolution law. The damage initiation refers to the beginning of degradation of the interface. The process of degradation begins when the interface stresses satisfy the defined interface damage initiation criteria. In this study, the stiffness was only employed without limiting the contact stresses.

5.3 Simulation Results

In order to study the masonry behavior using FEM and compare the output and failure modes with experimental results, the control and retrofitted specimens were studied using the input shown above. The results of FEM analysis are described in the following sections.

5.3.1 Prism FEM Results

The NCMW control prism and NCMWR on two sides prisms were studied in this Section and compared with the experimental results discussed in Chapter 3. FEM outputs were represented by the load-displacement curve shown in Figure 5-4 to 5-7 accompanying with the experimental results for each prism model. The FEM results showed good agreement with the experimental tests in terms of the ultimate load, deflection, initial stiffness and failure modes. It could be noticed that the initial stiffness of FEM analysis is similar to the experimental tests, but the FEM gives a slight ductility at the ultimate load compared with the experimental results.

Regarding the failure modes, Figure 5-8 shows how the mid-face crack started on the web and propagated through the prism causing immediate failure to the control specimen. Also, Figure 5-9 shows how the mid-face crack in the web started and propagated through the whole web in the plastered specimens. The prism continued carrying the load with the development of the web crack accompanying with the crushing of the block till failure, which coincides with the experimental results. The contours output of tension and compression damage parameters were used to observe the crack development and failure of the specimens. The retrofitted prisms followed the same crack pattern starting by the web crack, then full failure controlled by crushing of concrete blocks.

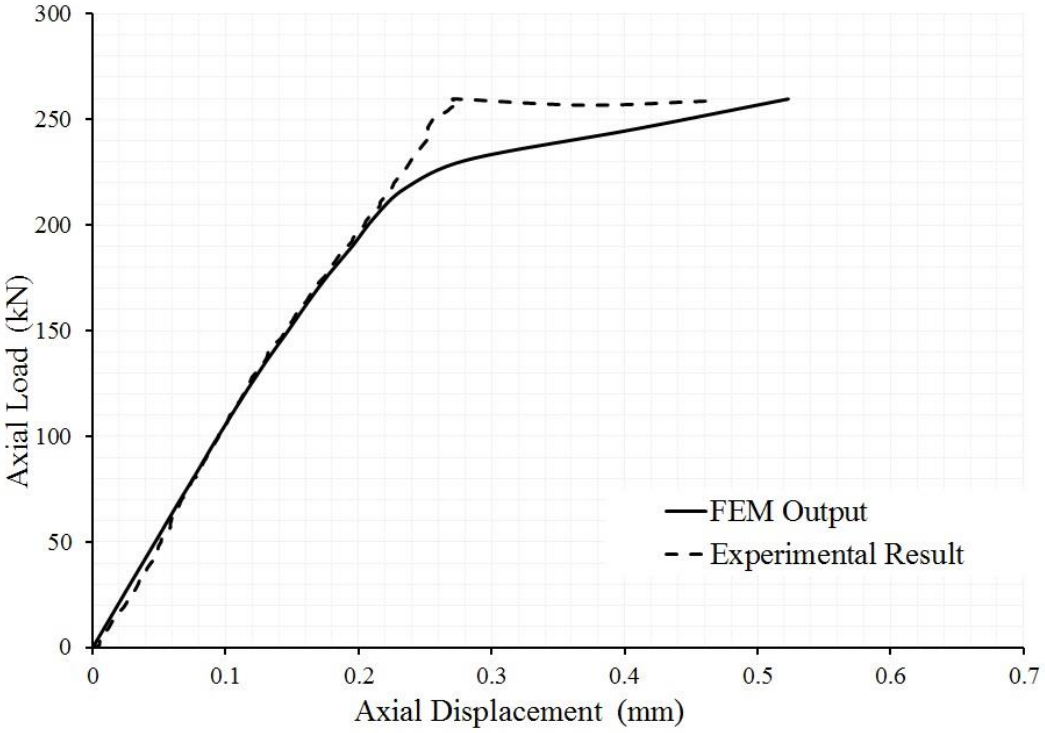

Figure 5-4: FEM Axial Load-Displacement Curve of Control Prism

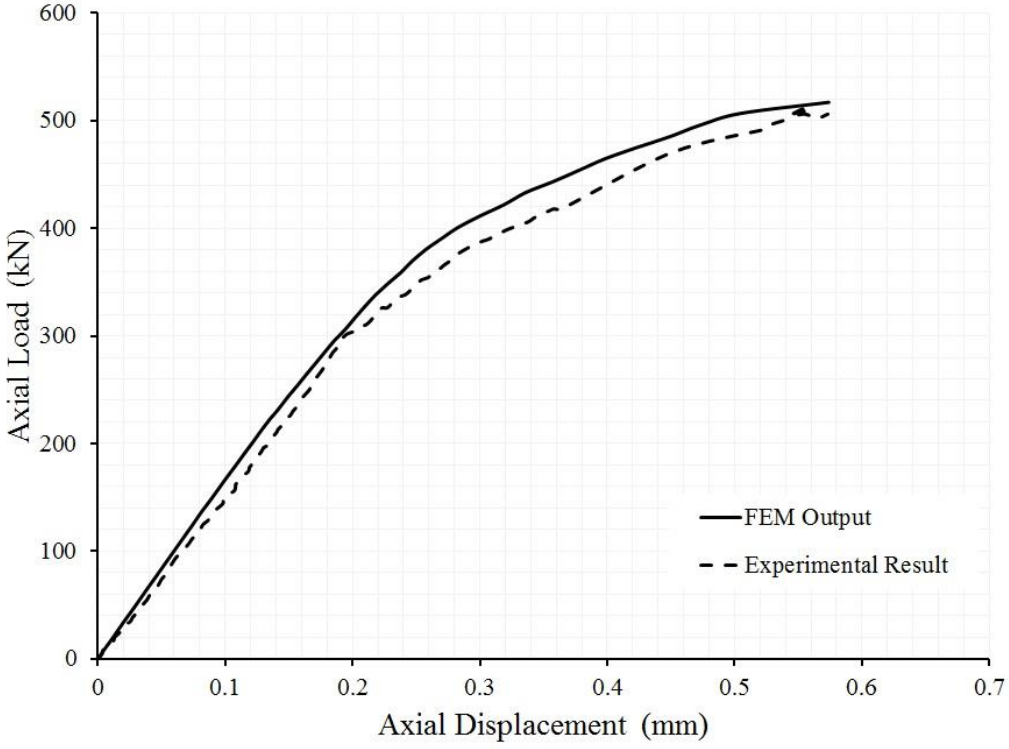

Figure 5-5: FEM Axial Load-Displacement Curve of NCMWR 10 mm Prism

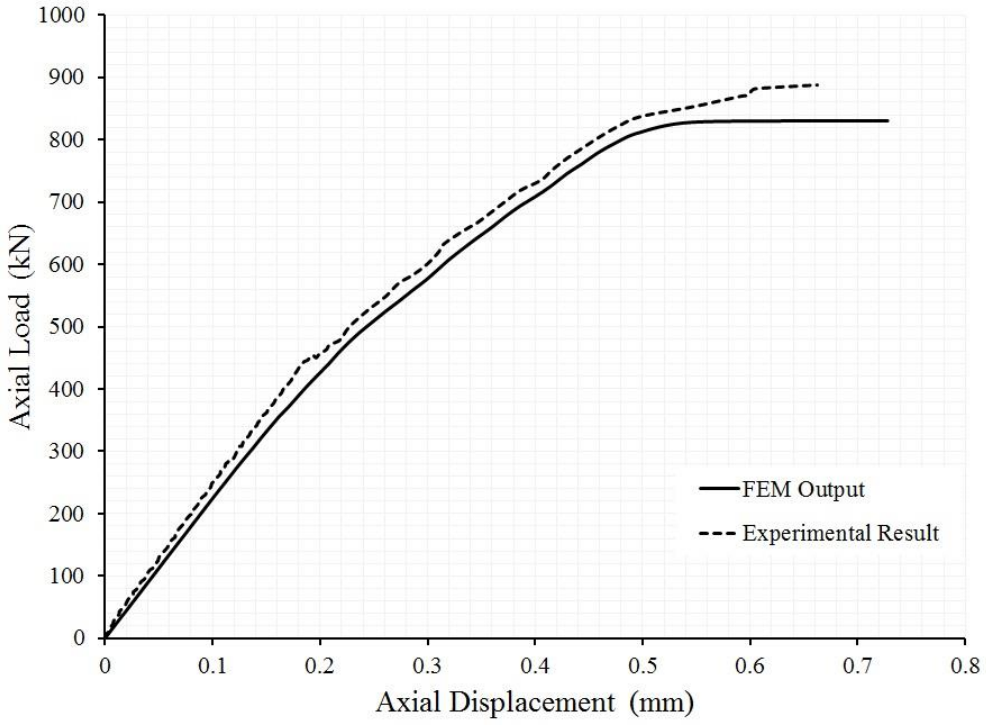

Figure 5-6: FEM Axial Load-Displacement Curve of NCMWR 20 mm Prism

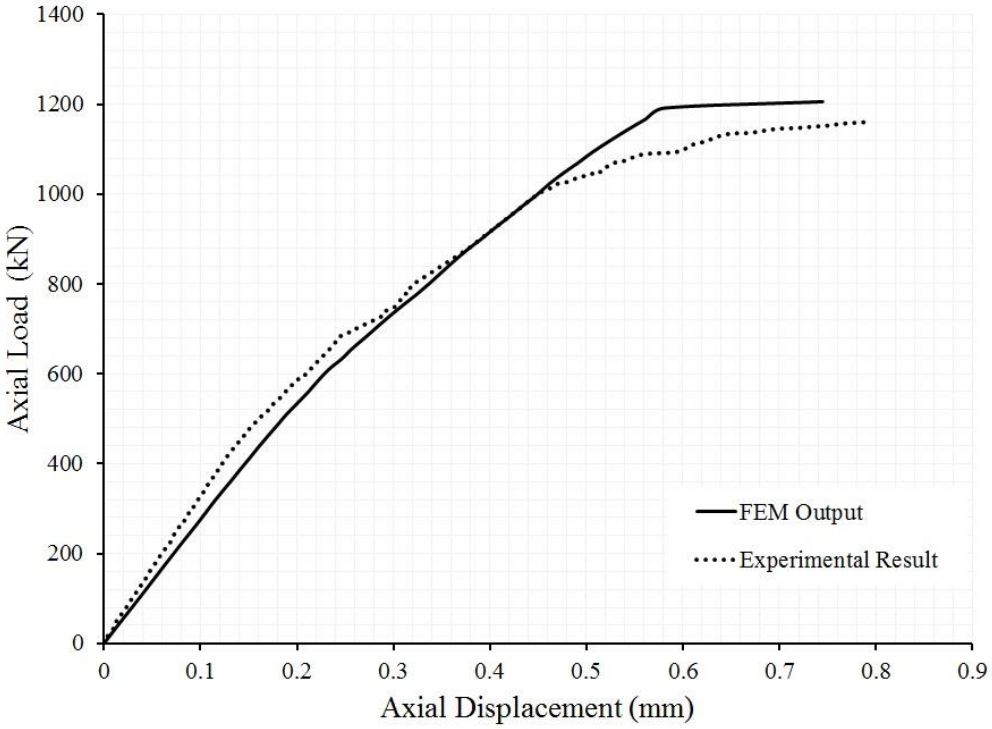

Figure 5-7: FEM Axial Load-Displacement Curve of NCMWR 30 mm Prism

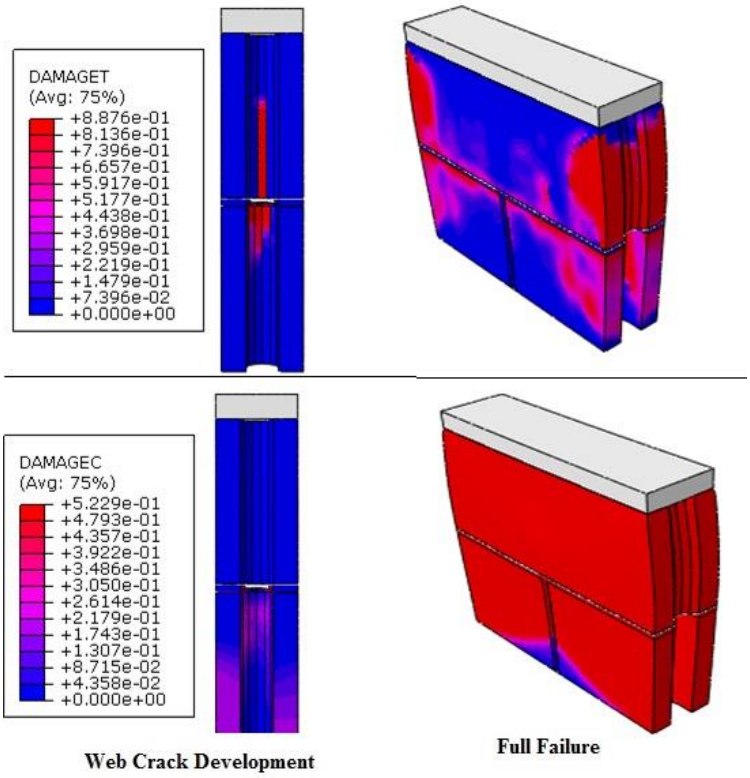

Figure 5-8: FEM Failure Mode of Control Prism

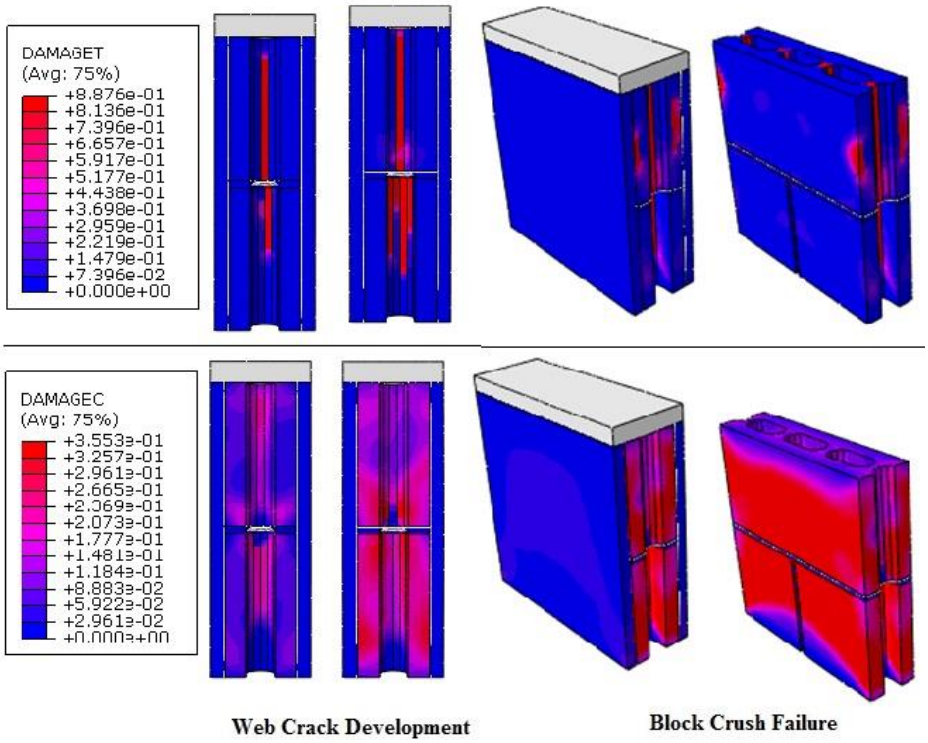

Figure 5-9: FEM Failure Mode of NCMWR Prisms

The web crack of FEM analysis started at a load of 220 kN and reached full web crack at a load of 260 kN in the case of control prism. For the retrofitted prisms, the web crack started at a load of 288 kN, 403 kN and 562 kN and developed a full web crack at 336 kN, 504 kN and 662 kN for 10 mm, 20 mm and 30 mm plaster thickness, respectively. The FEM results of the ultimate axial load were recorded with good agreement with the experimental results. The maximum difference was found 7% between the FEM and experimental results, as shown in Table 5-2.

Table 5-2: Comparison Results of Prism Test Results (FEM & Experimental)

Prism's Name	Ultimate Axial Load		
	Experimental (kN)	FEM (kN)	Difference %
NCMW Control	260	260	0.0
NCMWR 10 mm	510	517	-1.4
NCMWR 20 mm	890	830	6.7
NCMWR 30 mm	1160	1200	3.4
Difference %: the percentage difference between FEM and Experimental			

5.3.2 Full Wall FEM Results

The tested walls in this study were modeled in ABAQUS environment where the details of the model are shown in Figure 5-1 and the input is described in Section 5.2. The pre-compression load applied in FEM was similar to the experimental one. After that, the model was subjected to lateral cyclic loading controlled by the lateral displacement where it followed the displacement regime of the experimental test up to the occurrence of the crack in push and pull. In order to calibrate the FEM properly, all the processes of modeling, inputs and loading were assembled to be similar to the experimental test. The output of each wall model is described as follows:

- **FEM of NCMW Wall (Control Specimen)**

This model was adopted to simulate the control wall subjected to cyclic lateral load and calibrate the output result and failure mode with the experimental investigation. The FEM lateral load-displacement hysteresis was captured and plotted in Figure 5-10. Compared with the experimental test, which had a brittle behavior at the first crack (Push), the FEM result shows a slight ductility after the occurrence of the first crack, as shown in the combined plot in Figure 5-11.

In the first and second cycles, the experimental test shows residual displacement at 0 load while in the FEM simulation the displacement was zero at the zero load. Figure 5-12 shows the failure mode represented by damage parameters in tension. Similar to the experimental test, FEM simulation shows a propagation of diagonal cracks in the third cycle of push and pull.

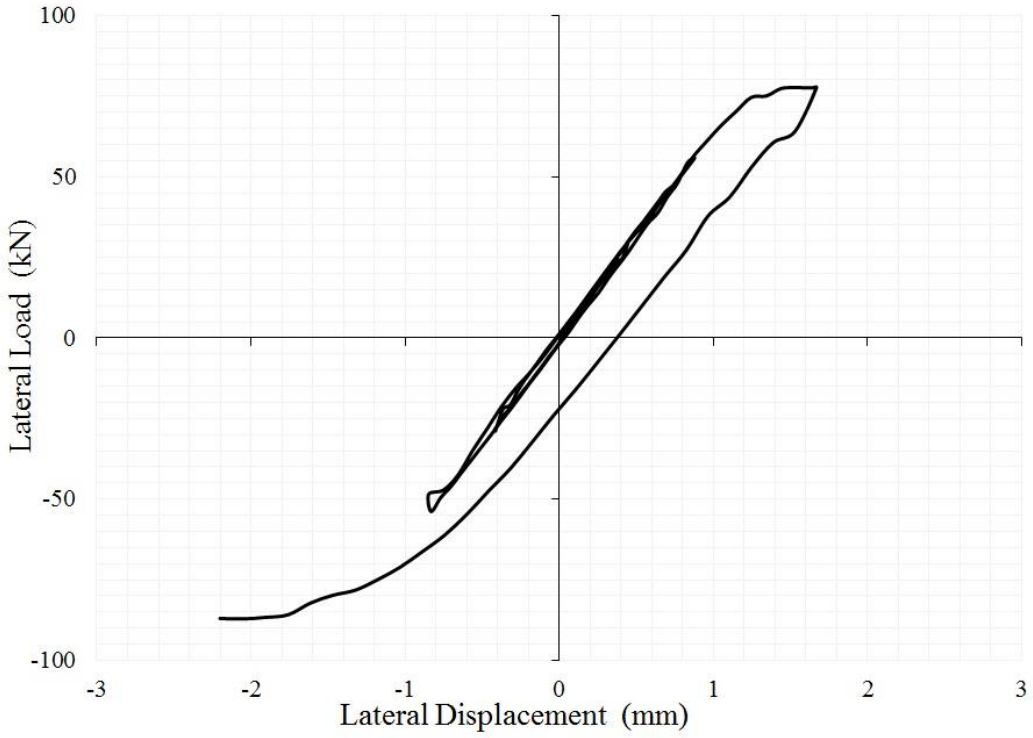

Figure 5-10: FEM Lateral Load Displacement Hysteresis of NCMW Wall

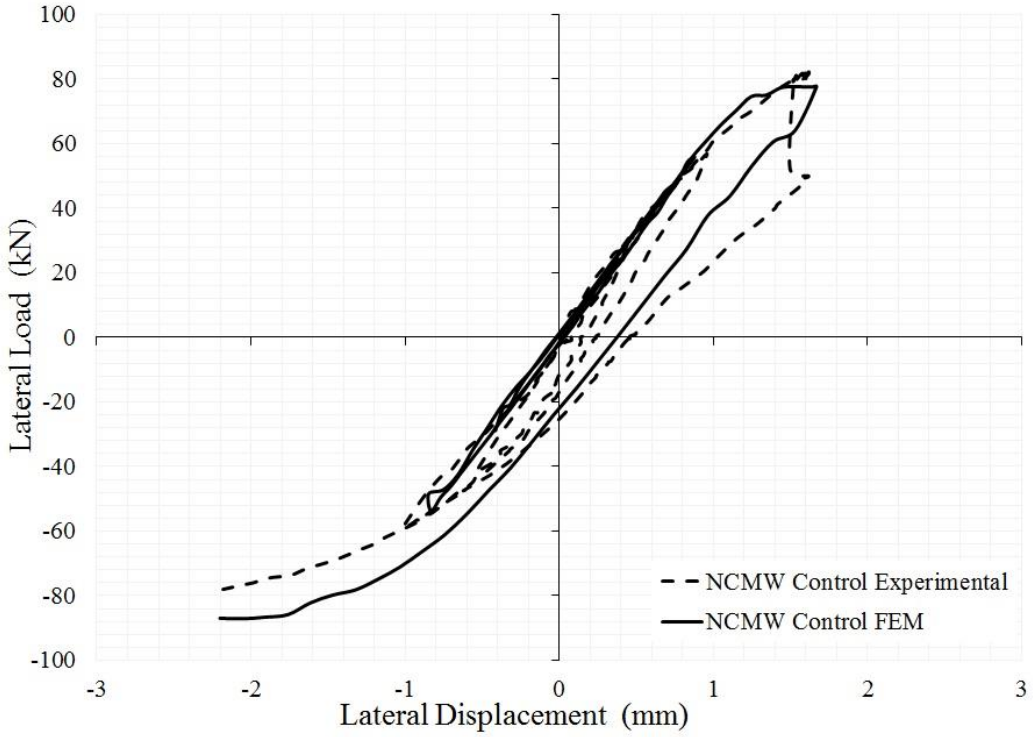

Figure 5-11: FEM and Experimental Lateral Load Displacement Hysteresis of NCMW Wall

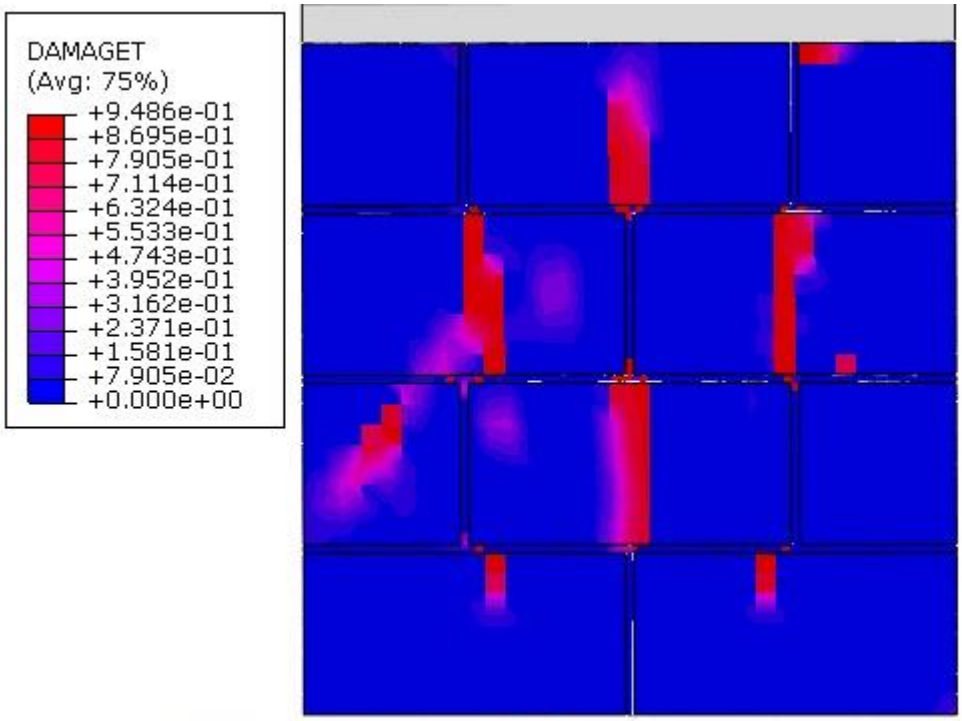

(a) Damage Parameters in Tension

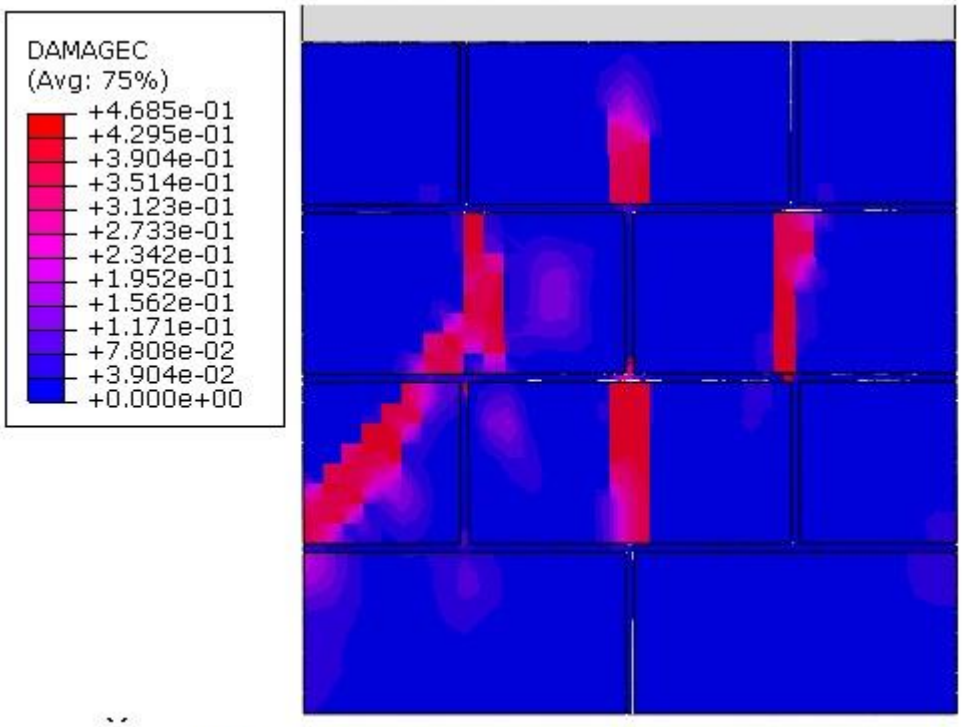

(b) Damage Parameters in Compression

Figure 5-12: Failure Mode of NCMW Wall (FEM)

- **FEM of NCMWJ Wall (SFRM Joint)**

The wall specimen built with SFRM in the bed-head joints was simulated in order to understand the change in the behavior when changing the joints mortar numerically. It is important to mention that, coinciding also to the experimental results, the FEM showed a development in the lateral capacity and crack propagation compared with the control specimen. However, the FEM results show a lateral capacity of NCMWJ less than the experimental test. The FEM lateral load-displacement hysteresis was captured and plotted in Figure 5-13. The FEM result shows a nonlinear behavior after the occurrence of the first crack which coincides with the experimental behavior, as shown in the combined plot in Figure 5-14.

In the first and second cycles, the experimental test shows the residual displacement at 0 load while in the FEM simulation the displacement was zero at the zero load. On the other hand, FEM and experimental results had the same residual displacement in the third cycle and close values in the fourth cycle. Figure 5-15 shows the failure mode represented by damage parameters in tension and compression, respectively. Similar to the experimental test, FEM simulation shows a propagation of diagonal cracks in the third and fourth cycles of push and pull.

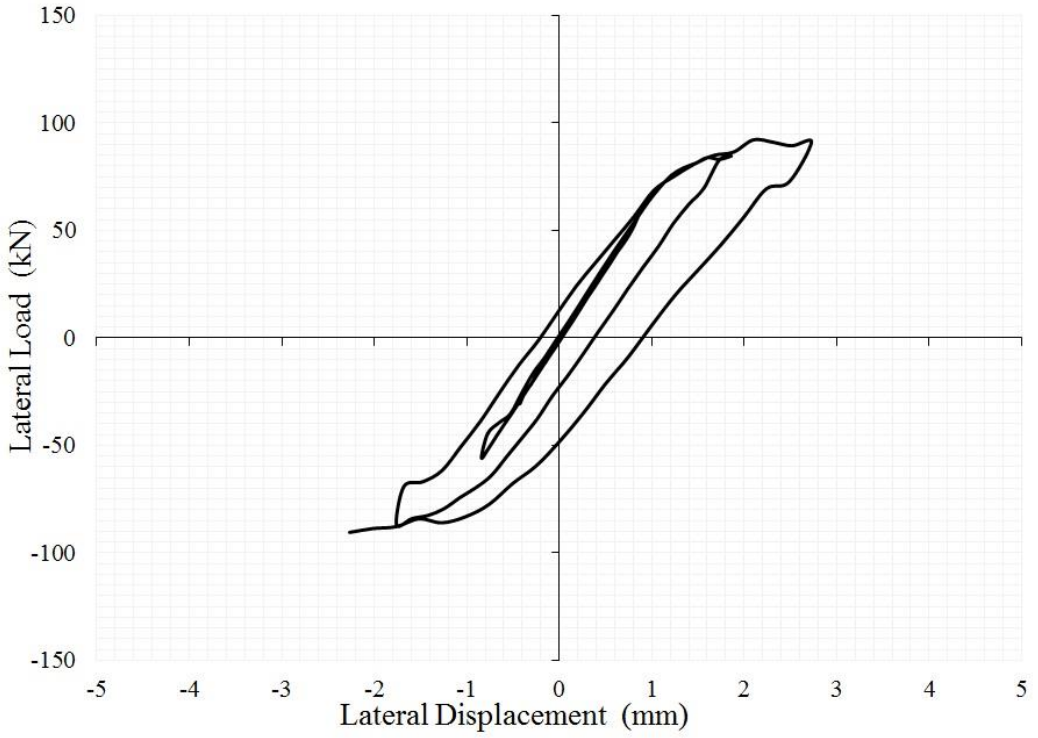

Figure 5-13: FEM Lateral Load Displacement Hysteresis of NCMWJ Wall

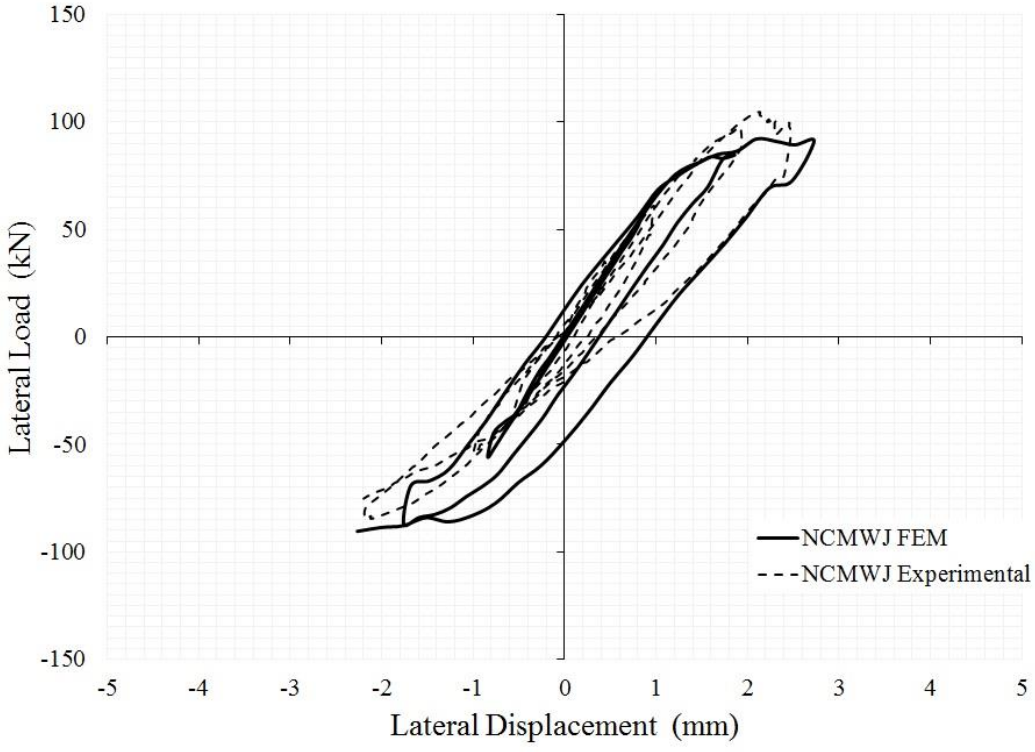

Figure 5-14: FEM and Experimental Lateral Load Displacement Hysteresis of NCMWJ Wall

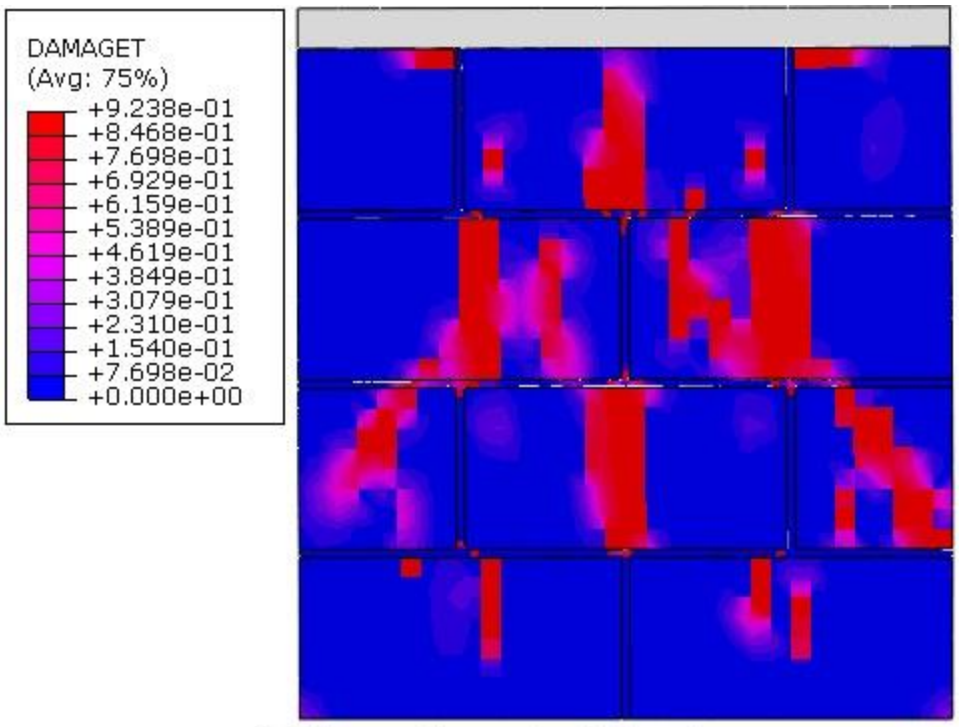

(a) Damage Parameters in Tension

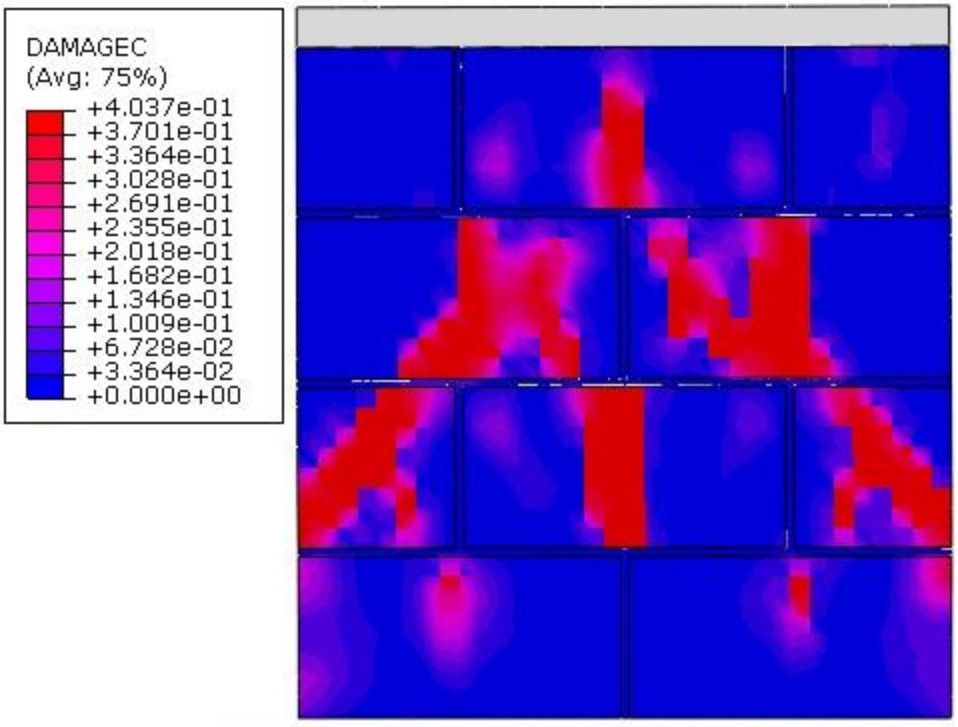

(b) Damage Parameters in Compression

Figure 5-15: Failure Mode of NCMWJ Wall (FEM)

- **FEM of NCMWR Wall (Plaster on One Side)**

The NCMWR wall retrofitted in one side using SFRM plaster was simulated in order to understand the effect of one side retrofitting on the behavior of the URM wall numerically. Matching the experimental results, the FEM showed a development in the lateral capacity and crack propagation compared with the control specimen. However, the FEM results show a lateral capacity of NCMWR slightly more than the experimental test. The FEM lateral load-displacement hysteresis was captured and plotted in Figure 5-16. Nonlinearity started at the load corresponding to the capacity of the control specimen, meaning that the SFRM started to work and prevent splitting of the concrete block. The combined plot in Figure 5-17 shows how the FEM results are overlapped the experimental test results.

Similar to the control specimen, the experimental test shows residuals displacement at 0 load while in the FEM simulation the displacement was zero at the zero load in the first and second cycles. On the other hand, FEM and experimental results had the same residual displacement in the third and fourth cycles. Figure 5-18 shows the failure mode represented by damage parameters in tension and compression, respectively. Similar to the experimental test, FEM simulation shows a propagation of diagonal cracks in the third and fourth cycles of push and pull.

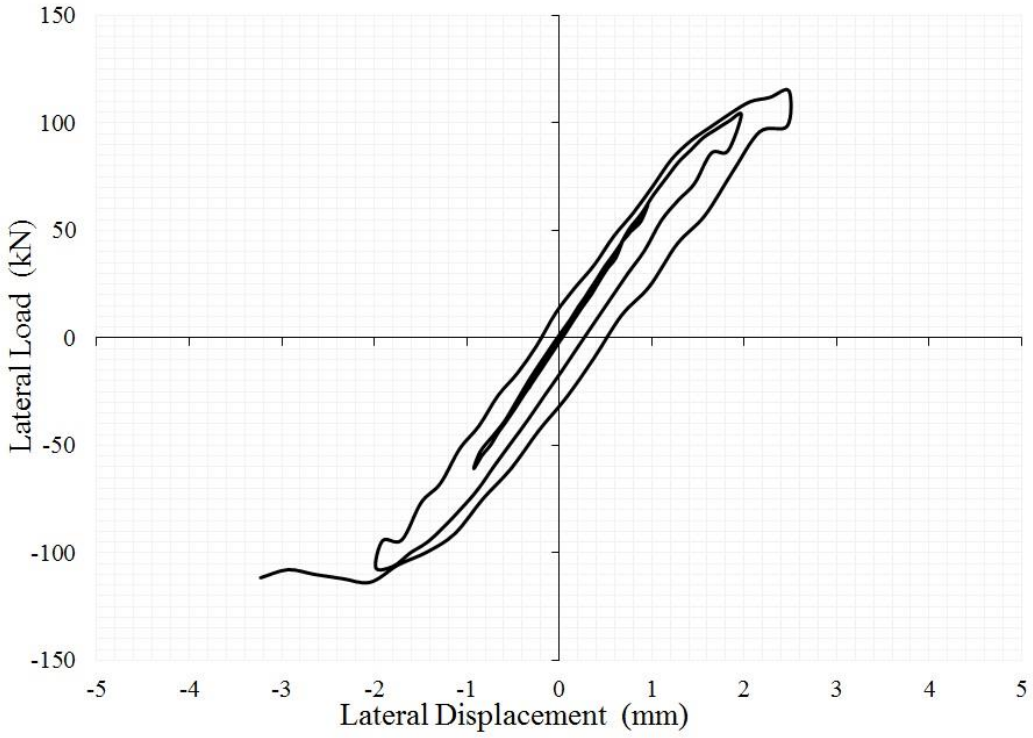

Figure 5-16: FEM Lateral Load Displacement Hysteresis of NCMWR One Side Wall

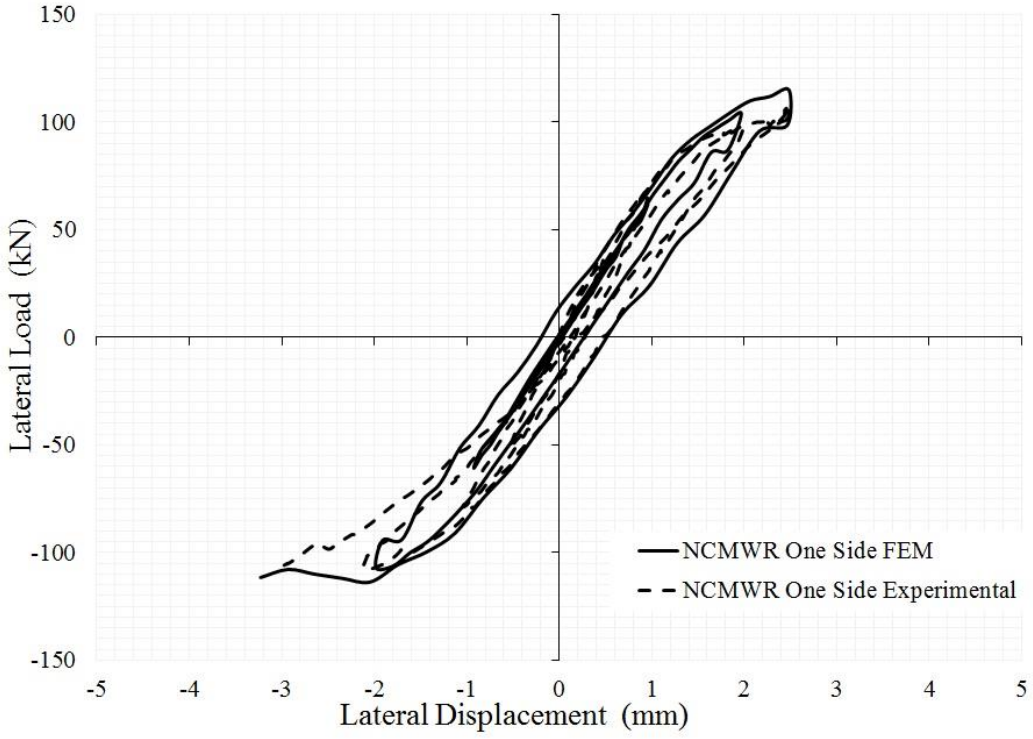

Figure 5-17: FEM and Experimental Lateral Load Displacement Hysteresis of NCMWR One Side Wall

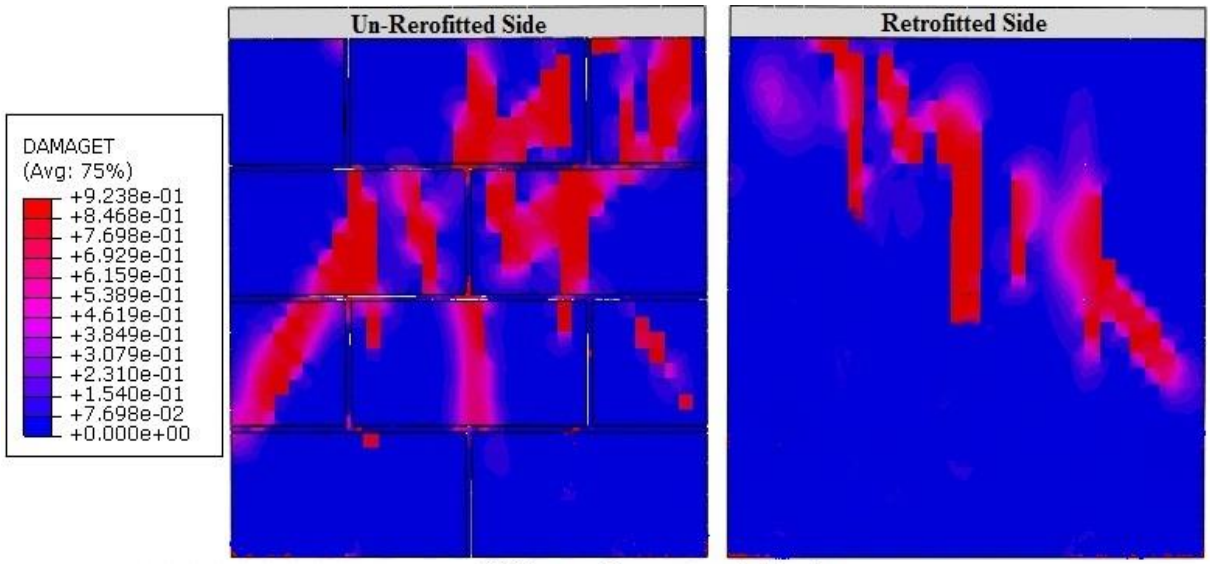

(a) Damage Parameters in Tension

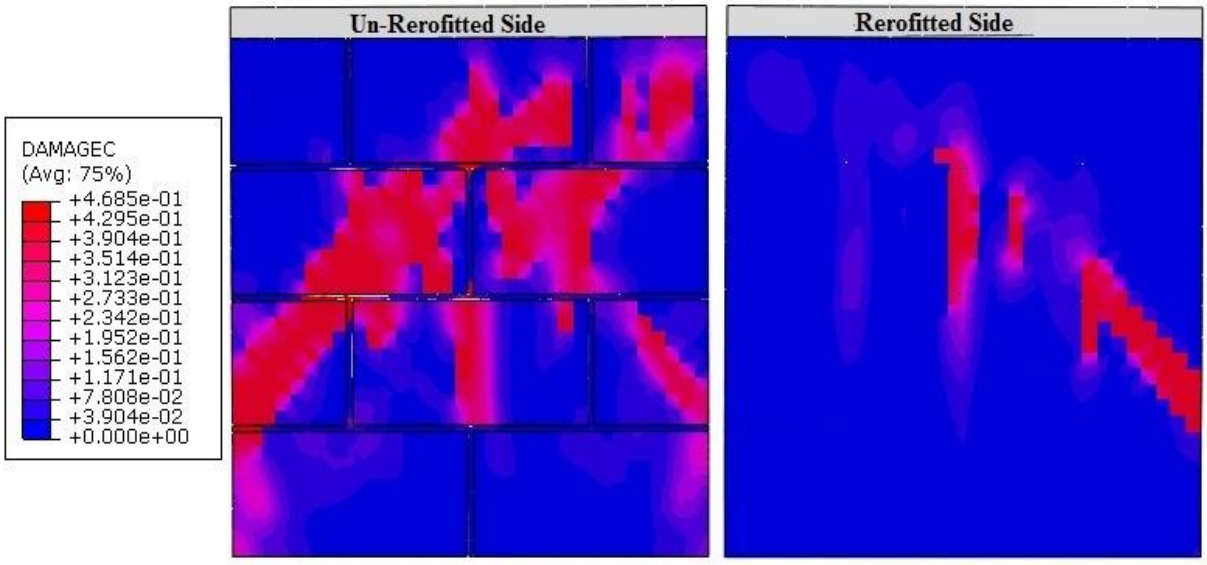

(b) Damage Parameters in Compression

Figure 5-18: Failure Mode of NCMWR One Side Wall (FEM)

- **FEM of NCMWR Wall (Plaster on Two Sides)**

- Applying 35% of the wall compressive capacity similar to the experimental test.

The retrofitted wall using SFRM as plaster on two sides was studied also numerically in ABAQUS environment. The purpose of this study was to calibrate the simulation output results and behavior with the experimental test. Also, the result of this model was compared with the control one.

Obviously, the FEM showed an increase the lateral capacity of the URM wall when retrofitted in two sides using SFRM plaster. However, the FEM results showed a lateral capacity of NCMWR slightly less than the experimental test. The FEM lateral load-displacement hysteresis was captured and plotted in Figure 5-19. The linearity behavior continued up to a load 1.5 times the capacity of the control specimen then the nonlinearity started. This can be related to the increase in the stiffness of the retrofitted wall. The combined plot in Figure 5-20 shows how the FEM results are overlapped the experimental test results.

Like other specimens, the experimental test shows residual displacement at 0 load while in the FEM simulation the displacement was zero at the zero load in the first and second cycles. On the other hand, the FEM and experimental results had the same residual displacement in the fourth cycles while in the third cycle the FEM results showed stiffer behavior. Figure 5-21 shows the failure mode represented by damage parameters in tension and compression, respectively. Similar to the experimental test, FEM simulation shows a propagation of rocking cracks but there is a start of diagonal cracks in the fourth cycles for FEM compared with the experimental test.

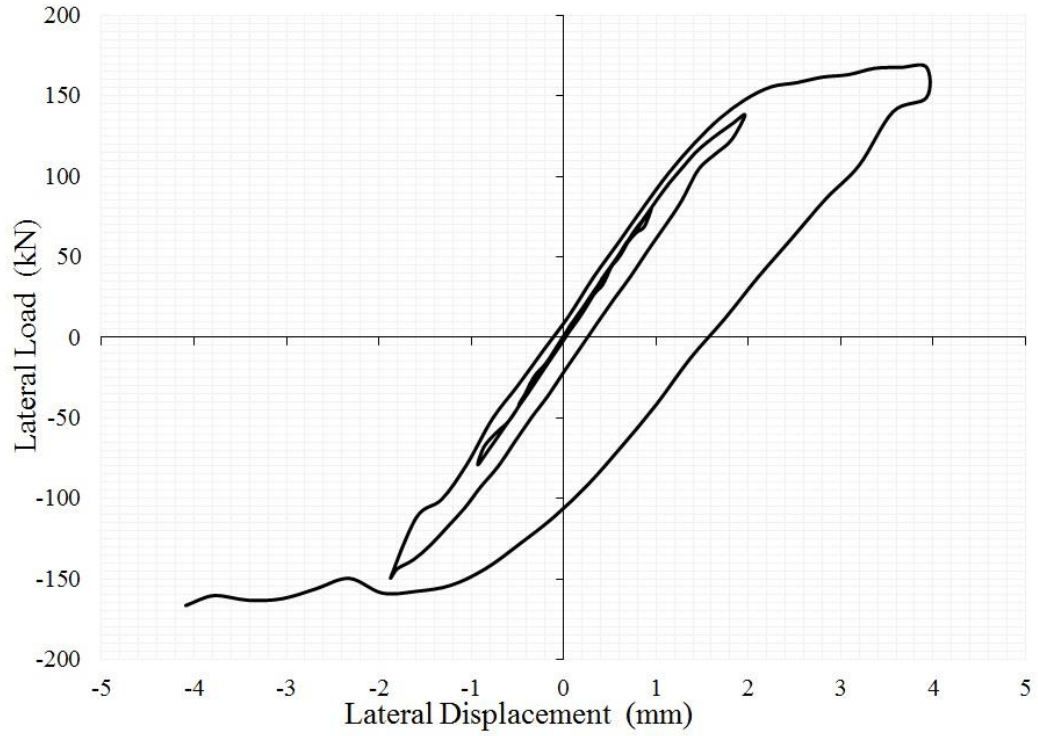

Figure 5-19: FEM Lateral Load Displacement Hysteresis of NCMWR Two Sides Wall

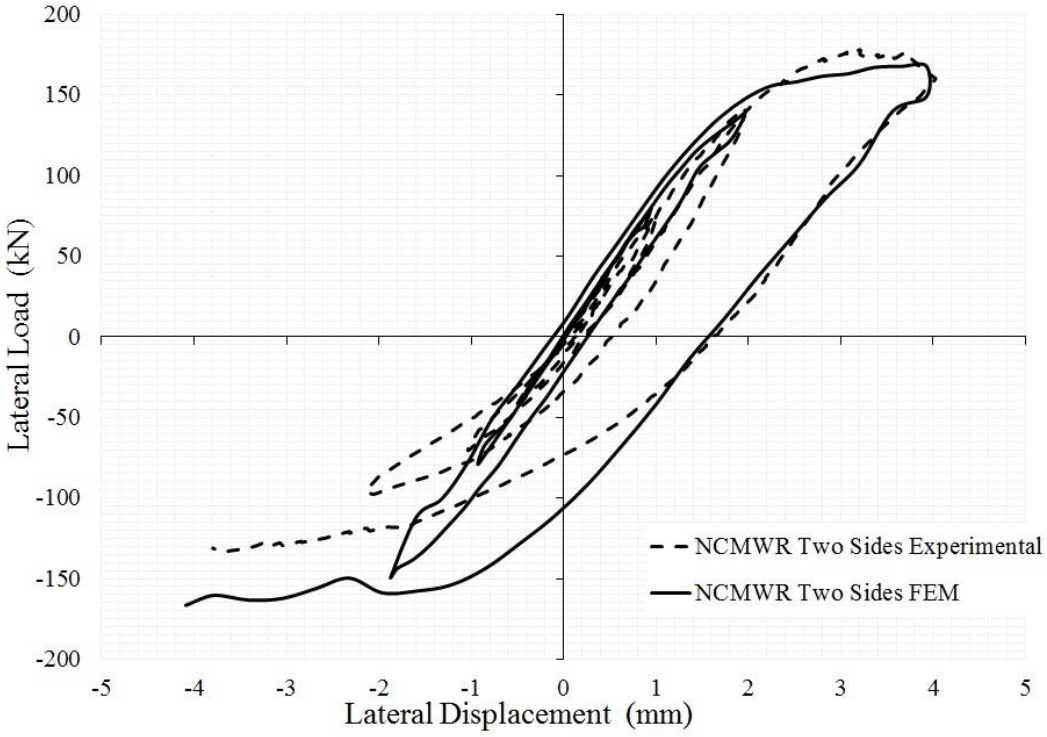

Figure 5-20: FEM and Experimental Lateral Load Displacement Hysteresis of NCMWR Two Sides Wall

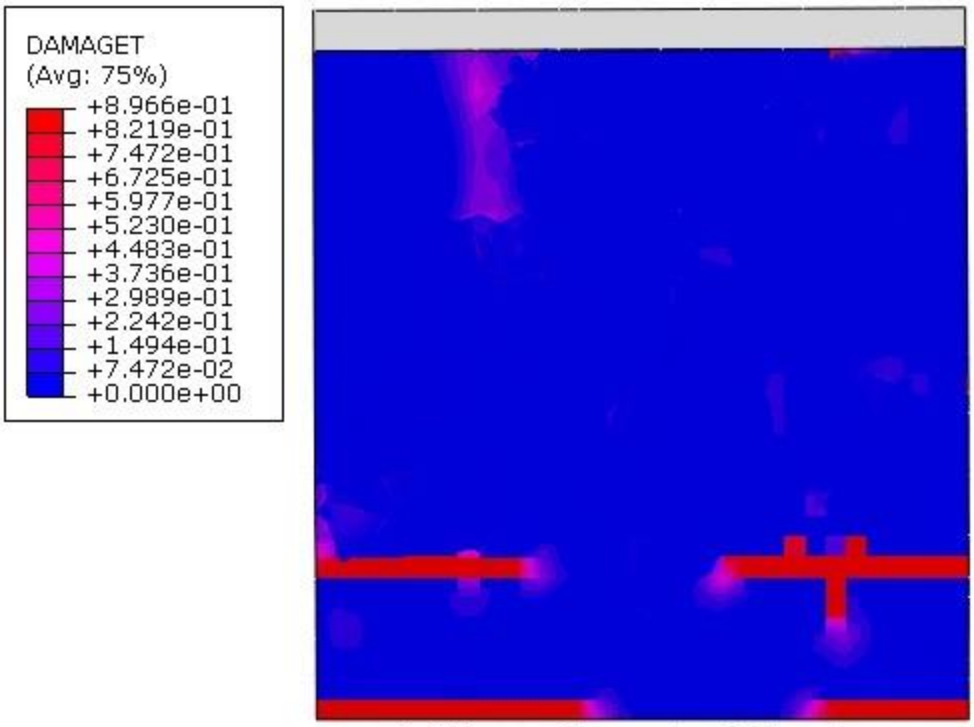

(a) Damage Parameters in Tension

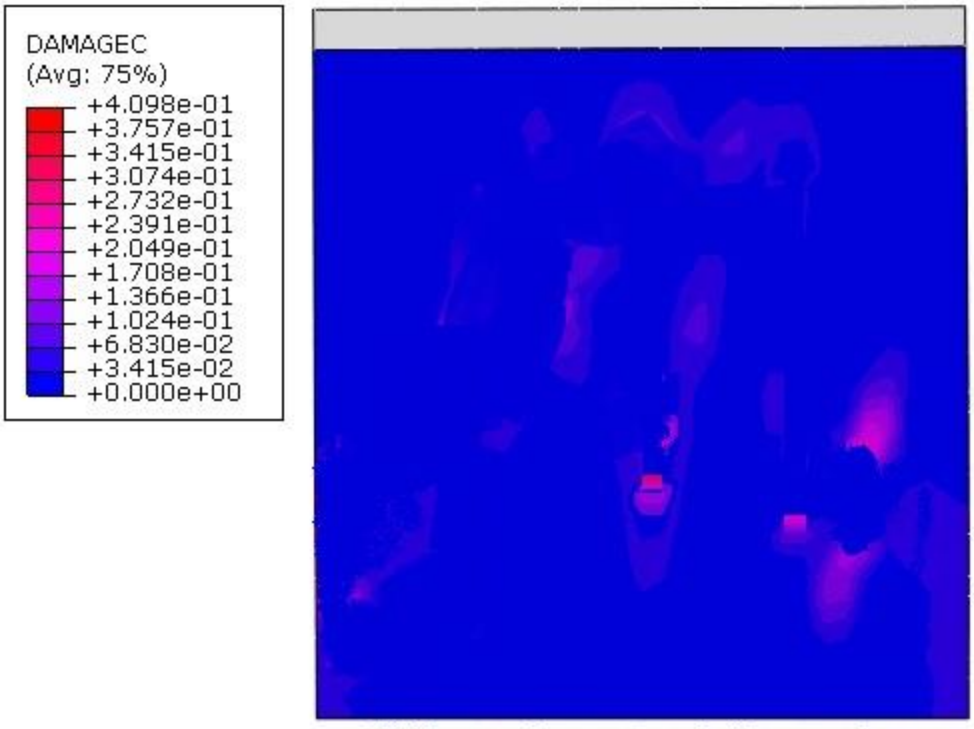

(b) Damage Parameters in Compression

Figure 5-21: Failure Mode of NCMWR Two Sides Wall (FEM) with 35% Pre-compression

- Applying 45% of the wall compressive capacity to get a diagonal cracks failure.

Due to the limitation on the laboratory testing frame, NCMWR on two sides was analyzed using FEM by applying 45% of its compressive capacity. Diagonal cracks failure was expected in this analysis due to the level of pre-compression stress which was exerted on the model. The output results of this study showed diagonal cracks as expected at a lateral load of 142 kN in the fourth cycle of both push and pull, as shown in Figure 5-22.

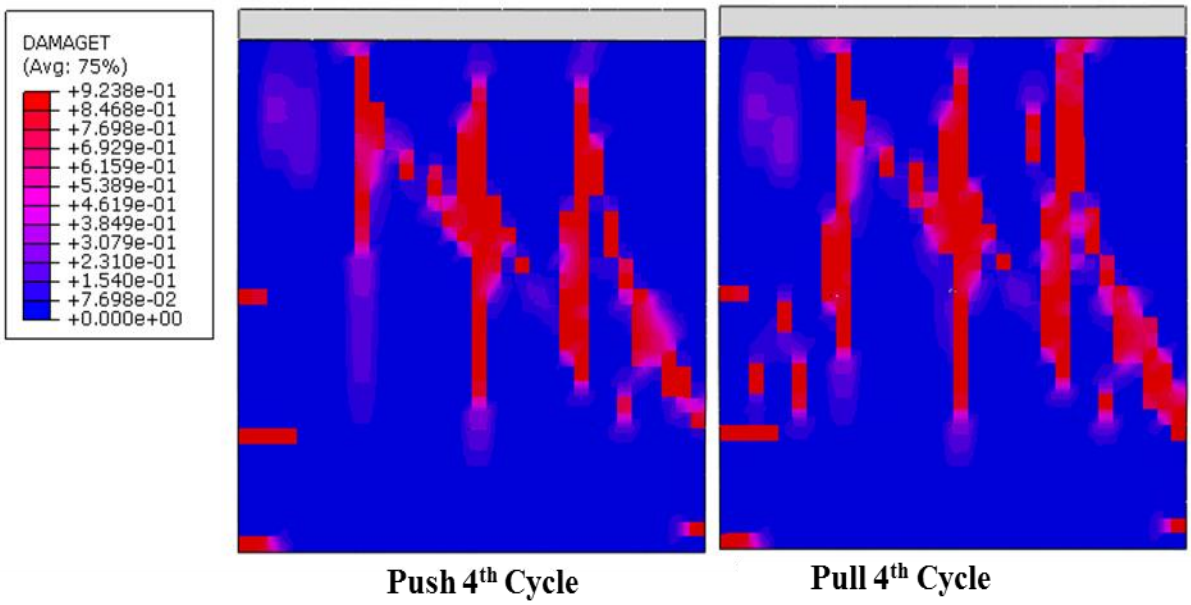

Figure 5-22: Failure Mode of NCMWR Two Sides Wall (FEM) with 45% Pre-compression

5.4 Mechanistic Modeling of URM Wall Behavior

5.4.1 Introduction

Masonry walls exhibit different mechanistic responses when subjected to in-plane loading. These responses are based on the intensity of axial loading applied and wall aspect ratio. Failure patterns and load-deformation response of the walls are also highly influenced by the material properties. The different modes of failure as a function of pre-compression load include sliding, rocking, staggered head/bed joint failure, cracks through wall blocks and crushing of wall blocks or bricks. The behavior has also been suggested by Mann and Müller [39] due to a set of remarkable experiments carried out on shear walls, as shown in Figure 3-1.

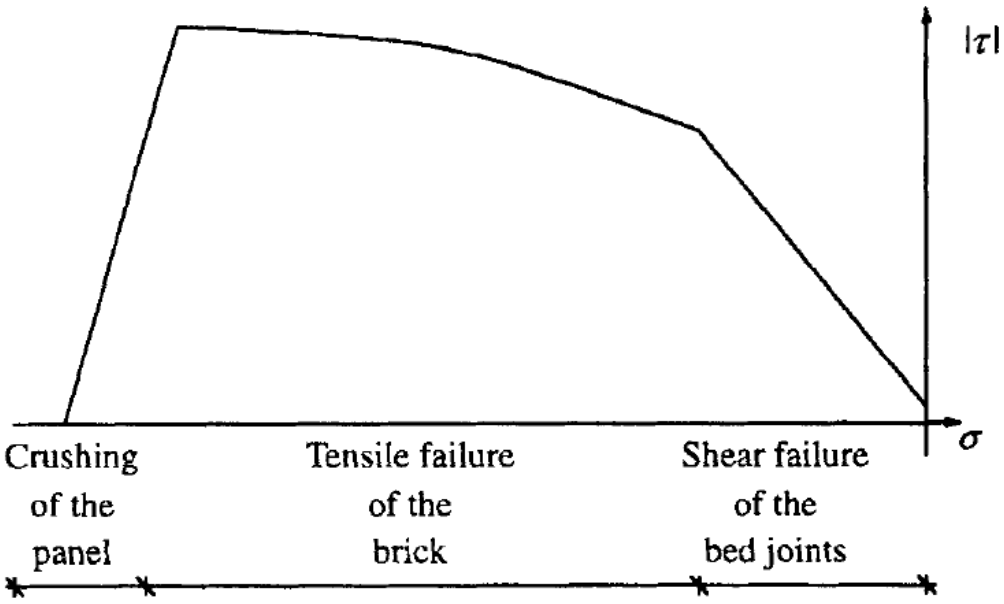

Figure 5-23: Shear-axial Interaction Diagram for URM Walls (Mann and Müller).

Several attempts have been conducted toward understanding and predicting the behavior of masonry walls using the mechanistic framework of analysis. Each failure mode is characterized by different failure pattern, sequences, and gives different levels of lateral resistance. But in this Section, the failure due to cracks through wall blocks will be discussed which occurred in NCMW, NCMWJ and NCMWR one side specimens. Also, the rocking failure is going to be analyzed for the NCMWR two sides as occurred experimentally.

5.4.2 Failure Mode with Cracks through Wall Blocks

In this failure mode, the degree of confinement is high in which it prevents the wall from sliding in a staggered pattern. In this failure mode, the combination of axial and lateral forces result in an initiation of the cracks through the wall bricks due to a principal diagonal tensile stress exceeding the tensile strength of the brick, as shown in Figure 5-24.

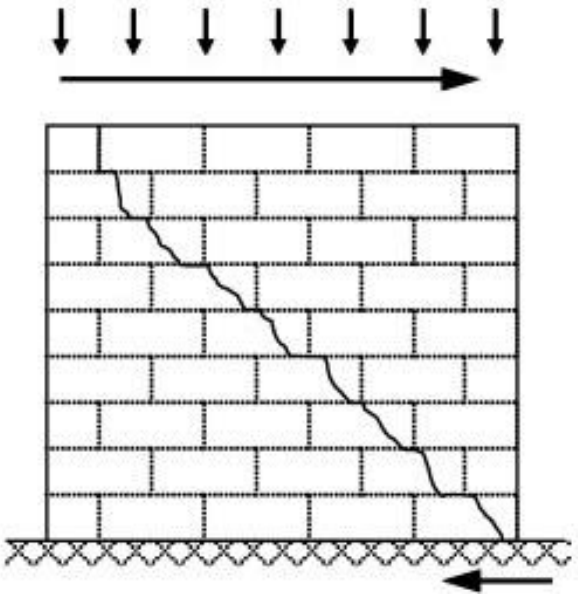

Figure 5-24: Cracks through Wall Blocks

Assuming that this failure occurs when the maximum tensile stress of the masonry (f_{ut}) becomes equal to a combination of 80% of the tensile strength of the block (f_{bt}) and 20% of the tensile strength of the joint mortar (f_{jt}). The lateral shear required to induce the tensile crack in the masonry block may be found from Eq. (5.3), Li et al. [40] and Paulay et al. [41].

$$V_m = d_m \times t_m \times \frac{f_{ut}}{2.3} \sqrt{1 + \frac{\sigma_n}{f_{ut}}} \qquad (5.3)$$

$$f_{ut} = 0.8\, f_{bt} + 0.2\, f_{jt} \qquad (5.4)$$

where:

V_m : Shear capacity of the masonry wall

σ_n : Axial pre-compression applied stress

d_m : Width of the wall

t_m : Effective thickness of the wall

f_m : Compressive strength of the masonry wall.

f_{ut} : Tensile strength of the masonry

f_{bt} : Tensile strength of the brick

f_{jt} : Tensile strength of the joints mortar.

Generally, the level of axial force is around 40-60% of wall axial capacity. The lateral resistance of the wall, in this case, is the highest of all the failure modes.

Also, the contribution of the plaster can be accounted by applying Eq. (5.3) with an equivalent area of the plaster. Therefore, we can use Eq. (5.5) to predict the shear capacity of the plastered walls.

$$V = d_m \left(t_m + n t_p\right) \frac{f_{ut}}{2.3} \sqrt{1 + \frac{\sigma_n}{f_{ut}}} \qquad (5.5)$$

where:

t_p : Thickness of the plaster

n : Elastic moduli ratio $= E_p/E_b$

E_p : Elastic modulus of plaster.

E_b : Elastic modulus of concrete block.

5.4.3 Rocking and Toe Crushing Failure

Walls with a higher axial loading and stronger mortar type may be set into a rocking motion. Due to the mechanism of this type of response, the toe of the wall is generally subjected to high compression force because the entire force is transferred to the base through the toe contact area. This generally results into a local crushing at the toe of the wall, followed by the general collapse of the wall [4].

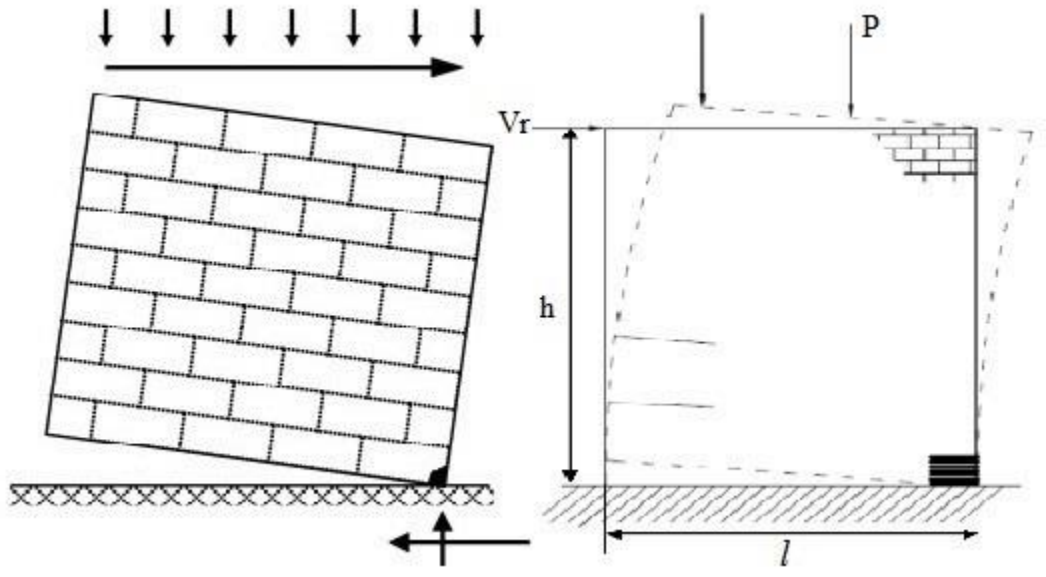

Figure 5-25: Rocking and Toe Crushing Failure Mode

In the tested URM concrete wall retrofitted with 10 mm SFRM plaster on two sides, crack start at the base mortar with a small hear-crack on the plaster. Then the wall was rotating

during the application of lateral load due to the rocking failure in the base without an occurrence of toe crushing. Therefore, Eq. (5.7) is developed using equilibrium principle where the resultant axial stress is equated to the flexural strength of the base mortar.

$$\sigma = -\sigma_n + \frac{M\ c}{I} = -\sigma_n + \frac{V_{r1}\ h\frac{l}{2}}{\frac{1}{12}\ t_m\ l^3} = f_{tm} \qquad (5.6)$$

$$V_{r1} = \frac{t_m\ l^2}{6\ h}\ (\sigma_n + f_{tm}) \qquad (5.7)$$

where:

V_{r1} : Rocking strength at the initiation of the crack.

σ_n : Applied vertical axial compression.

l : Length of the wall.

h : Height of the wall.

t_m : Thickness of the wall.

The lateral strength of URM walls based on expected rocking failure strength in accordance with Eq. (5.5) according to FEMA 273 [42] (NEHRP Guidelines for the Seismic Rehabilitation of Buildings). The Eq. (5.5) is used to determine the rocking strength capacity before the toe crushing and after the occurrence of the rocking crack as expected using Eq. (5.4).

$$V_r = 0.9\ \alpha\ P\ \left(\frac{l}{h}\right) \qquad (5.8)$$

where:

V_r : Rocking shear strength.

α : Factor equal to 0.5 for fixed-free cantilever wall, or equal to 1.0 for fixed-fixed pier.

P : Expected vertical axial compression force.

5.4.4 Shear Capacity of the Tested Walls

- NCMW and NCMWJ

Equations (5.3) & (5.4) are used to predict the shear capacity of the control wall and the wall with SFRM in the joints. The numerical values of the parameters to be substituted in the equations are shown in Table 5-3.

Table 5-3: Numerical Values of Parameters of Eq. (5.3) & Eq. (5.4)

Name of the parameter	**value**
Brick tensile strength	f_{bt} =1.6 MPa
Joint tensile strength NCMW	f_{jt} = 2.5 MPa
Joint tensile strength NCMWJ	f_{jt} = 5.0 MPa
width of the wall	d_m = 810 mm
Effective thickness of the wall	t_m = 72 mm
Axial pre-compression on wall	σ_n = 4.0 MPa

Substituting the value in Eq. (5.3) and Eq. (5.4):

NCMW shear capacity $V_m = 81\ kN$

NCMWJ shear capacity $V_m = 94\ kN$

- NCMWR 10 mm Two Sides

To determine the occurrence of the rocking crack, Eq. (5.7) is used. Then Eq. (5.8) is used in order to determine the shear capacity of the URM wall plastered on two sides which based on expected rocking strength.

Crack initiation:

$$V_{r1} = \frac{t_m\, l^2}{6\, h}\ (\sigma_n + \ f_{tm}) = \left(\frac{92 \times 810^2}{6 \times 770}\right)\frac{(5.4 + 7)}{1000} = 161\ kN$$

The value of $f_{tm} = 7MPa$ for the base mortar (EMACO S88 CT provided by BASF) as reported by attached data to the product.

$$V_r = 0.9\ \alpha\ P\ \left(\frac{l}{h}\right)$$

$$V_r = 0.9\ \times\ 0.5 \times 400\ (1) = 180\ \ kN$$

- <u>NCMWR 10 mm One Side</u>

Eq. (5.5) is used in order to determine the shear capacity of the URM wall plastered on one side and controlled by diagonal cracks. The numerical values of the parameters to be substituted in Eq. (5.5) are shown in Table 5-4.

Table 5-4: Numerical Values of Parameters of Eq. (5.5)

Name of the parameter	**value**
Brick tensile strength	f_{bt} =1.6 MPa
Joint tensile strength NCMW	f_{jt} = 2.5 MPa
Elastic moduli ratio	$n = E_p/E_b = 28/16.5 = 1.7$
width of the wall	d_m = 810 mm
Effective thickness of the wall	t_m = 72 mm
Thickness of the plaster	t_p = 10 mm
Axial pre-compression on wall	σ_n = 4.5 MPa

Substituting the value in Eq. (5.4) and Eq. (5.5):

NCMWR plastered on one side shear capacity, $V_m = 106\ kN$

The experimental, FEM and mechanistic analysis results are compared in Table 5-5. The proposed mechanistic model, as well as FEM analysis, predicted the shear capacity of the tested walls with a difference of 4% and 6% with the experimental tests, respectively. It is important to mention that, the diagonal cracks failure occurred in the first three walls due to the moderate level of pre-compression. However, the failure of the fourth walls, NCMWR on two sides, was rocking because of the low level of pre-compression. Therefore, a FEM analysis was conducted, as shown in Figure 5-22, where diagonal cracks failure occurred at a load of 142 kN. Also, the shear capacity under 45% pre-compression was calculated to be 148 kN using the proposed mechanistic model, Eq. (5.5). Both FEM and mechanistic results showed the powerful of the calibrated FEM and proposed a mechanistic model in predicting the behavior and shear capacity of URM walls.

Table 5-5: Comparison Results of the Wall Lateral Tests

Specimen	**Shear Capacity kN**					Mode of Failure
	Experimental	**FEM**		**Mechanistic**		
		Value	Difference % (*)	Value	Difference %(*)	
NCMW	82.0	77.6	5.4	81.0	1.2	Diagonal Cracks
NCMWJ	96.0	91.2	5.0	94.0	2.1	Diagonal Cracks
NCMWR one side	110.0	115.0	4.5	106.0	4.1	Diagonal Cracks
NCMWR two sides	178.0	168.0	5.6	180.0	-1.1	Rocking Failure
(*) Percentage difference with the experimental results.						

CHAPTER 6

CONCLUSIONS AND RECOMMENDATIONS

Experimental and FEM simulations were carried out in this study for different prism and wall specimens. The main purpose of this study was to understand the response of masonry wall to axial and lateral loadings. SFRM plaster was used in this work as a retrofitted material in order to strengthen the axial and lateral load resistance of the concrete masonry walls. This method of surface treatment opens the door for enhancing the existing masonry structures against any lateral loading without any destruction of building's element or distortion of architectural appearance.

6.1 Conclusions

This research investigates the effect of using SFRM as a surface treatment for retrofitting concrete block masonry walls to enhance the performance of the concrete masonry structures. The following conclusions could be drawn:

The masonry components (concrete blocks and type M mortar) exhibited a good strength in compression but weak in tension. The SFRM mortar on the other hand exhibits enhanced strength in both tension and compression. Therefore, SFRM can be used to compensate the weakness in the wall performance.

The use of SFRM in joints or as plaster in retrofitting the URM concrete walls enhanced the axial and lateral resistance. The axial compressive strength of the masonry increased with the increase of plaster's thickness, which increases the area of the strong material

contribution in the prism strength. Based on the experimental results, the 20 mm thickness of SFRM plaster enhanced the axial load by the same amount of the non-plastered wall. Therefore, if the lateral load is not a major problem and there is a need for enhancing the gravity load, SFRM can be used as plaster.

Regarding the crack patterns, the weakest point is in the web of the hollow concrete blocks which makes all prism specimens follow the same crack patterns as a vertical crack at the web of the hollow concrete blocks.

The use of SFRM in bed-head joint improves the resistance of URM wall against in-plane stress by 17% of the shear capacity of the control one. Also, diagonal cracks developed through the block similar to the control under moderate to high axial pre-compression stress.

The use of SFRM as a plaster on one side improved the resistance of URM wall against in-plane stress by 34% of the shear capacity and 17% of the stiffness of the control one. Also, diagonal cracks developed through the block and plaster under moderate to high axial pre-compression stress.

The plastered wall on both sides exhibited a good enhancement in both shear strength and stiffness by 117% and 26%, respectively. But due to the low level of the axial pre-compression load exerted during the experiment, the rocking failure was the mode of failure in this wall.

It is important to mention that, the rough surface of the block provides a strong bond between the block and the plaster. Therefore, no de-bonding between the SFRM plaster and block was observed during the experimental tests.

I order not to increase the seismic weight of the building, SFRM is recommended to be used as plaster instead of normal mortar. This is due to the enhancement of the wall with only 10 mm thick plaster.

CDP approach implemented in ABAQUS can be used competently to model concrete masonry structures. The continuum-based technique adopted for concrete blocks, type M mortar and SFRM mortar results in a good agreement (5%-6%) difference between experimental and numerical load-deflection response of the prism and full wall. The mode of failure and development of cracks in the wall were also captured with significant accuracy using the plastic-damage model. Time and memory consumption of the computer during the analysis, as well as the accuracy of the analysis results, should be put in mind when meshing the model. This FEM simulation can be used to expand the study of masonry performance for different factors before conducting any experimental program.

A mechanistic model was developed based on the principle of transformer section using the elastic moduli ratio. It predicted the shear capacity of the wall with a (2%-4%) difference with the experimental results.

6.2 Recommendations

From this work, it can be noticed that there are several studies that have to be conducted in order to come up with the full database on masonry structure retrofitted using SFRM plaster. Some of these topics can be summarized as follows:

1. Aspect ratio and plaster thickness for concrete masonry wall need to be studied experimentally and numerically to come up with a mathematical model that represents the effect of plaster thickness and aspect ratio on the performance of the wall.

2. Cyclic tests should be conducted with different levels of pre-compression stress to understand the interaction of shear and axial stress of such walls.
3. The out-of-plane behavior of concrete masonry walls needs to be characterized experimentally and numerically.
4. Additional research is required to comprehend the behavior of wall with an opening in both in-plane and out-of-plane loading.
5. Additional research is required to establish appropriate contact properties between concrete blocks and mortar.
6. Different FEM approaches such as macro, micro and macro-micro modeling have to be conducted in order to identify the most accurate one for modeling URM walls.
7. Additional study is required to find out mesh size sensitivity of the model in ABAQUS environment in the case of both monotonic and cyclic loading.
8. The performance of SFRM with cheap and low-quality materials such as clay bricks, instead of the blocks needs to be studied.

References

[1] S. Bhattacharya, S. Nayak, and S. C. Dutta, "A critical review of retrofitting methods for unreinforced masonry structures," *Int. J. Disaster Risk Reduct.*, vol. 7, pp. 51–67, 2014.

[2] M. Elgawady, P. Lestuzzi, and M. Badoux, "A review of conventional seismic retrofitting techniques for URM," *13th Int. Brick Block Mason. Conf.*, pp. 1–10, 2004.

[3] B. Al-Gohi, M. K. Rahman, and M. H. Baluch, "A review of seismic retrofit of masonry walls," *Turkish-Saudi Work. Struct. Earthq. Eng.*, 2010.

[4] W. Yi, S. Oh, and J. Lee, "Shear capacity assessment of unreinforced masonry wall," *13th World Conf. Earthq. Eng.*, no. 1698, pp. 1–12, 2004.

[5] D. Jain, A. K. Saxena, and S. Saraswat, "A review of effect of microsilica in concrete," *Corona J. Sci. Technol.*, vol. 3, no. I, pp. 14–18, 2014.

[6] U. Sharma, A. Khatri, and A. Kanoungo, "Use of micro-silica as additive to concrete-state of art," *Res. India Publ.*, vol. 5, no. 1, pp. 9–12, 2014.

[7] C. Akis, L. Bank, V. Brown, E. Cosenza, J. Davalos, J. Lesko, A. Machida, S. Rizkalla, and T. Triantafillou, "Fiber-reinforced polymer composites for construction state-of-the-art review," *J. Compos. Constr.*, vol. 6, no. 2, pp. 73–87, 2002.

[8] B. Al-Gohi, "An experimental and numerical study of retrofitted masonry walls under cyclic loading," *PhD, KFUPM, KSA*, p. 381, 2013.

[9] Saudi Geologist Survey, "www.sgs.org.sa," 2006. .

[10] M. ElGawady, P. Lestuzzi, and M. Badoux, "A review of retrofitting of unreinforced masonry walls using composites," *Proc., 4th Int. Conf. ...*, pp. 1–8, 2004.

[11] V. Haach, G. Vasconcelos, and P. P. B. Lourenço, "Experimental analysis of reinforced concrete block masonry walls subjected to in-plane cyclic loading," *J. Struct. Eng.*, vol. 136, no. April, pp. 452–462, 2009.

[12] A. Mosallam and S. Banerjee, "Enhancement in in-plane shear capacity of unreinforced masonry (URM) walls strengthened with fiber reinforced polymer composites," *Compos. Part B Eng.*, vol. 42, no. 6, pp. 1657–1670, 2011.

[13] P. Bischof and R. Suter, "Retrofitting masonry walls with carbon mesh," *Polymers (Basel).*, vol. 6, no. 2, pp. 280–299, 2014.

[14] G. Vasconcelos, S. Abreu, R. Fangueiro, and F. Cunha, "Retrofitting masonry infill walls with textile reinforced mortar," *15th World Conf. Earthq. Eng. Lisbon Port.*,

2012.

[15] H. Basaran, A. Demir, and M. Bagci, “The behavior of masonry walls with reinforced plaster mortar,” *Adv. Mater. Sci. Eng.*, vol. 2013, 2013.

[16] M. ElGawady, P. Lestuzzi, and M. Badoux, “Retrofitting of masonry walls using shotcrete,” *2006 NZSEE Conf. Yeni*, no. 45, pp. 45–54, 2006.

[17] L. Facconi, A. Conforti, F. Minelli, and G. a. Plizzari, “Improving shear strength of unreinforced masonry walls by nano-reinforced fibrous mortar coating,” *Mater. Struct.*, pp. 2557–2574, 2014.

[18] H. Köksal, C. Karakoc, and H. Yildirim, “Compression behavior and failure mechanisms of concrete masonry prisms,” *J. Mater. Civ. Eng.*, vol. 17, no. February, pp. 107–115, 2005.

[19] G. Mohamad, P. B. Lourenço, E. Rizzatti, H. R. Roman, and E. Y. Nakanishi, “Failure mode, deformability and strength of masonry walls,” *15th Int. Brick Block Mason. Conf.*, vol. 01, no. c, 2012.

[20] J. Machado and A. Lima, “The effect of mortar bedding type and hollow concrete block geometry on the mechanical behavior of high-strength structural masonry,” *15th Int. Brick Block Mason. Conf. Florianóp. – Brazil*, 2012.

[21] F. L. D. E. Oliveira and J. B. D. E. Hanai, “Axial compression behavior of concrete masonry wallettes strengthened with cement mortar overlays Comportamento à compressão axial de pequenas,” *IBRACON Struct. Mater. J.*, vol. 1, no. 2, pp. 158–170, 2008.

[22] A. A. Shah, “Applications of ferrocement in strengthening of unreinforced masonry columns,” *Int. J. Geol.*, vol. 5, no. 1, pp. 21–27, 2011.

[23] G. Sarangapani, B. V. Reddy, and K. Jagadish, “Brick-mortar bond and masonry compressive strength,” *J. Mater. Civ. Eng.*, vol. 17, no. 2, pp. 229–237, 2005.

[24] T. Nagarajan, S. Viswanathan, S. Ravi, and V. Srinivas, “Experimental approach to investigate the behaviour of brick masonry for different mortar ratios,” *Int. Conf. Adv. Eng. Technol.*, pp. 586–592, 2014.

[25] H. a. Toutanji and Tahar El-Korchi, “The influence of SF on the compressive strength of cement paste and mortar,” *Cem. Concr. Res.*, vol. 25, no. 7, pp. 1591–1602, 1995.

[26] R. Duval and E. H. Kadri, “Influence of silica fume on the workability and the compressive strength of high-performance concretes,” *Cem. Concr. Res.*, vol. 28, no. 4, pp. 533–547, 1998.

[27] M. Mazloom, A. A. Ramezanianpour, and J. J. Brooks, “Effect of silica fume on mechanical properties of high-strength concrete,” *Cem. Concr. Compos.*, vol. 26, no. 4, pp. 347–357, 2004.

[28] S. Bhanja and B. Sengupta, “Influence of silica fume on the tensile strength of concrete,” *Cem. Concr. Res.*, vol. 35, no. 4, pp. 743–747, 2005.

[29] S. F. Lee, X. H. Wang, and S. Jacobsen, “Mix design and the effect of silica fume and steel fiber on rheological and mechanical properties of mortars,” *Nord. Concr. Res.*, vol. 41, no. 3, pp. 33–50, 2010.

[30] B. H. Al-Gohi, M. H. Baluch, M. K. Rahman, A. Ilki, and C. Demir, “Behavior of heritage masonry walls retrofitted with CFRP,” *2nd Conf. smart Monit. Assess. Rehabil. Civ. Struct.*, no. September, pp. 1–8, 2013.

[31] M. Bolhassani, A. a. Hamid, A. C. W. Lau, and F. Moon, “Simplified micro modeling of partially grouted masonry assemblages,” *Constr. Build. Mater.*, vol. 83, pp. 159–173, 2015.

[32] ABAQUS 2013., “Abaqus 6.13 online documentation.,” *Dassault Systèmes*. .

[33] J. Lubliner, J. Oliver, S. Oller, and E. Oñate, “A plastic-damage model for concrete,” *Int. J. Solids Struct.*, vol. 25, no. 3, pp. 299–326, 1989.

[34] J. H. Lee and G. L. Fenves, “Plastic-damage model for cyclic loading of concrete structures,” *J. Eng. Mech.*, vol. 124, no. 8, pp. 892–900, 1998.

[35] A. Dogariu and F. Campitiello, “Calibration of a FE model of masonry shear panels strengthened by metal sheathing,” *Proc. 3rd WSEAS Int. Conf. Finite Differ. - Finite Elem. - Finite Vol. - Bound. Elem. F-and-B ’10*, pp. 258–263, 2010.

[36] M. Vindhyashree, P. Kumar, P. G. Coordinator, and P. Kumar, “Numerical simulation of masonry prism test using ANSYS and ABAQUS,” vol. 4, no. 07, pp. 1019–1027, 2015.

[37] ASTM C140-11a, “Standard test methods for sampling and testing concrete masonry units and related units,” pp. 1–17, 2012.

[38] J. A. Thamboo, “Development of thin layer mortared concrete masonry,” *PhD, Queensland University of Technology, Australia*. 2014.

[39] W. Mann and H. Muller, “Failure of shear-stressed masonry- an enlarged theory, tests and application to shear walls,” *Proc. Br. Ceram. Soc.*, vol. 30, pp. 223–235, 1982.

[40] T. Li, N. Galati, J. G. Tomialan, and N. Antonio, “Analysis of unreinforced masonry concrete walls strengthened with glass fiber-reinforced polymer bars,” *ACI Struct. J.*, vol. 102, no. 4, pp. 569–577, 2005.

[41] T. Paulay and M. J. N. Priestley, “Seismic design of reinforced concrete and masonry buildings,” *John Wiley Sons, Inc., New York*, p. 744, 1992.

[42] FEMA 273, “NEHRP guidelines for the seismic rehabilitation of buildings,” *Washington, D.C.*, p. 435, 1997.

Vitae

Name:	Madyan Abdulwahab Saleh Alshugaa
Nationality:	Yemeni
Date of Birth:	1/1/1987
Email:	madyan.alshugaa@gmail.com
Address:	Ba'adan, Ibb, Yemen
Academic Background:	MS in Civil Engineering, King Fahd University of Petroleum and Minerals (KFUPM), Dhahran, Saudi Arabia. BS in Civil Engineering, King Fahd University of Petroleum and Minerals (KFUPM), Dhahran, Saudi Arabia.